

AD-A254 347



PL-TR-91-2270

ELF/VLF Generation

DTIC
ELECTE
JUL 22 1992
S C D

2

Dennis Papadopoulos
Robert D. Short

ARCO Power Technologies, Inc.
1250 Twenty Fourth St., NW
Suite 850
Washington, DC 20037

31 August 1991

Scientific Report No. 2

Approved for Public Release, Distribution Unlimited



Phillips Laboratory
Air Force Systems Command
Hanscom Air Force Base, MA 01731-5000

92 7 20 189

92-19254



This technical report has been reviewed and is approved for publication.

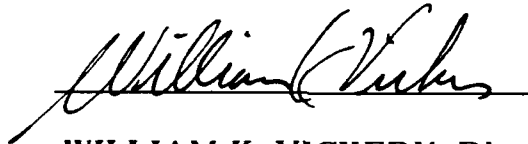


JOHN L. HECKSCHER

Contract Manager



JOHN E. RASMUSSEN, Chief
Ionospheric Modification Branch



WILLIAM K. VICKERY, Director
Ionospheric Physics Division

This document has been reviewed by the ESD Public Affairs Office (PA) and is releasable to the National Technical Information Service (NTIS).

Qualified requestors may obtain additional copies from the Defense Technical Information Center. All others should apply to the National Technical Information Service.

If your address has changed, or if you wish to be removed from the mailing list, or if the addressee is no longer employed by your organization, please notify PL/TSI, Hanscom AFB, MA 01731-5000. This will assist us in maintaining a current mailing list.

Do not return copies of this report unless contractual obligations or notices on a specific document require that it be returned.

REPORT DOCUMENTATION PAGE

FORM APPROVED
OMB No. 0704-0188

Public reporting burden for this collection of information is estimated to average 1 hour per response, including the time for reviewing instructions, searching existing data sources, gathering and maintaining the data needed, and completing and reviewing the collection of information. Send comments regarding this burden estimate or any other aspect of this collection of information, including suggestions for reducing this burden, to Washington Headquarters Services, Directorate for Information Operations and Reports, 1215 Jefferson Davis Highway, Suite 1204, Arlington, VA 22202-4302, and to the Office of Management and Budget, Paperwork Reduction Project (0704-0188), Washington, DC 20503.

1. AGENCY USE ONLY (Leave blank)	2. REPORT DATE 31 August 1991	3. REPORT TYPE AND DATES COVERED Scientific No. 2	
4. TITLE AND SUBTITLE ELF/VLF Generation		5. FUNDING NUMBERS PE 62101F PR 4643 TA 10 WU AM Contract F19628-89-C-0174	
6. AUTHOR(S) Robert D. Short Dennis Papadopoulos		8. PERFORMING ORGANIZATION REPORT NUMBER	
7. PERFORMING ORGANIZATION NAME(S) AND ADDRESS(ES) ARCO Power Technologies, Inc 1250 Twenty-Fourth Street, NW Suite 850 Washington, DC 20037		10. SPONSORING/MONITORING AGENCY REPORT NUMBER PL-TR-91-2270	
9. SPONSORING/MONITORING AGENCY NAME(S) AND ADDRESS(ES) Phillips Laboratory Hanscom AFB, MA 01731-5000 Contract Manager: John Heckscher/GPID		11. SUPPLEMENTARY NOTES	
12a. DISTRIBUTION / AVAILABILITY STATEMENT Approved for public release; Distribution unlimited		12b. DISTRIBUTION CODE	
13. ABSTRACT (Maximum 200 words) A preliminary analysis of the results of the ELF experimental campaigns conducted in the May - September, 1990 time frame using the HIPAS transmitter in conjunction with the UCLA ELF receiver at the NOAA site and the mobile NUSC receiver is presented. Following a discussion of the critical physics issues and scalings relating to practical implementation of ionospherically generated ELF to submarine communications, the results of the two campaigns are presented. The data show conclusively that the measured ELF are low frequency signals generated by modulated ionospheric currents and not by nonlinear interference effects of the modulated HF. For the HIPAS parameters the received ELF signals are consistent with an equivalent Horizontal Magnetic Dipole (HMD) located at an altitude of 75 km radiating with an average dipole moment $M \sim 6 \times 10^8 \text{ A-m}^2$. The maximum M value achieved during the campaign was $9 \times 10^8 \text{ A-m}^2$. Results related to conversion efficiency scaling with HF polarization, low duty and painting operation, ELF frequency and ionospheric conditions, along with suggestions for future studies are also presented.			
14. SUBJECT TERMS ELF Generation, Ionospheric Modifications, Ionospheric Heating, Current Modulation		15. NUMBER OF PAGES 90 16. PRICE CODE	
17. SECURITY CLASSIFICATION OF REPORT Unclassified	18. SECURITY CLASSIFICATION OF THIS PAGE Unclassified	19. SECURITY CLASSIFICATION OF ABSTRACT Unclassified	20. LIMITATION OF ABSTRACT SAR

TABLE OF CONTENTS

1.0 Physics Issues on ELF/VLF Generation.....	1
1.1 Overview.....	1
1.2 Ideal Efficiency Limits - Scalings.....	2
1.3 Critical Physics Issues Related to Practical ELF Implementation.....	5
2.0 Experimental Campaigns.....	8
2.1 Goals and Limitations.....	8
2.2 Data Sets.....	9
3.0 Analysis of the Results - Issues - Uncertainties-Conclusions.....	11
3.1 Verification of Ionospheric ELF Source.....	11
3.2 Dominant Moment.....	11
3.3 Correlation Between Far and Near Site Measurements.....	14
3.4 Scaling of X vs O Polarization.....	14
3.5 Low Duty Operation Scaling.....	15
3.6 Pointing Operation.....	16
3.7 Effect of Ambient Conditions.....	16
3.8 Scaling with ELF Frequency.....	16
Acknowledgements	
References.....	18
Figures.....	20

DTIC QUALITY INSPECTED 2

Accession For	
NTIS GRAB	<input checked="" type="checkbox"/>
DTIC TAB	<input type="checkbox"/>
Unannounced	<input type="checkbox"/>
Justification	
By _____	
Distribution/	
Availability Codes	
Dist	Avail and/or Special
A-1	

1.0 Physics Issues on ELF/VLF Generation

1.1 Overview

Generation of ELF/VLF waves by utilizing the properties of the ionosphere as an active medium has been extensively studied theoretically and experimentally during the last decade (Stubbe et al 1982; Barr and Stubbe 1984 a,b; Ferraro et al 1982; Belyaev et al 1987; Chang et al 1982; Tripathi et al 1982; Papadopoulos et al 1983; Papadopoulos and Chang 1985; Papadopoulos et al 1990). Among the various techniques proposed for converting RF to low frequency power the most successful to-day has been the modulation of quasi-stationary ionospheric currents flowing in the lower ionosphere ($h=65-100$ km). These currents are driven by winds in the middle and lower latitude ionosphere (often called S_q - currents), and by the field aligned mapping of magnetospheric electric fields in the high latitude ionosphere. Figure 1 shows the experimental set up for typical ionospheric ELF/VLF generation by current modulation.

The practicality for utilization of the concept as a communication technique depends critically on the efficiency with which ground RF power can be converted to ELF/VLF power in the ionosphere, and subsequently coupled and propagated in the wave-guide formed by the conducting earth and the ionosphere. Current experimental evidence from the Tromso RF heater operated by the Max Planck Institute (Barr and Stubbe 1991) and from the recent experimental campaigns using HIPAS (Bannister 1990, Papadopoulos 1990, McCarrick et al 1990) indicates that the observed ELF radiation fields are consistent with an equivalent horizontal magnetic dipole (HMD) situated at an altitude of 75 km and having a magnetic moment $M = 2-4 \times 10^8$ A-m². The polarization of the observed radiation is interpreted as produced by a modulated Hall current. Since the value of M quoted above was achieved at the expense of 1 MW RF power on the ground, the resultant conversion efficiency is of the order of

$$\eta = 5 \times 10^2 \text{ A-m}^2/\text{W} \quad (1)$$

To place this into prospective we note that the current ground based Navy "ELF" facility in Michigan has a value of $M = 2 \times 10^{10}$ A-m². As a result, unless the conversion efficiency can be substantially improved, ground RF power in excess of 50 MW will be required in

order to achieve ELF radiation power comparable to the ground based "ELF". The practicality of the ionospheric source for ELF communications depends critically on improving dramatically the currently achieved conversion efficiency.

1.2 Ideal Efficiency Limits - Scalings

A measure of the potential efficiency improvement and the parameters on which it depends can be found by comparing the value of the efficiency given by Equation 1 to the one expected under the following conditions:

1. The electron energy content Q at the end of the RF pulse, which is taken as half the period τ of the ELF wave, is equal to

$$Q = \frac{\alpha P \tau}{2} \quad (2)$$

where α is the efficiency with which energy is transferred from the RF to the electron gas on a time $\tau/2$ and P is the ground RF power.

2. The electron gas cools on a time scale comparable to $\tau/2$ following the termination of the RF pulse.

3. The energy is absorbed at altitudes where the electrons were and remained magnetized during the pulse (magnetized in the sense that the electron neutral collision frequency remains smaller than the cyclotron frequency).

4. The ionospheric ELF source can be represented as an horizontal magnetic dipole M , given by

$$M = E \sum_p S \Delta z \quad (3)$$

where E is the value of the ambient ionospheric electric field, S is the modified area, Σ_p is the modified height integrated Pedersen conductivity, and Δz the width in altitude of the energy deposition rate.

The height integrated Pedersen conductivity is given by

$$\Sigma_p = \frac{e^2}{m} \int dz \int d\varepsilon \frac{\nu(\varepsilon)}{\Omega^2 + \nu^2(\varepsilon)} f(\varepsilon) \quad (4)$$

where $\nu(\varepsilon)$ is the electron neutral collision frequency as a function of the energy ε , Ω the electron cyclotron frequency and the electron distribution function $f(\varepsilon, z)$ is normalized to the local electron density $n(z)$ as

$$n(z) = \int d\varepsilon f(\varepsilon, z) \quad (5)$$

We assume next that $\Omega \gg \nu$, and that, for the relevant energy range, ν is proportional to energy so that

$$\nu(\varepsilon) = \nu_0 (\varepsilon / T_0) \quad (6)$$

where ν_0 and T_0 are the ambient values of the electron collision frequency and temperature in the modified region. From Equations (4-6) we find that

$$S \Sigma_p = \frac{\nu_0}{\Omega} \frac{e^2}{m\Omega} \frac{1}{T_0} \left(S \int dz \int d\varepsilon \varepsilon f(\varepsilon) \right) \quad (7)$$

Notice that

$$Q = S \int dz \int d\epsilon \text{eff}(\epsilon) \quad (8)$$

The value of the magnetic moment M in units of $\text{A}\cdot\text{m}^2$ can thus be written by using Equations (2, 3, 7, 8) as

$$M = \frac{1}{2} \Delta z \left(\frac{E}{B} \right) \left(\frac{v_0}{\Omega} \right) \frac{\alpha P \tau}{T_0} \quad (9)$$

In Equation (9) T_0 is expressed in units of eV, while the rest of the quantities are in MKS units. Using $T_0 = .02$ eV and $B = 3 \times 10^{-5}$ Tesla, Equation (9) gives the following expression for the conversion efficiency

$$\eta = 4 \times 10^5 \times \left(\frac{v_0}{\Omega} \right) \left(\frac{\Delta z}{10 \text{ mV}} \right) \left(\frac{\tau}{3 \text{ msec}} \right) \frac{\text{A}\cdot\text{m}^2}{\text{W}} \quad (10)$$

Taking the value of v_0 / Ω as $1/4$, we find that, for typical values of the electric field, the ideal efficiency is by more than 200 times larger than the observed one, which corresponds to larger ELF power by a factor of 4×10^4 .

The above simple analysis highlights the overall energetics of the conversion, as well as its scaling with ambient parameters, and identifies the critical research issues that will lead to improved efficiency. It is clear current facilities achieve values of α of 5×10^{-3} . This is approximately the ratio of the time required to heat their electrons to their saturated value (50 μsec) to the ELF period. A research priority is thus, the development of techniques that improve the value of α . Studies using the limited capabilities of HIPAS should attempt to explore control of the altitude of the energy deposition, so that the cooling rates are close to the desired ELF frequencies, and procedures (e.g. fast transmitter sweeping) that maximize the energy deposition of the RF into the electron gas.

1.3 Critical Physics Issues Related to Practical ELF Implementation

In order to optimize the conversion efficiency and assess the availability of the ionospheric ELF channel, several experimental and theoretical studies related to the physics of the RF to ELF conversion and to the coupling and propagation in the earth-ionosphere wave-guide are required. It is expected that the planned HAARP facility will allow for a comprehensive study of these issues. It is, however, possible, in the interim, to address some of the issues using existing RF heaters, such as HIPAS or the HEATER facility in Tromso. Both facilities have limited maximum ERP and frequency range, so that extreme care is required in the planning as well as the interpretation of the experiments. We list below some important physics issues that can be addressed, at least to some extent, with the current facilities.

1. What is the dominant equivalent ELF radiating moment in the ionosphere and how does it depend on ambient conditions, modification height, RF mode polarization, frequency, ERP and gain?

The initial thinking was that the ionospheric ELF source could be modeled as an equivalent horizontal electric dipole (HED) (Barr and Stubbe 1984b; Papadopoulos et al 1990). This, however, led to inconsistencies between ground observations and simultaneous observations from satellites (James 1985), which can be reconciled if the radiating source is an HMD rather than an HED (Papadopoulos et al 1990). The measurements from the latest series of HIPAS experiments appear to be consistent with a radiating HMD (Bannister 1990, Papadopoulos 1990). Further confirmation of the nature of the source is required as well as its resolution into VED, HED and HMD components. An important issue concerns the controllability of the source components.

2. What is the polarization of the low frequency horizontal magnetic fields on the ground and how does it vary with the modification altitude?

The ionospheric ELF source is located in a strongly anisotropic medium. This anisotropy is reflected in the structure of the ambient ionospheric currents shown schematically in Figure 2. There is a critical altitude z_0 , typically between 70-75 km, at which $v_0 = \Omega$. At this altitude the ambient current flows at a 45° angle relative to the ambient electric field (ie

the Hall and Pedersen currents are equal). For altitudes much below the critical altitude the current flows along the direction of the ambient electric field (Pedersen current), while at altitudes much higher than z_0 , the current flows perpendicular to both the electric and magnetic field (Hall current). Thus, the anisotropy of the medium creates a rotation of the ambient current by a 90° angle. The modification affects predominantly the weaker current (Papadopoulos et al 1990), so that at low altitudes the perturbed current is the Hall current, while at high altitudes it is the Pedersen current. One can define a new critical altitude z_1 , where the value of Ω equals the modified value of ν . If the dominant energy deposition is in the vicinity of z_1 the observed polarization will be close to circular, while it will be elliptical otherwise. The polarization axis of the ellipse will rotate counterclockwise with source altitude. The detailed polarization structure will, of course, depend on the ELF frequency, whether the measurements were in the near or far zone, phase lags due to propagation, reflection etc. We, however, believe that in conjunction with propagation and other theoretical studies polarization measurements can provide a unique way to characterize the source and its properties using HIPAS or Tromso. Such studies could, furthermore, lead to important novel ionospheric diagnostic techniques.

3. What is the scaling of the ELF signal with the incident RF power density, RF frequency, and ELF frequency?

This is, perhaps the most important issue in terms of practical ELF implementation. Papadopoulos et al (1989, 1990) introduced an index n that connects the ELF strength to the incident power density S and modified area A as

$$\text{ELF signal strength} \sim A \times S^n \quad (11)$$

This is related to the total HF power P as

$$\text{ELF signal strength} \sim A \times (P/A)^n \sim A^{1-n} \times P^n \quad (12)$$

Notice that for constant P and for values of n approaching or larger than one the conversion efficiency increases by increasing the power density. For values of n smaller than .5 the

opposite is true. A theoretical analysis of this scaling can be found in Papadopoulos et al (1989,1990), while some recent experimental results in Barr and Stubbe (1991).

4. What is the coupling efficiency of the ionospheric source to the earth-ionosphere wave-guide as a function of the source altitude, frequency and polarization? Are there any techniques to improve it?

For an ionospheric source located on the bottom part of the ionosphere, most of the energy enters the wave-guide. For a higher altitude source the fraction of the energy that enters the wave-guide depends on whether the ionospheric source generates a propagating or evanescent mode, the form and scale of the gradient of the local refractive index, and the frequency and polarization of the low frequency waves. It has, furthermore, been suggested (Gurevich et al 1991) that by sweeping the ionospheric source at a speed that matches the phase velocity of the excited wave dramatic directional increases in the coupling efficiency can be achieved. These issues require proper experimental investigation.

5. What is the extent of availability of a useful ELF signal and how can we reduce its dependence on the ambient ionospheric conditions?

In addition to these issues, investigations should be conducted to determine:

i. The absolute phase of the ELF signals with respect to the HF modulation as a function of the frequency, polarization, distance etc.

ii. The variation of of the major axis of the ELF polarization as a function of the ionospheric conditions and ELF parameters.

iii. The phase stability of the signal at various frequencies and modulation modes, etc.

A comprehensive plan on performing these investigations as well as identifying the required diagnostics is a major goal of APTT's research plan for the current year.

2.0 Experimental Campaigns

2.1 Goals and Limitations

Two experimental campaigns were conducted during the May-September 1990 time frame using the HIPAS facility in conjunction with diagnostic ELF receivers provided by NUSC. Each campaign covered 12 days with approximately six hours of operation daily. The two campaigns can be characterized as preliminary to a more comprehensive plan for continuous operation using permanent ELF/VLF receivers.

The first campaign conducted in May 1990 had as goals the unambiguous confirmation that the signals received were real ELF signals rather than spurious modulated HF reflections, the characterization of the ELF equivalent moment and radiation pattern for frequencies in the range of 40-200 Hz, and the absolute calibration of the UCLA ELF receiver. This range was not available to the Tromso facility. Measurements were performed using the UCLA ELF receiver located at the NOAA tracking station in Gilmore Creek. This site is 35 km northwest of the HIPAS heater. During the May campaign, the NUSC receiver was positioned at a variety of distances between 20 and 200 km (Figure 3 from Bannister 1990).

The second campaign conducted in September 1990 (Sept. 15-26) had as goals continuous monitoring of the signal from two sites, one located in the near and the other in the far field, with calibrated receivers, a test of the improvements of the HIPAS transmitter, identification of the polarization, examination of phase stability and a preliminary study of the scaling of the magnetic moment with frequency and mode of operation (eg sweeping operation). The near site was the NOAA site, while the far site using the NUSC receiver, was located in Talkeetna, 300 km south of HIPAS (Figure 3).

The HIPAS heater was used in both campaigns. During the second campaign a new ground screen was installed under two of the eight antennas of the transmitting HIPAS array. As a result the total ERP might have increased by 20%. Furthermore, the limit on beam scanning time, controlled now by the bandwidth of the final amplifiers, was reduced to about 5 μ secs. In terms of studying the conversion efficiency scaling, the HIPAS facility was limited by ERP, and frequency range. In terms of interpreting the experimental results an important limitation of HIPAS is that the power distribution in the far zone has not yet been measured.

A description of the UCLA and NUSC ELF sensors utilized in the campaigns can be found in McCarrick et al (1990). We simply note here, that the UCLA receiver was simultaneously measuring the north-south and east-west magnetic fields with calibrated coils. Maximum sensitivity was achieved for frequencies between 5-50 Hz. The vertical electric field was also measured but the sensor was not calibrated so that only relative local measurements are meaningful. The NUSC ELF receiver consisted of a single air-core loop and had maximum sensitivity in the range of 70-200 Hz.

Measurements and various preliminary conclusions of the campaigns have been discussed in Bannister (1990), McCarrick et al (1990), and Papadopoulos (1990). For completeness we present below the data set of measurements for both receivers as presented in McCarrick et al (1990). As will be discussed later the variability of the ionospheric conditions makes the physical interpretation of the results and the resultant scaling rather difficult. This was in particular true during the second campaign due to lack of communications between the far site and HIPAS. As a result only prearranged operational modes were used and no adjustments due to variation in the ambient conditions was used.

2.2 Data Sets

A comprehensive set of data for the two campaigns was presented and partly analyzed in McCarrick et al (1990) and Bannister (1990). For completeness and archival reasons as well as consistency in our presentation and discussion we reproduce them below.

Figures 4 and 5 refer to results and analysis from the May campaign. Figure 4 shows the instantaneous ELF signal and phase measured at the NOAA site along with three axis magnetometer data from the College Alaska Geophysical Observatory (McCarrick et al 1990). The magnetic perturbations measured on the ground are resolved along the geographically north-south (positive north), east-west (positive east), and vertical (positive down) directions and are conventionally denoted by H, D, and Z, respectively. To facilitate their interpretation Figure 6 shows their latitudinal profiles for a current jet in the ionosphere (Kisabeth and Rostoker, 1971). Figure 5 shows nightly averaged measurements from the NUSC receiver as a function of the receiver location along with a comparison based on simple HMD ionospheric source as presented by Bannister (1990). The coordinate system used in the notation is shown in Figure 7.

The data from the September campaign are shown in Figures 8-10. Figure 8 shows the summary of the ELF data received at the NOAA site and at Talkeetna, with the frequency and modulation sequence shown at the top of each plot. The Talkeetna data were mostly five minute samples although some 100 sec samples were also taken. Figure 9 shows the complete set of data received at the NOAA site along with the three axis magnetometer and 30 MHz riometer data from College, Alaska. Averaged data are shown in Figure 10.

All of the above data were obtained with HIPAS operating at a frequency of 2.85 MHz and a power level of 8x100 kW with an effective radiated power (ERP) of 50 MW. In the absence of absorption this corresponds to a power density $S = .7 \text{ mW/ m}^2$ and an equivalent quiver energy of $5 \times 10^{-4} \text{ eV}$ for X-mode polarization.

3.0 Analysis of the Results - Issues - Uncertainties-Conclusions

3.1 Verification of Ionospheric ELF Source

There have been occasional doubts as to whether the origin of the received ELF signals is ionospheric or plain ionospheric demodulation of the amplitude modulated HF. As discussed by the NUSC and UCLA groups in the ONR review, laboratory tests of the ELF receiver response to HF power levels, lack of correlation between the ELF signal and the demodulated HF signal and far zone (ie New London) detection of the signals leaves no doubt as to the ionospheric origin of the source.

A particularly convincing example of the ionospheric nature of the ELF source is presented by the data shown in Figure 11 from McCarrick et al (1990). The figure shows the NS component of the ELF signal and its associated phase. It, also, shows the College station magnetometer traces and the 30 MHz riometer absorption. Of importance is the magnetometer H-trace, which shows the horizontal NS component of the magnetic field. The positive direction is defined as northward. Eastward electrojet currents cause positive deviation on the value of H, while westward produce negative bays. In Figure 11 it is clear that when the H component oscillates through zero the ELF phase oscillates between -90 and +90 degrees till it, finally, locks at +90 when the westward electrojet dominates. Similar behavior has been detected during the other runs. This reinforces previous confirmation by the USSR and Max Planck groups.

3.2 Dominant Moment

Bannister (1990) analyzed the signals received by the NUSC receiver during the two campaigns, using a simplified propagation model based on radiation due to an HMD in the ionosphere. An examination of the data shown in Figures 5 and 10 leads to the conclusion that the radiation pattern observed can be accounted by an ionospheric source located at an altitude of 75 km, in the form of an HMD making an angle of 17° north of east, with an average value of $M=1.7 \times 10^8$ A-m² for the May campaign and of 6×10^8 A-m² for the September campaign. Table 1 reproduced from Bannister's presentation shows several types of averaged values of M as well as the peak values observed during the campaign.

Table 1
September 1990 Nightly Averages

Date	35 km Hns (dBA/m)	330 km H0 (dBA/m)
9/15	-137.1(12)	-159.6(10)
9/16	-136.5(12)	-156.2 (6)
9/17	-138.3(12)	-161.6(10)
9/18	-136.1(12)	-153.9(12)
9/19	-138.1(12)	-161.2 (9)
9/20	-----	-161.6 (5)
9/21	-134.4(12)	-158.3(12)
9/22	-139.7 (8)	-160.2 (5)
9/23	-135.9 (9)	-161.0 (6)
9/24	-137.6(12)	-157.4(12)
9/25	-136.6 (6)	-163.4 (6)
September Average	-136.9	-158.6

The implications of these results to the physics issues can be seen by expressing the magnetic moments due to the Hall and Pedersen conductivity modifications as

$$M_H = E \times \delta \Sigma_H \times \Delta x A \quad (13)$$

$$M_P = E \times \delta \Sigma_P \times \Delta x A \quad (14)$$

Since the direction of the observed M is 170° the ratio

$$M_H/M_P = \delta\Sigma_H/\delta\Sigma_P = \tan 17^\circ = 3$$

but

$$\delta\Sigma_H/\delta\Sigma_P = \delta\nu/\Omega = 1/3$$

where $\delta\nu$ is the average change in the collision frequency at the modified height. These lead to the following two possible conclusions:

i. If we assume that the modification height was at 75 km where the neutral density is $\sim 6 \times 10^{14} \text{ \#/cm}^3$ the average effective temperature modification is of the order of 230 K. This temperature is by a factor of three lower than predicted by the one dimensional heating model.

ii. The alternative is to accept the modified temperature of approximately 800 K and accept that the neutral density in the modified region is $2 \times 10^{14} \text{ \#/cm}^3$, which will either place the modified region at 80 km or revise the neutral density profile.

We utilized APTI's one dimensional code to simulate the modifications resulting with the HIPAS parameters used in the experiment. Since the density profile of the D region was not known we used profiles 3 and 5 from Barr and Stubbe (1984) which correspond to nighttime with 1.8 dB absorption and to daytime with .8 dB absorption. These allow us to bracket the changing ionospheric profile. Figure 12 shows the results from profile 3. Figure 12 a-c show the modified temperature, and Hall and Pedersen conductivities as a function of altitude and time to saturation. The dominant modification is at about 72 km altitude. The ratio of Hall to Pedersen conductivity is close to 2 corresponding to about 26° direction of M. The extent of the modification gives a value of M of about $6 \times 10^8 \text{ A-m}^2$ if we assume that the ionospheric electric field was 10 mV/m. Figure 13 shows the same quantities as Figure 12 but for profile 5. Note that the maximum modification occurs now near 66 km. The ratio of Hall to Pedersen conductivity is approximately 12 giving an angle of about 50° , while for an assumed electric field of 10 mV/m the value of M is approximately $2 \times 10^8 \text{ A-m}^2$. More detailed comparison of the experimental and theoretical results is ongoing.

3.3 Correlation Between Far and Near Site Measurements

Figures 14 a-d show a comparison of the signals received in the NOAA site and the far site at Talkeetna during the September campaign for selected intervals all with vertical operation of the heater. The intervals have been selected to highlight variations in the relative strength of the received signals. Figure 14a was taken for 154 Hz modulation with the transmitter operation alternating every 1/2 hour between normal and 30% duty cycle (54 μ s on and 168 μ sec off). Notice that over the entire period of 6 hours the ratio of the two signals was essentially constant at about 15 dB. This is consistent with the loss expected at the far site. Figures 14b-d were taken for 154 Hz modulation and normal operation. Notice that the signal ratios had extremely large variations during the 18 hours of data shown. The variation was at times larger than 40 dB. It is very difficult to draw reliable conclusions from these data. From basic physics considerations we expect that the variation is predominantly related to changes in the heating altitude due to modifications of the ambient electron density profile. This changes the ratio of the Hall to Pedersen conductivity and the direction of the equivalent HMD. It could also affect the near site measurement due to finite effective antenna effects, although we do not expect major variations for normal vertical incidence operation. For example in Figure 14d we note that following 10.30 pm while the field intensity is increasing in the near zone it is reduced by almost 10 dB in the far zone. Since the near field is measured by cross dipoles we can attribute the difference to rotation of the HMD due to variation of the heating altitude. The September data guide us towards exploring the properties and scaling of the ionospheric source by simultaneous measurements at more than two sites with crossed dipoles of the relative ratios of the NS and EW field components. Vertical electric field measurements would also aid in diagnostics. We are currently exploring the far to near site ratios using a 1D code to determine the causes of the variability.

3.4 Scaling of X vs O Polarization

The physical basis of the differences between modulation with X vs O mode polarization lies in the fact that the quiver energy, which determines the interaction strength, is weaker for the O-mode than the X-mode by a factor β^2 given approximately by

$$\beta = (1 - \Omega/\omega)/(1 + \Omega/\omega) \quad (15)$$

where Ω, ω are the electron cyclotron and HF frequency. For the 2.8 MHz case the O-mode quiver energy is reduced by a factor of 1/9. As a result, one expects lower values of the peak temperatures. On the other hand the O-mode is equivalent to a higher frequency, resulting in a larger value of Δ . The scaling and direction of M with respect to O and X mode polarization is an important issue. As noted in Papadopoulos et al (1990), we expect X-mode to produce larger values of M and large NS signals for low frequencies and low ERP's, when the modified Hall conductivity dominates. The opposite is true for the high frequency high ERP case.

During the September campaign only one night was devoted to this experiment. The results are shown in Figure 15. Although it appears that the X-mode signals are higher it is difficult to derive any serious conclusions. It would be of interest to examine the variation in the ratio of the NS to EW signal with polarization. We do not, currently, have these data.

As a benchmark we present in Figure 16 the results of the one dimensional code using the ionospheric model #3 and O-mode polarization for HIPAS parameters similar to the ones shown in Figure 14. The modeling shows the expected lower temperatures and broader absorption layer. However, for the model #3 electron density profile, shows that the Pedersen conductivity is by a factor of 4 larger than the Hall, corresponding to a direction of M of 75° , while the magnetic moment is three times larger than the X-mode.

It is clear that systematic investigations related to the ELF polarization and signal strength as a function of the RF polarization are very important and should be pursued in the future.

3.5 Low Duty Operation Scaling

One operating session was devoted to low duty cycle operation. The results for the only case tested are shown in Figure 17 along with type of pulsed sequence used. As discussed previously, this was the best case for consistent tracking of the far and near field results, as well as one the most stable electrojets. Contrary to previous experiments there was no evidence for increased conversion efficiency with the low duty cycle operation.

3.6 Painting Operation

Preliminary painting experiments with three spots are shown in Figure 18. The perturbed region was located overhead, 10 degrees north, and 10 degrees south. The dwell time was 54 μ sec per spot. It is rather difficult to interpret the results. They show clear differences between the near and far site. The far site shows a systematic, marginal, gain with painting, while the near site a loss. It is unclear whether these can be attributed to finite source size effects in the near zone, or directional gains in the far zone. The situation is clearer for the second day of painting runs shown in Figure 19 which, unfortunately, were performed under rather weak ionospheric electric field conditions. In this case the relative efficiency of 3 and 12 spot painting for long and short dwell times was tested. Sequences with 12 spots and long dwell time seemed to give strong signals in the far site while the 12 spot painting produced substantially better efficiency than the other operating modes at both sites. For the data of Figure 18 there was a 3 dB improvement on the average signal with 3 spots for the Talkeetna site. For the data of Figure 19 the 12 spot average signal at the far site was 12 dB higher than the normal operation and 7dB higher than the 3 spots. However, the data base is too small to draw any serious conclusions.

3.7 Effect of Ambient Conditions

McCarrick et al produced data correlating the ELF signals to riometer absorption, photometric, and magnetometer data for few cases. There were no significant systematic trends in the data. There is, however, one exception. A systematic reduction of the signals appeared when a strong aurora was overhead of HIPAS. This confirms theoretical predictions (Papadopoulos et al 1990) that electron profiles containing significant electron densities at low altitude (ie 60-70 km) result in low conversion efficiency.

3.8 Scaling with ELF Frequency

A very limited set of runs were performed with varying the ELF frequency. The three frequencies tested were 78, 154, and 198 Hz. Figure 20 shows the results. Fitting the values of 78 Hz and 154 Hz to a simple propagation model (Figure 21), Bannister concludes that the value of M at 78 Hz is by 3 dB larger than the one at 154 Hz. However, the limited data base does not allow for a definite conclusion. On a theoretical level scaling

with frequency can arise due to propagation effects or due to different heating and cooling to ELF time ratios. These phenomena need to be investigated in future campaigns.

Acknowledgements

We would like to thank Drs. P. Bannister, M. McCarrick, A. Wong and R. Wuerker for the conduct of the campaign, sharing of data and for many scientific discussions.

References

1. Bannister, P. ONR Review of HIPAS Research on ELF Generation, December, 1990. [Copy available from P. Bannister, Naval Underwater Sound Laboratory, Fort Trumbull, New London, Conn. 06320]
2. Barr, R. and Stubbe, P. "The Polar Electrojet Antenna' as a Source of ELF Radiation in the Earth-Ionosphere Waveguide," *J. Atmos. Terr. Phys.*, vol. 46, p. 315-320, 1984a.
3. Barr, R. and Stubbe, P. "ELF and VLF Radiation from the 'Polar Electrojet Antenna'," *Radio Science*, vol. 19, p. 1111-1122, 1984b.
4. Barr, R. and Stubbe, P. "ELF Radiation from the Tromso 'Superheater' Facility," *Geoph. Res. Lett* (impress), 1991.
5. Belyaev, P. P., Kotik, D. S., Mityakov, S. N., Polyakov, S. V., Rapport, V. O. and Trakhtengerts, V. Yu. "Generation of Electromagnetic Signals of Combination Frequencies in the Ionosphere," *Radio Physics*, vol. 30, p. 248, 1987.
6. Borisov, N. D., Gurevich, A. V. and Papadopoulos, K. "Generation of Radiation by Superluminal Movement of Heated Regions of the Ionosphere," Proceedings of the III URSI Symposium on Modifications of the Ionosphere by Powerful Radio Waves USSR, Academy of Science, 1991.
7. Chang, C. L., Tripathi, V., Papadopoulos K., J. Fedder, Palmadesso, P. J., and Ossakow, S. L. *Effect of the Ionosphere on Radiowave Systems*, edited by J. M. Goodman, p. 91, U.S. Government Printing Office, Washington, D.C. 1981.
8. Ferraro, A. J., Lee, H. S., Allshouse, R., Carroll, K., Tomko, A. A., Kelly, F. J. and Joiner, R. J. " VLF/ELF Radiation from the Ionosphere Dynamo Current System Modulated by Powerful HF Signals," *Atmos. Terr. Phys.*, vol. 44, p. 1113-1122, 1982.
9. James, H. G. "The ELF Spectrum of Artificially Modulated DIF Region Conductivity," *J. Atmos. Terr. Phys.*, vol. 47, p. 1129, 1985.
10. Kisbeth, J. L. and Rostoker, G. "Development of the Polar Electrojet During Polar Magnetic Substorm," *J. Geophys. Res.*, vol. 76, p. 6815, 1971.
11. McCarrick, M. J., Wong, A. Y., Wuerker, R. F. and Chouinard, B. *ONR Review of HIPAS Research on ELF Generation*, December, 1990. [Copy available from Dr. M.J. McCarrick, HIPAS Observatory Fairbanks, Alaska 99706]
12. Papadopoulos, K. and Chang, C. L. *Geophys. Res. Lett.*, vol. 12, p. 279, 1985.
13. Papadopoulos, K., Chang, C. L., Vitello, P. and Drobot, A. "On the Efficiency of Ionospheric ELF Generation," *Radio Science*, vol. 25, p. 1311, 1990a.
14. Papadopoulos, K., Ko, K., and Tripathi, V., "Efficient Parametric Decay in Dissipative Media," *Phys. Rev. Lett.*, vol 51, p. 463, 1983.

15. Papadopoulos, K. *ONR Review of HIPAS Research on ELF Generation*, December, 1990. [Copy available from Dr. K. Papadopoulos, APTI, 1250 24th Street, Washington, D.C. 20037]
16. Papadopoulos, K., Shanny, R., Susman, L., Machina, M. and Stambolis, P. "Electrojet Modulation ELF Communications," *Proceedings of AGARD EEP Symposium*, Bergen, Norway, 1990b.
17. Stubbe, P., Kopka, H., Reitveld, M.T. and Dowden, R. L. "ELF and VLF Wave Generation by Modulated Heating of the Current Lower Ionosphere," *J. Atmos. Terr. Phys.*, vol. 44, p. 1123, 1982.
18. Tripathi, V. K., Chang, C. L. and Papadopoulos, K. "Excitation of the Earth Ionosphere Waveguide by an ELF Source in the Ionosphere," *Radio Science*, vol. 17, p. 1321-1326, 1982.
19. Papadopoulos, K., Shanny, R., Susman, L. Machina, M. and Stambolis, P., "Electroject Modulation ELF Communications," in *Ionospheric Modification and its Potential to Enhance or Degrade the Performance of Military Systems, AGARD Conference Proceedings No. 485*, p. 37A, 1990. [Available from National Technical Information Service (NTIS), 5285 Port Royal Road, Springfield, VA 22161]

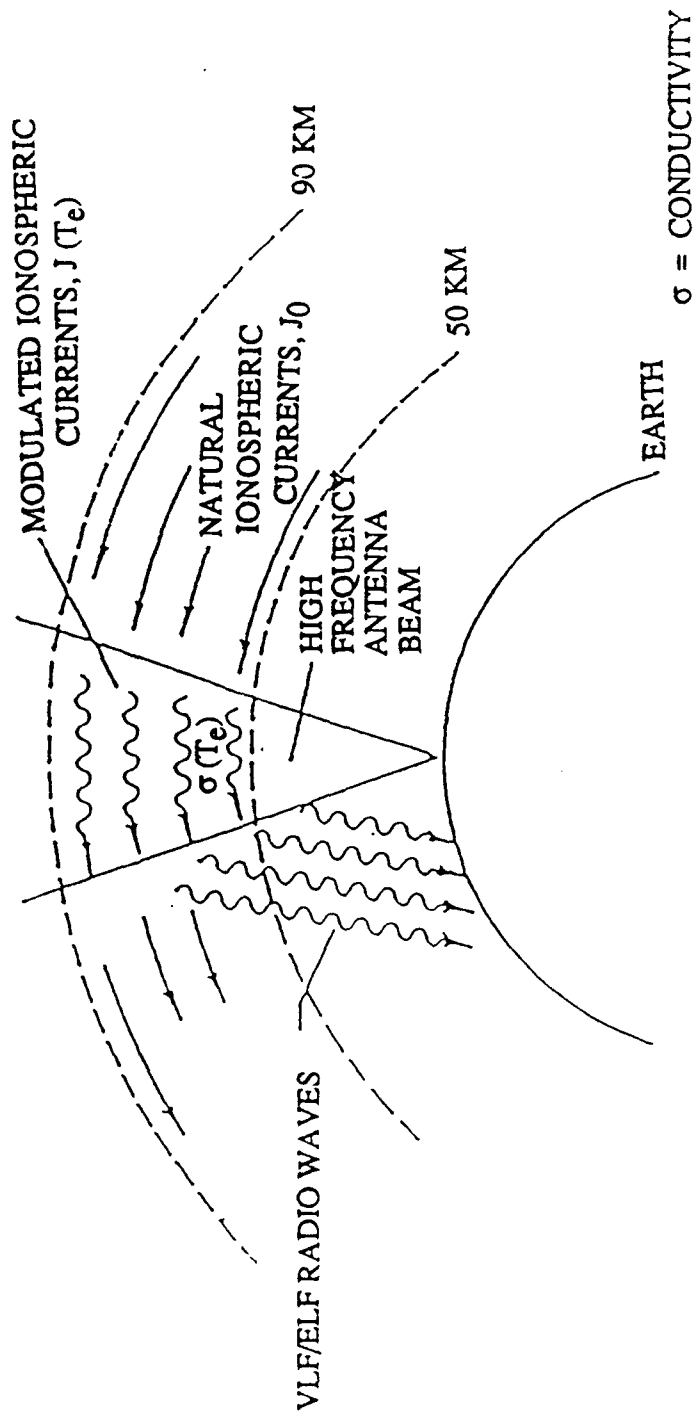


Figure 1 Set-up for Ionospheric ELF Generation

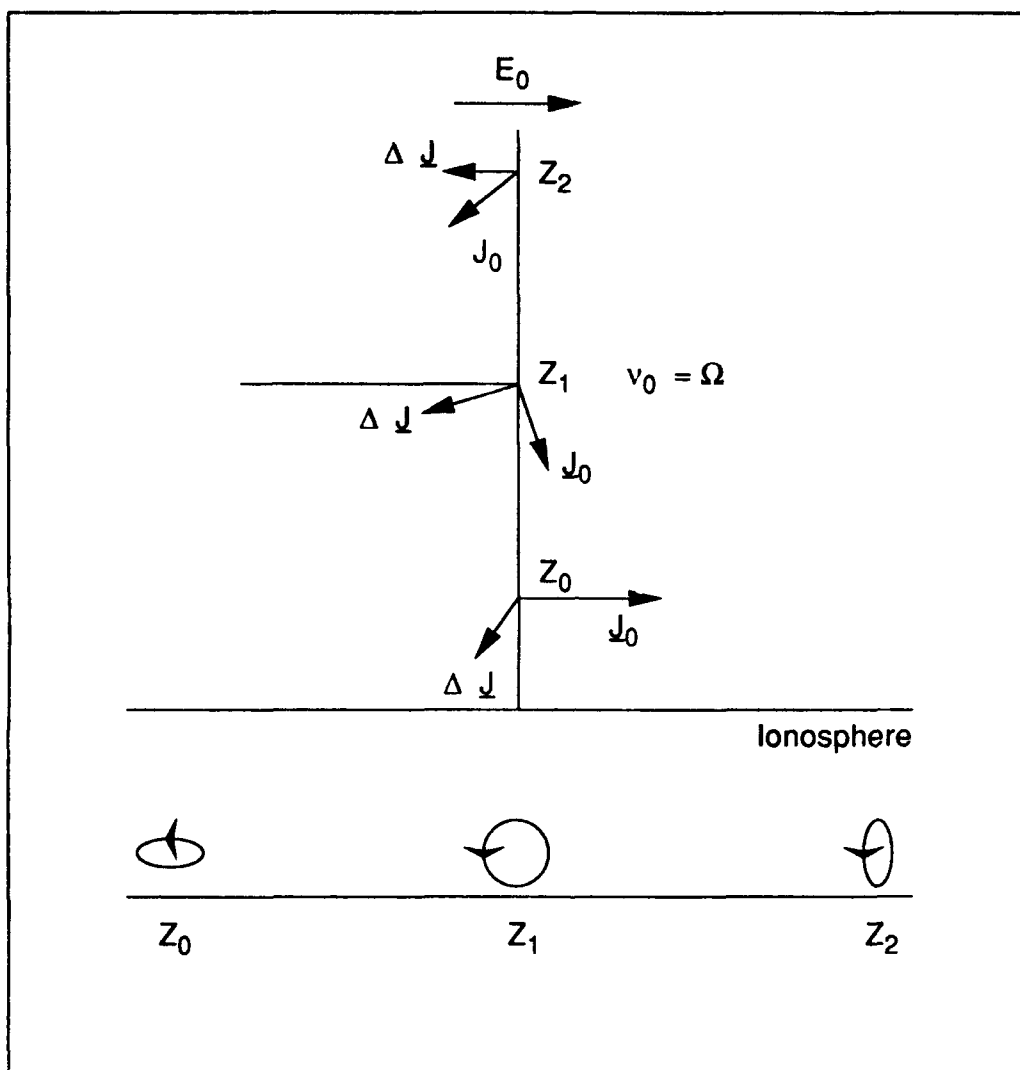


Figure 2. Schematic of Modified Ionospheric Current Polarization as a Function of the Source Altitude and of the Expected Signal Polarization on the Ground

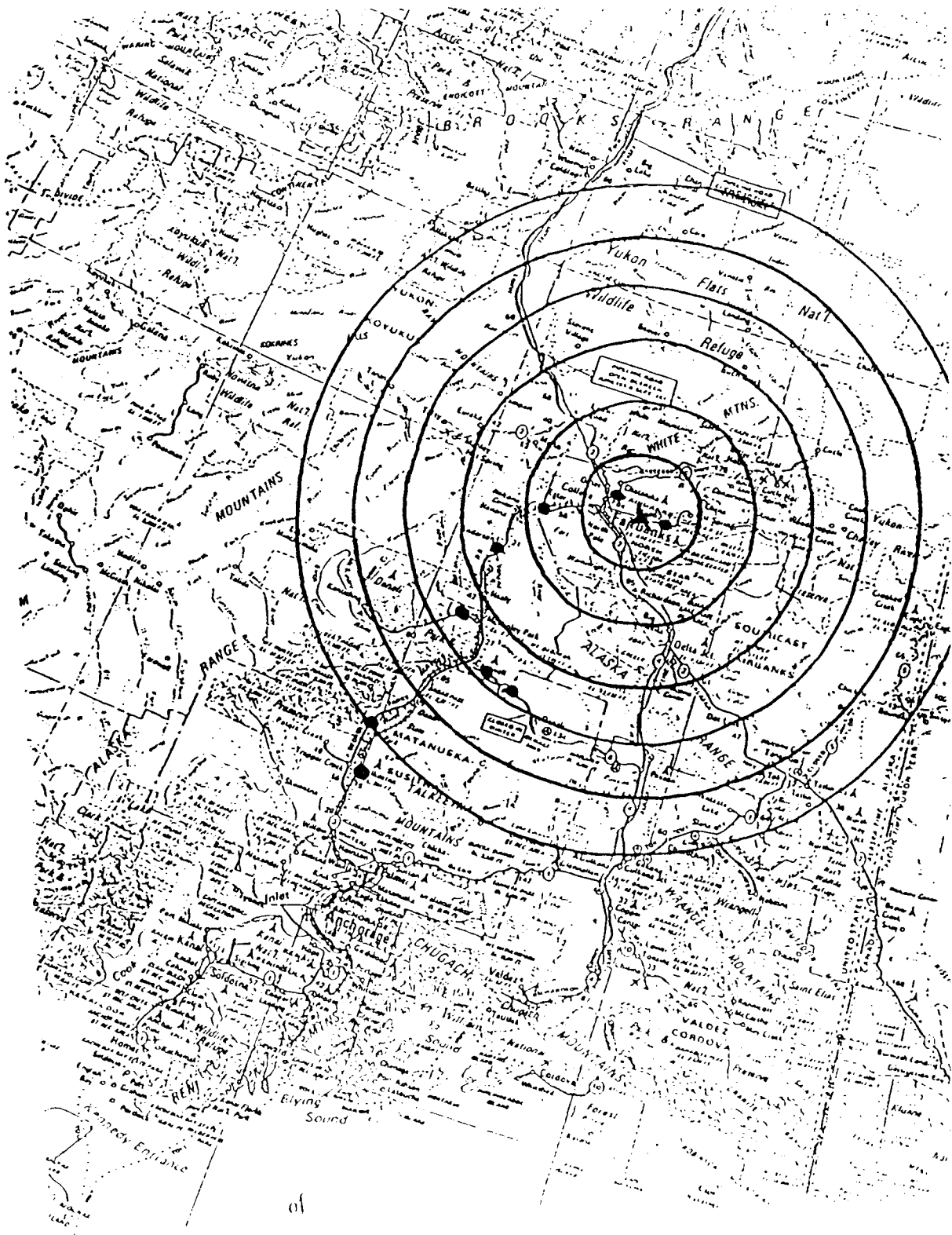
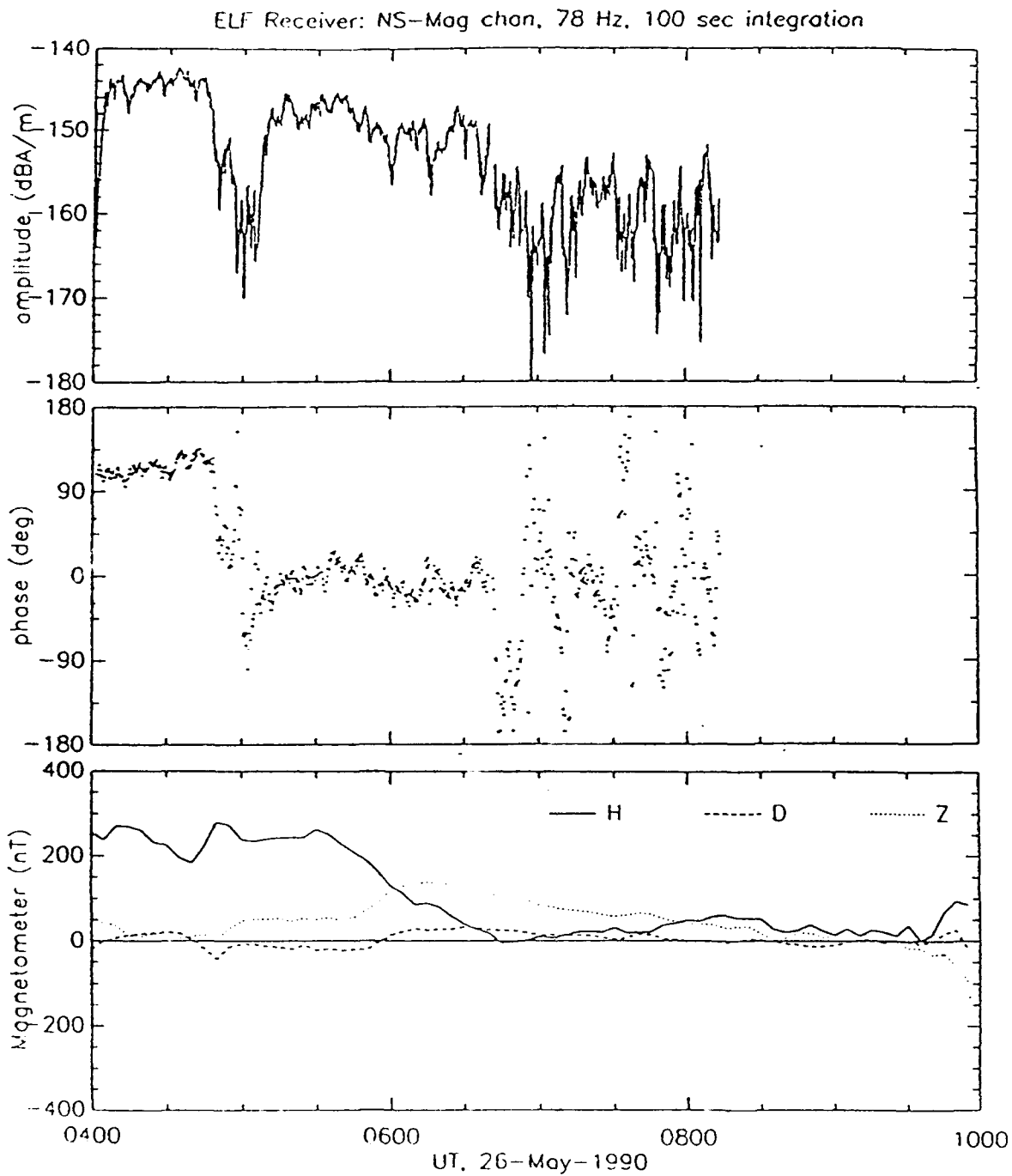


Figure 3 Locations of NUSC Receiver During the Experimental HIPAS Campaigns (from Bannister 1990)



ML900526 001

Figure 4 (a) Instantaneous ELF Signal and Phase Measurements at the NOAA Site Along with Magnetometer Data from the May 1990 Campaign (McCarrick et al 1990)

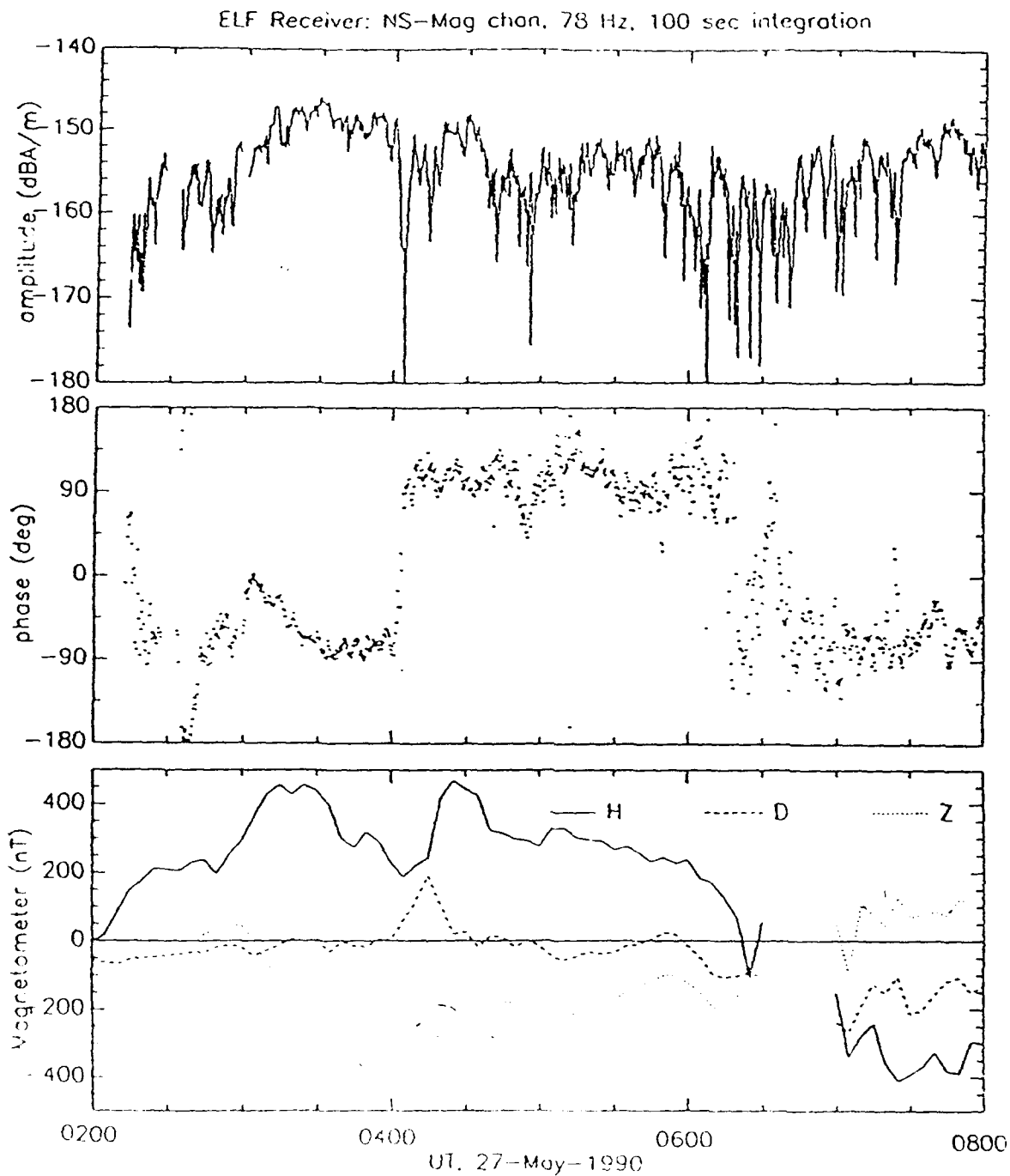
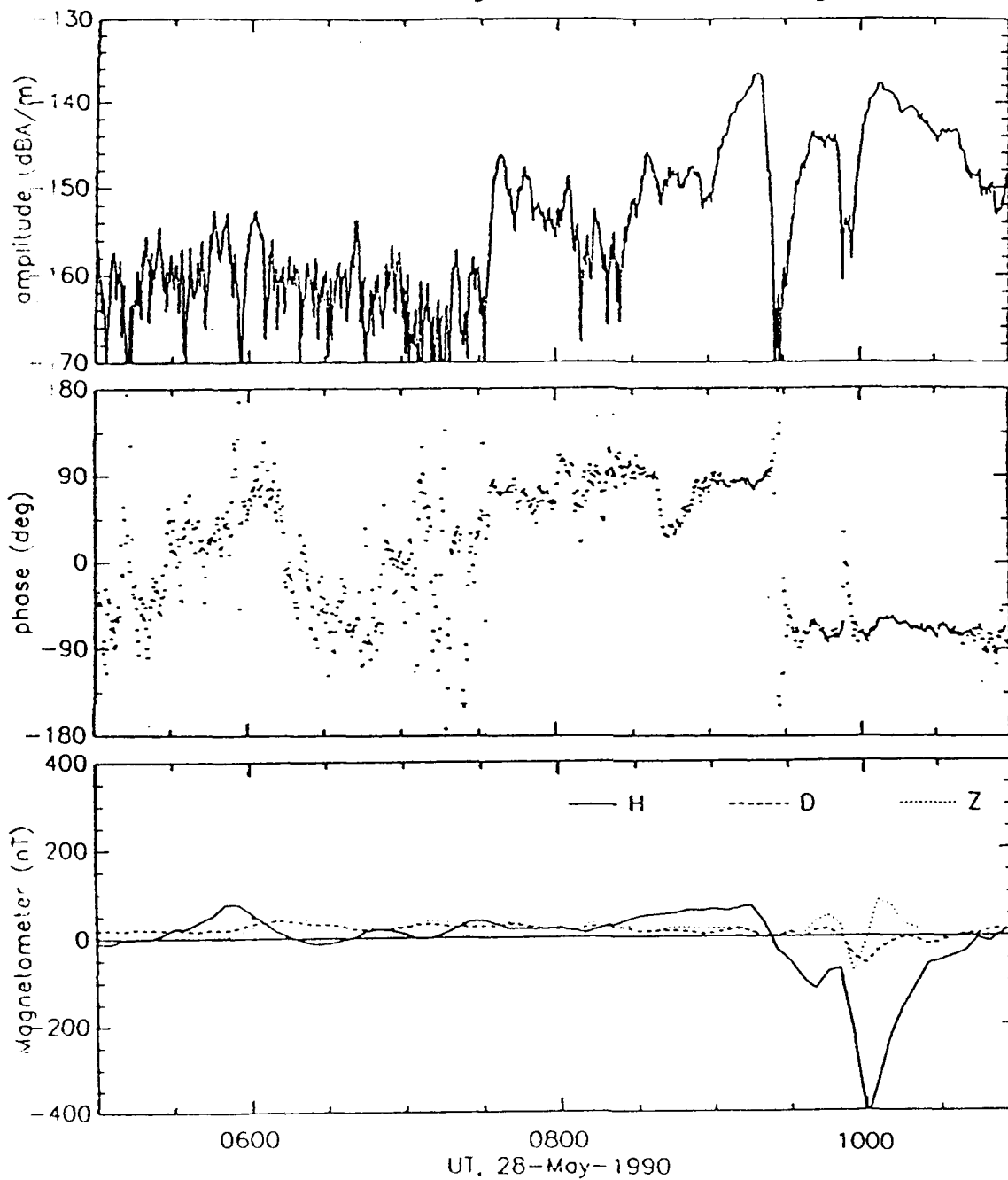


Figure 4 (b)

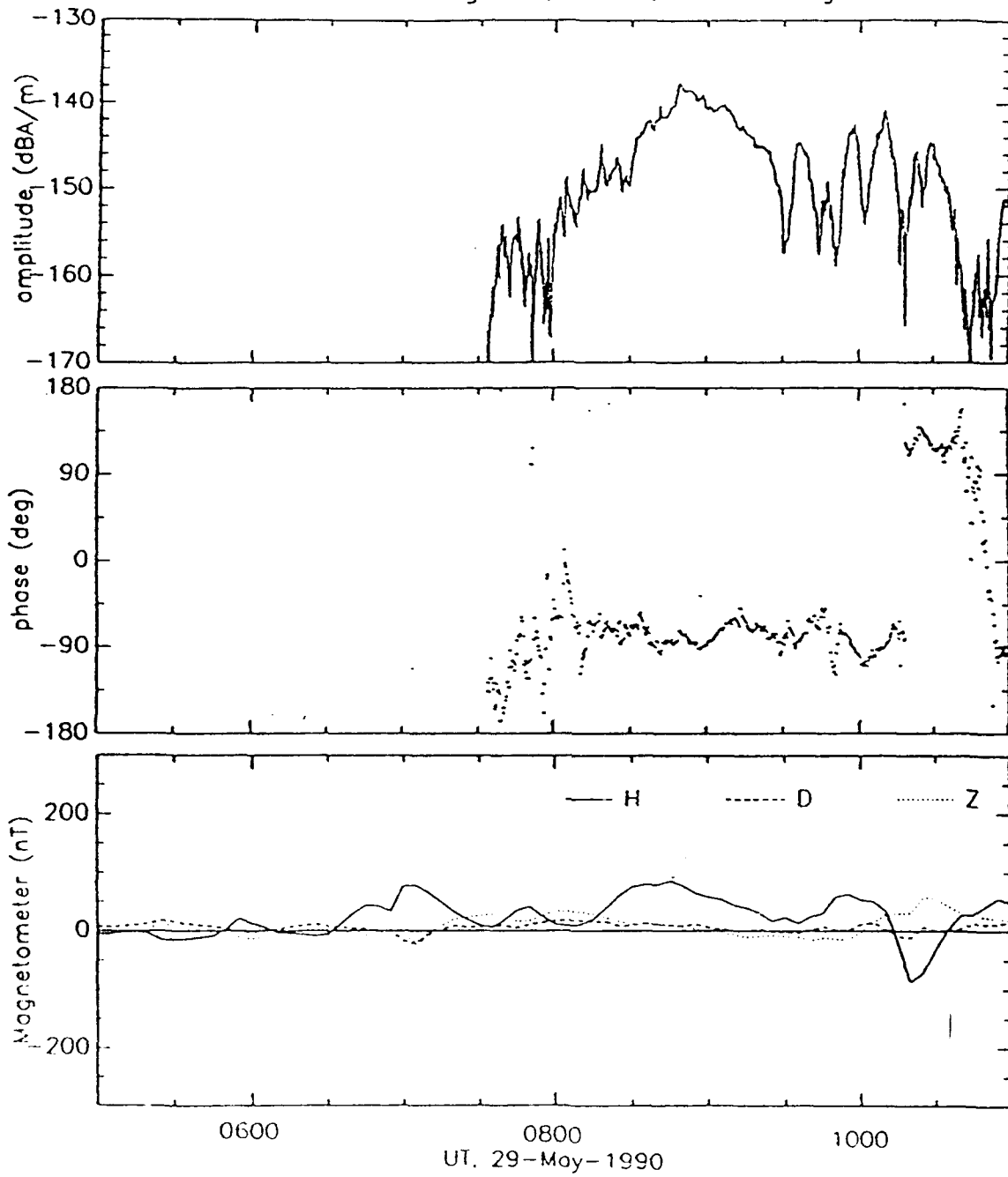
ELF Receiver: NS-Mag chan, 78 Hz, 100 sec integration



NL900528.D01

Figure 4 (c)

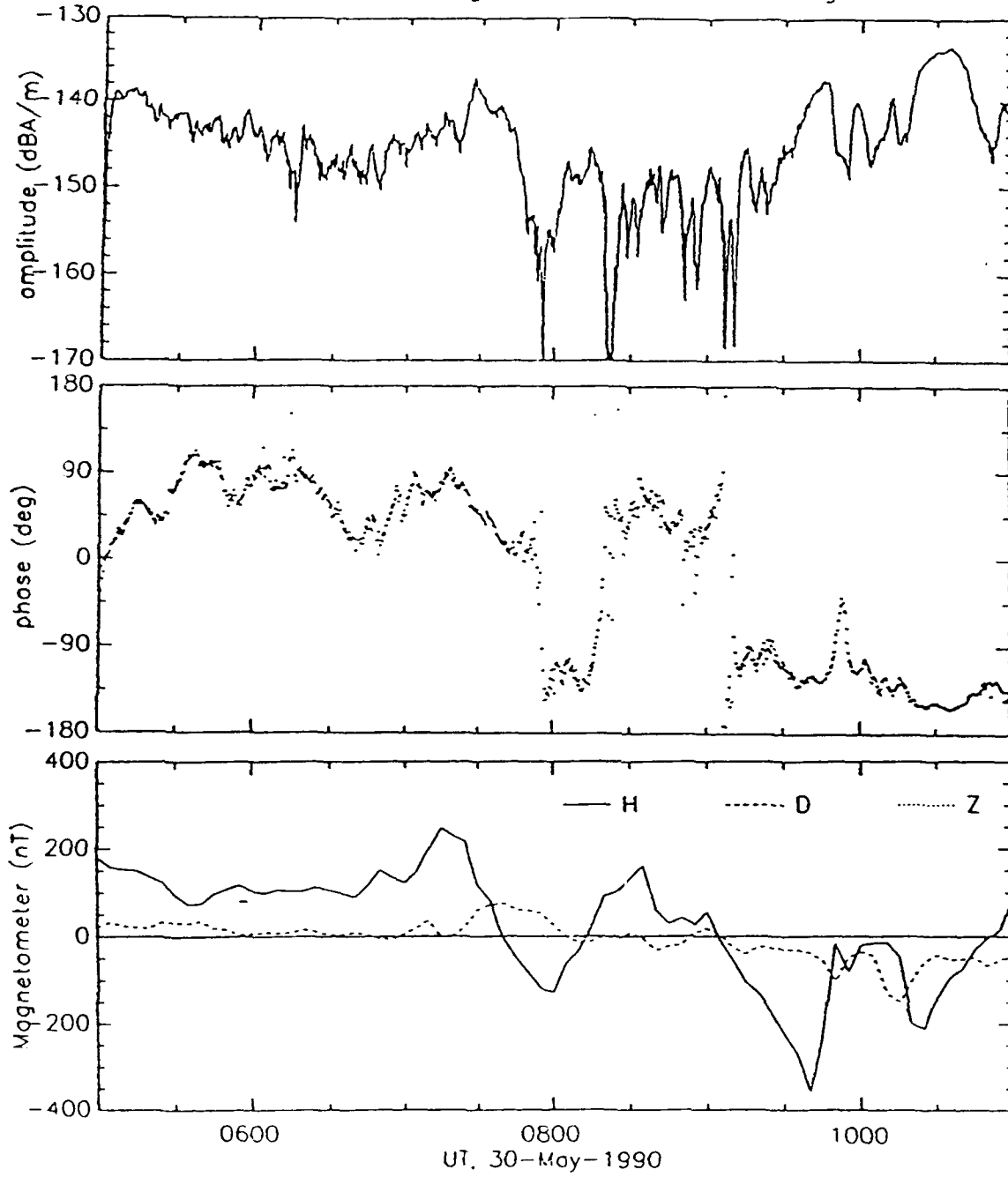
ELF Receiver: NS-Mag chan, 154 Hz, 100 sec integration



NL900529.DC1

Figure 4 (d)

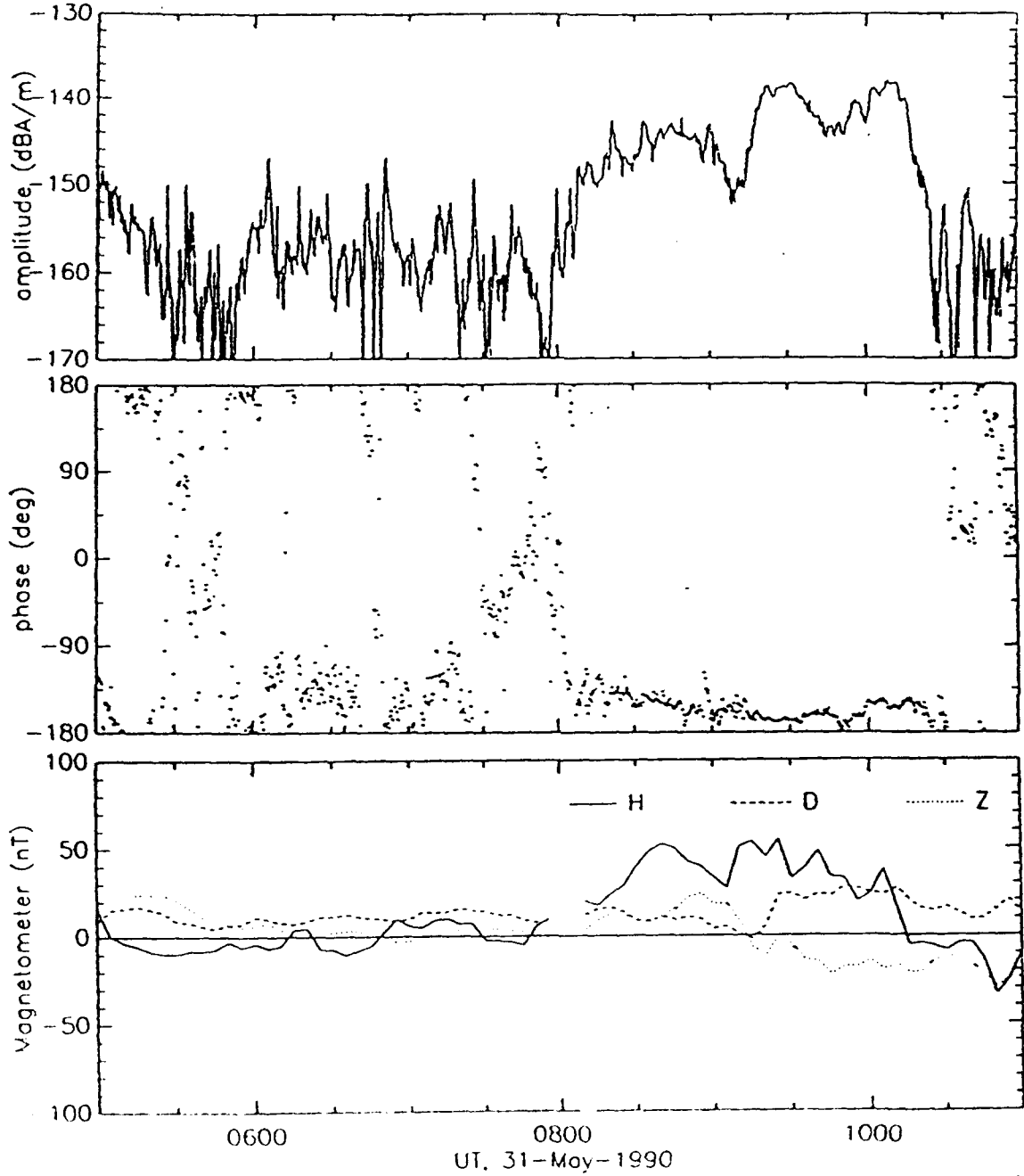
ELF Receiver: NS-Mag chan. 154 Hz, 100 sec integration



NL900530 001

Figure 4 (e)

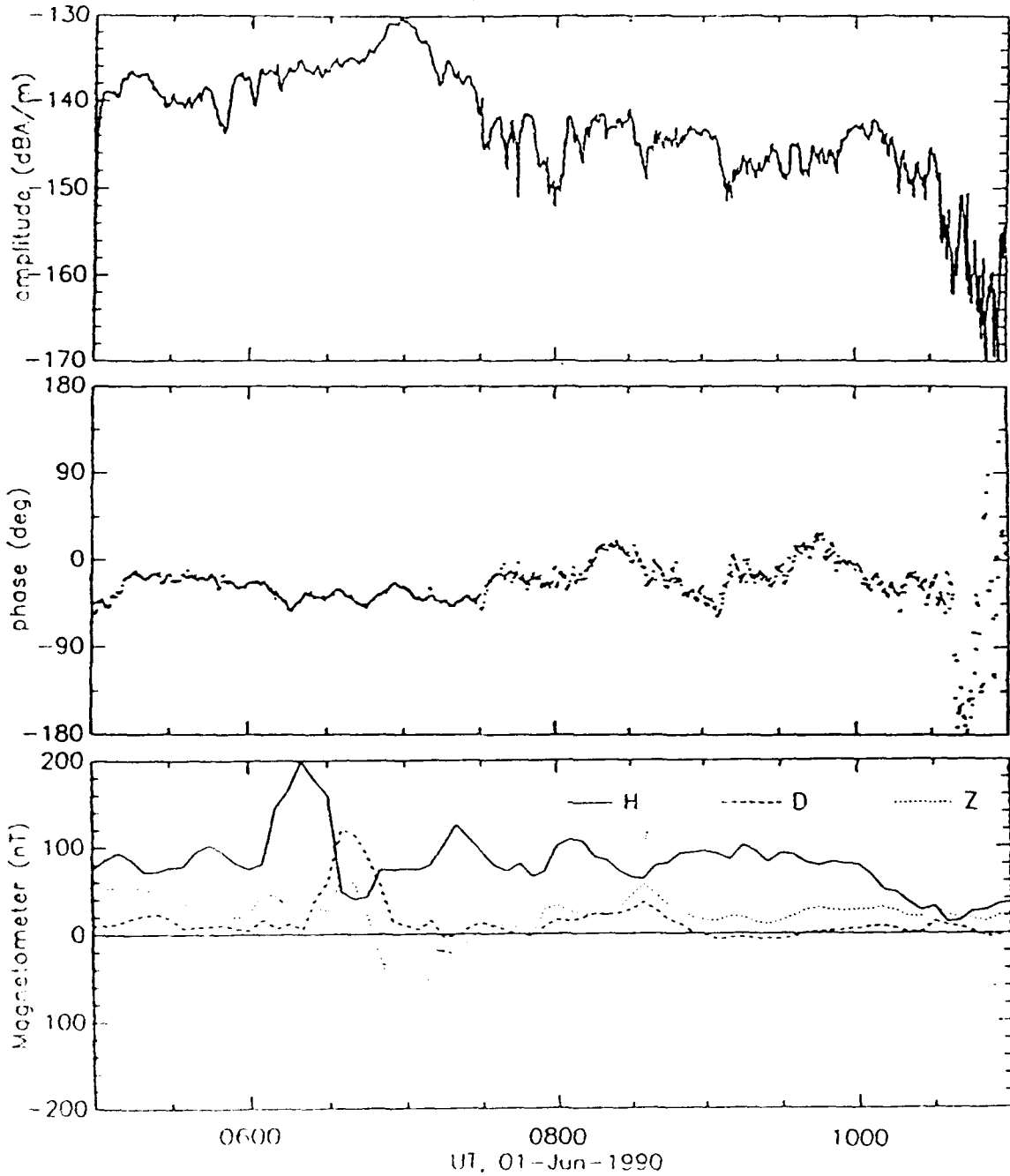
ELF Receiver: NS-Mag chan, 154 Hz, 100 sec integration



NL900531 D01

Figure 4 (f)

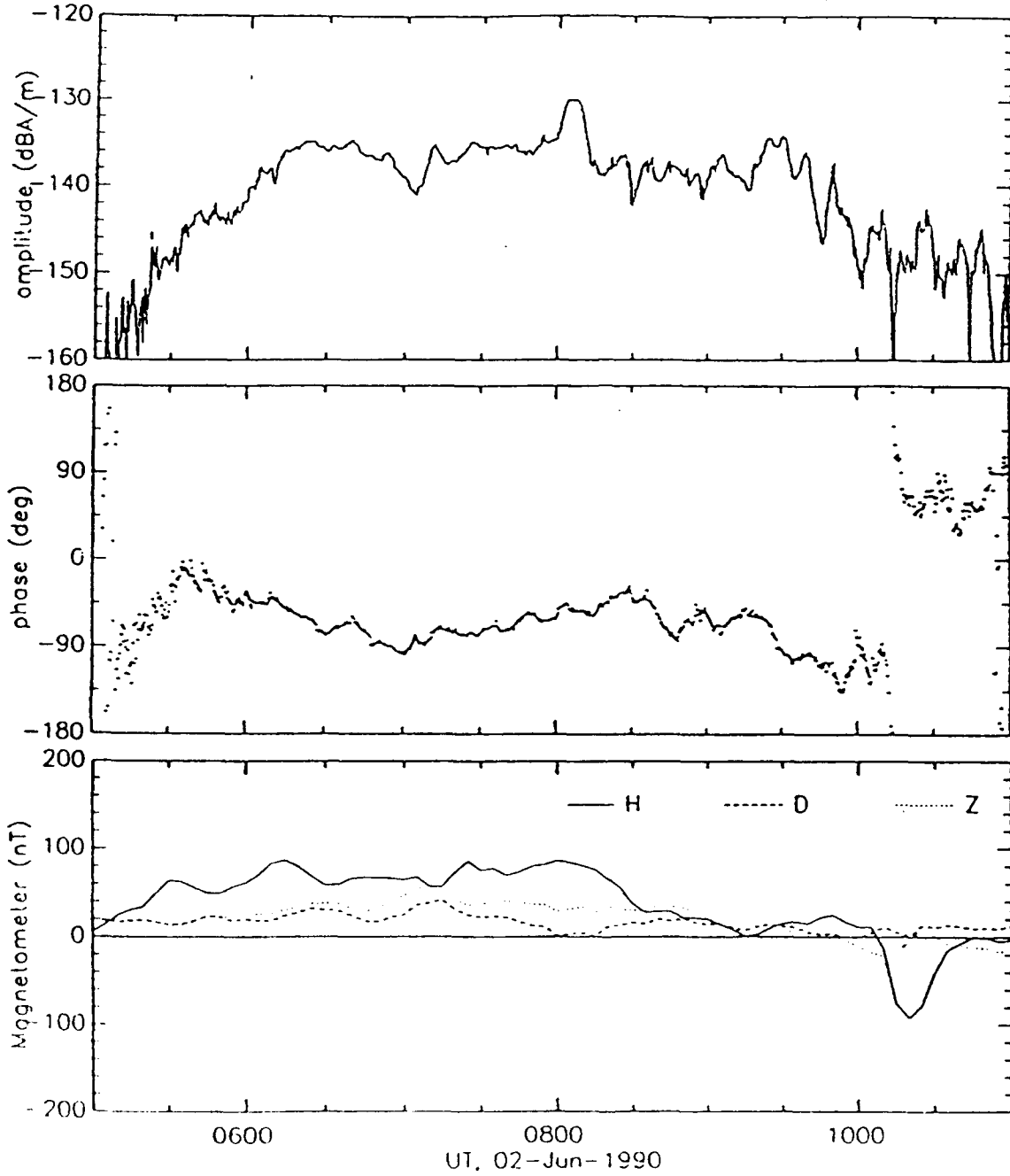
ELF Receiver: NS-Mag chan, 154 Hz, 100 sec integration



NL900601 1001

Figure 4 (g)

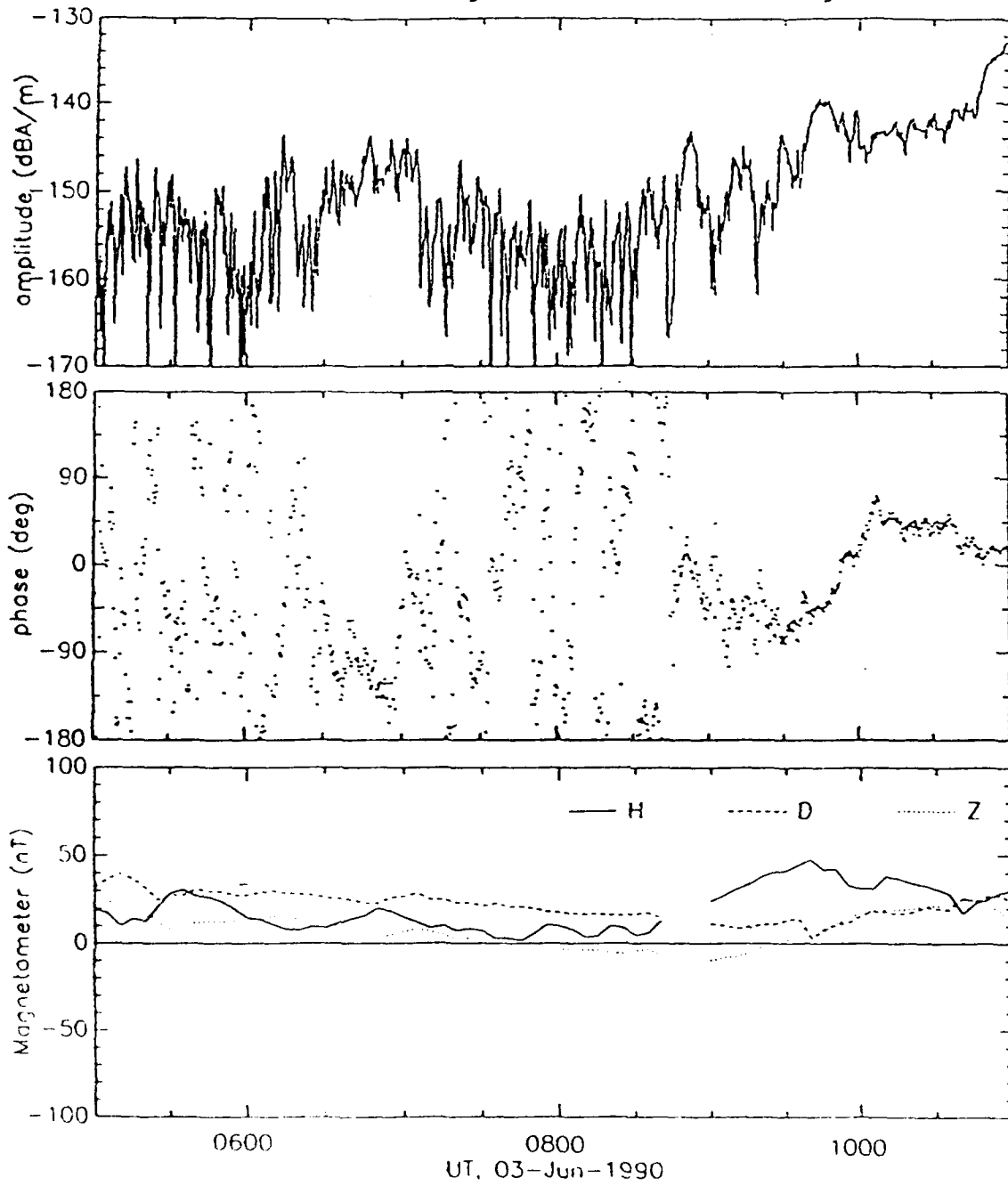
ELF Receiver: NS-Mag chan, 154 Hz, 100 sec integration



NL900602.D01

Figure 4 (h)

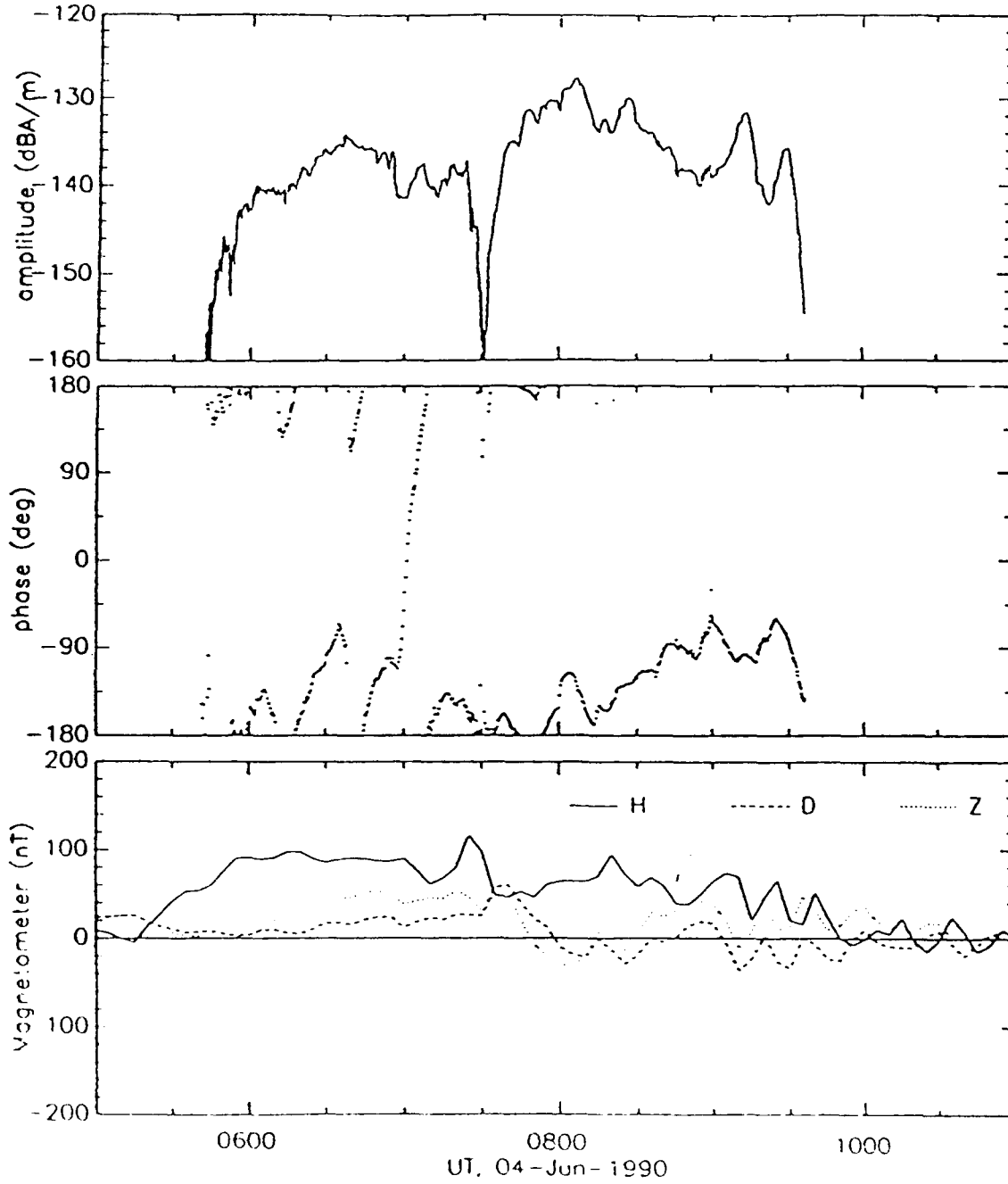
ELF Receiver: NS-Mag chan. 154 Hz. 100 sec integration



NL900603 001

Figure 4 (i)

ELF Receiver: NS-Mag chan. 154 Hz, 100 sec integration



PL 9006(1) 001

Figure 4 (j)

MAY/JUNE 1990 CAMPAIGN
2100-0300 ADST NIGHTLY AVERAGES
(ACTUAL MEASURED DATA)

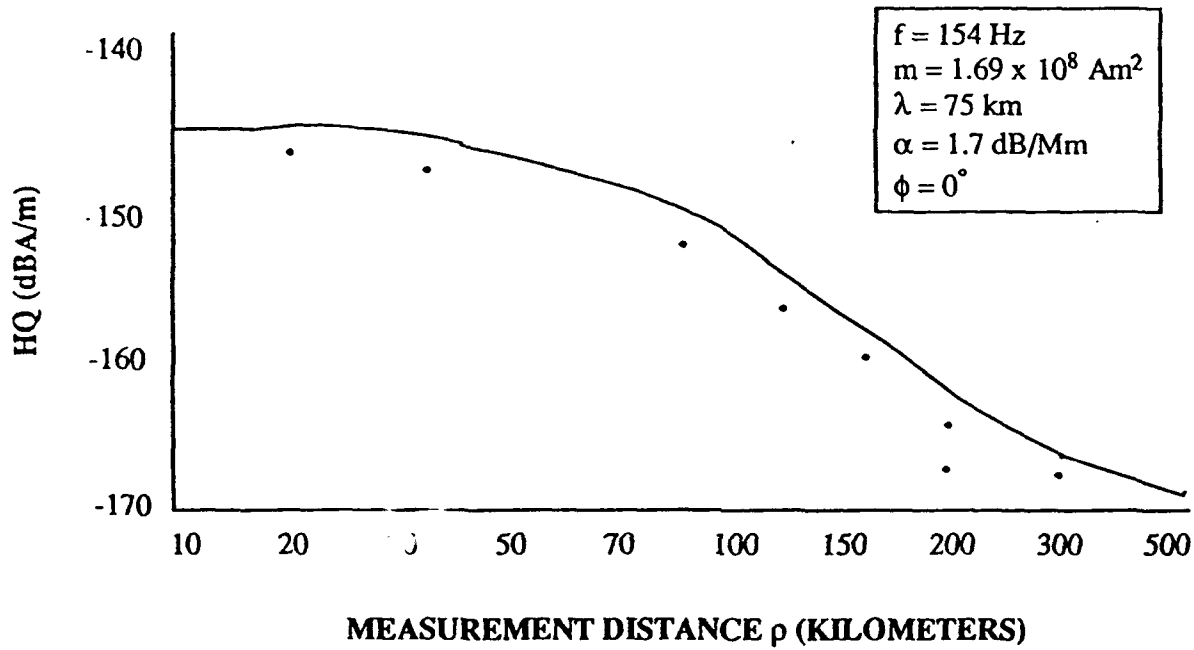


Figure 5 (a) Nightly Average Measurements from the NUSC Site Compared to Predictions from a Simple HMD Ionospheric Source at 75km, for the May 1990 Campaign (Bannister 1990)

MAY/JUNE 1990 CAMPAIGN
2100-0300 ADST NIGHTLY AVERAGES

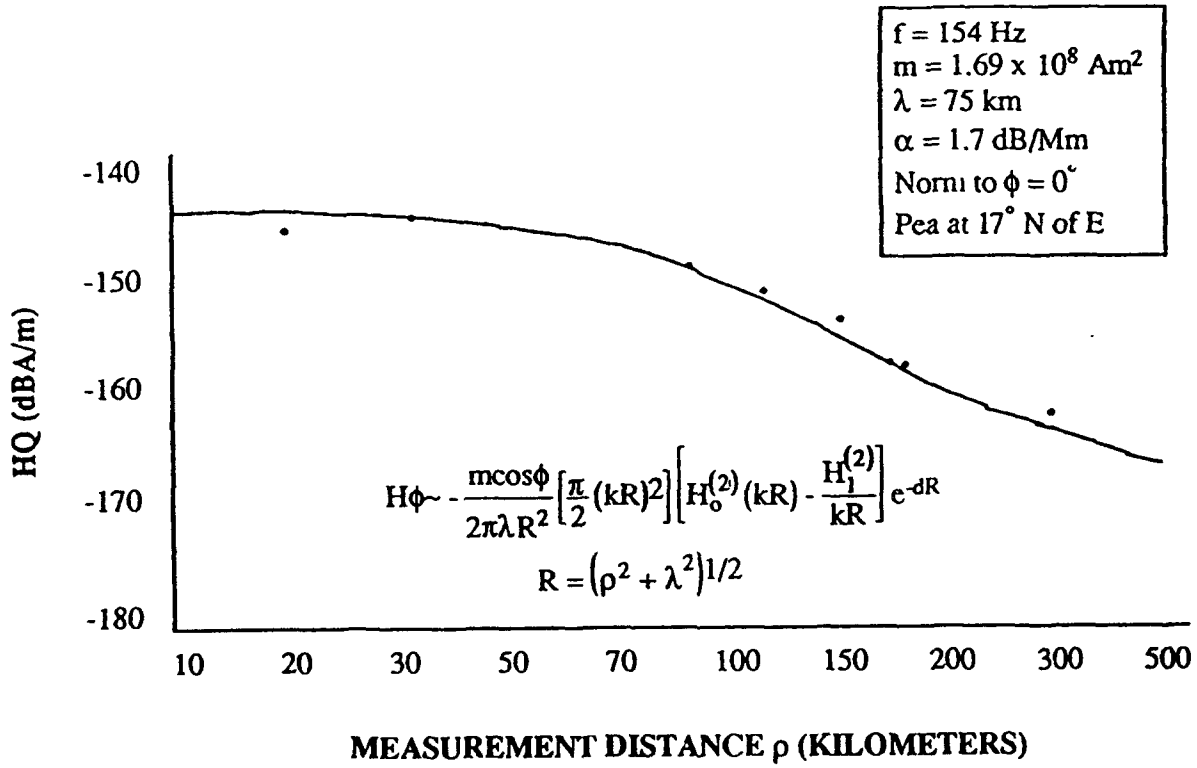


Figure 5 (b)

MAY/JUNE 1990 CAMPAIGN
0000-0300 ADST NIGHTLY AVERAGES

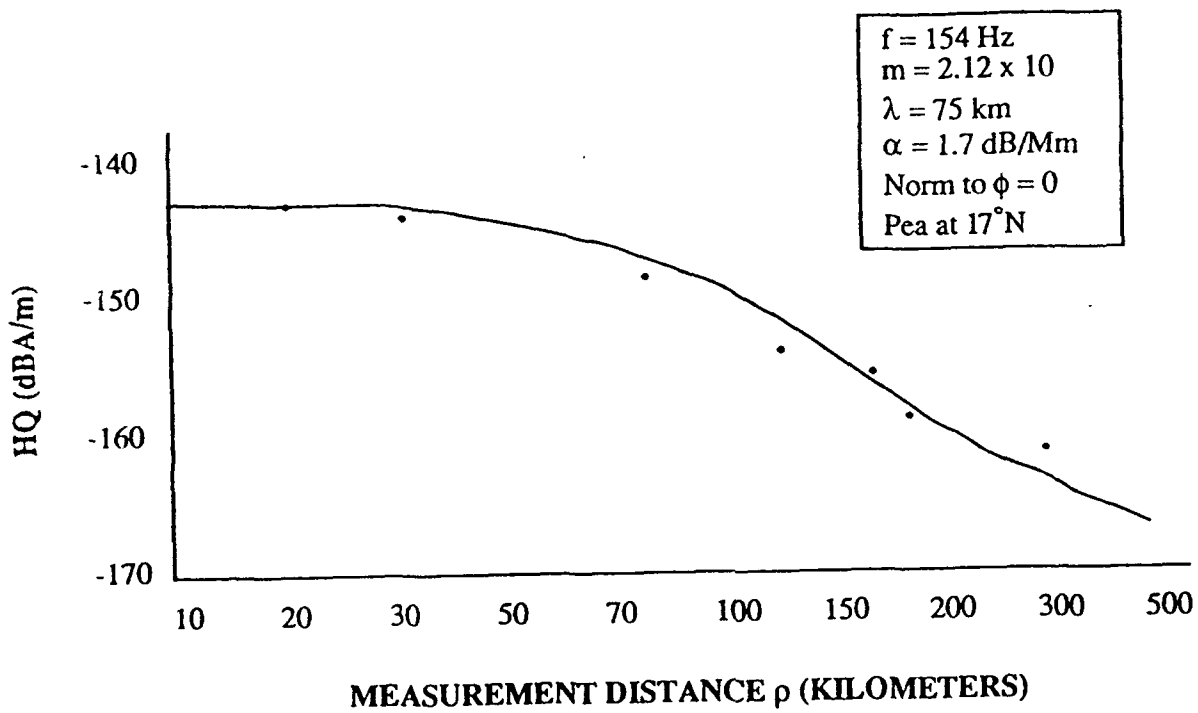


Figure 5 (c)

MAY/JUNE 1990 CAMPAIGN
HIGH VALUE AVERAGES
(VALUES > NIGHTLY AVERAGES)

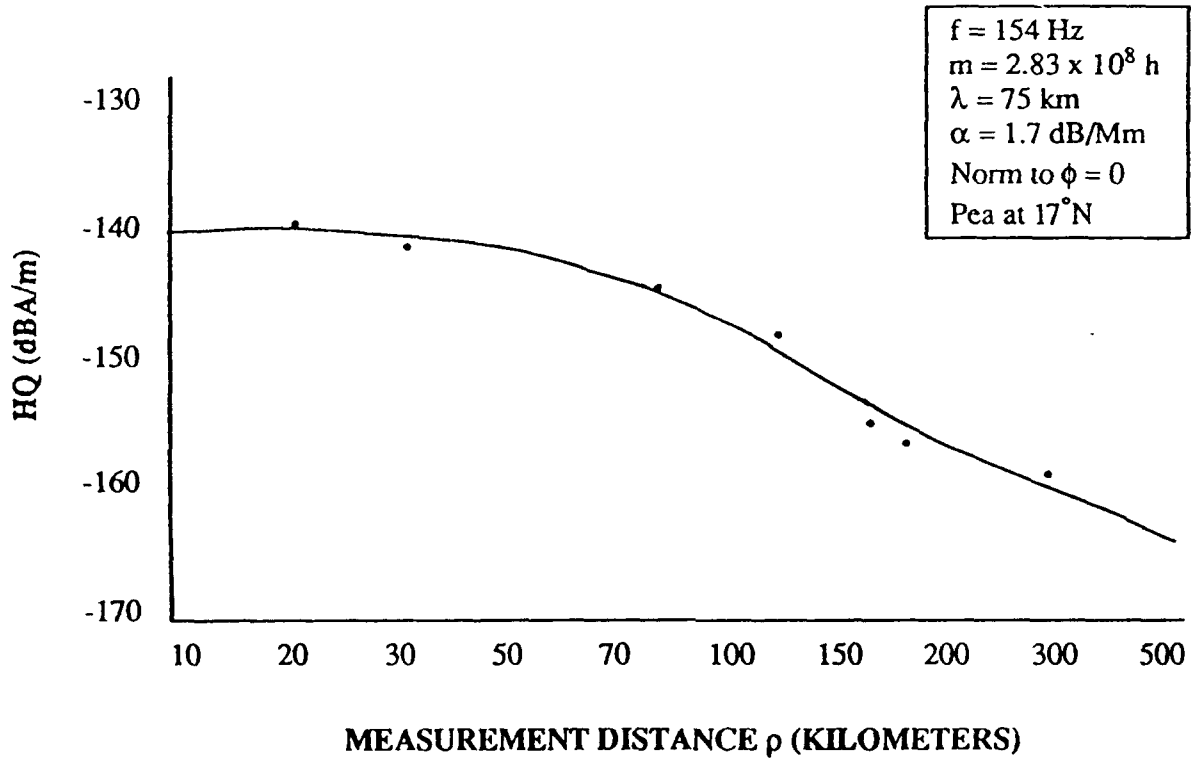


Figure 5 (d)

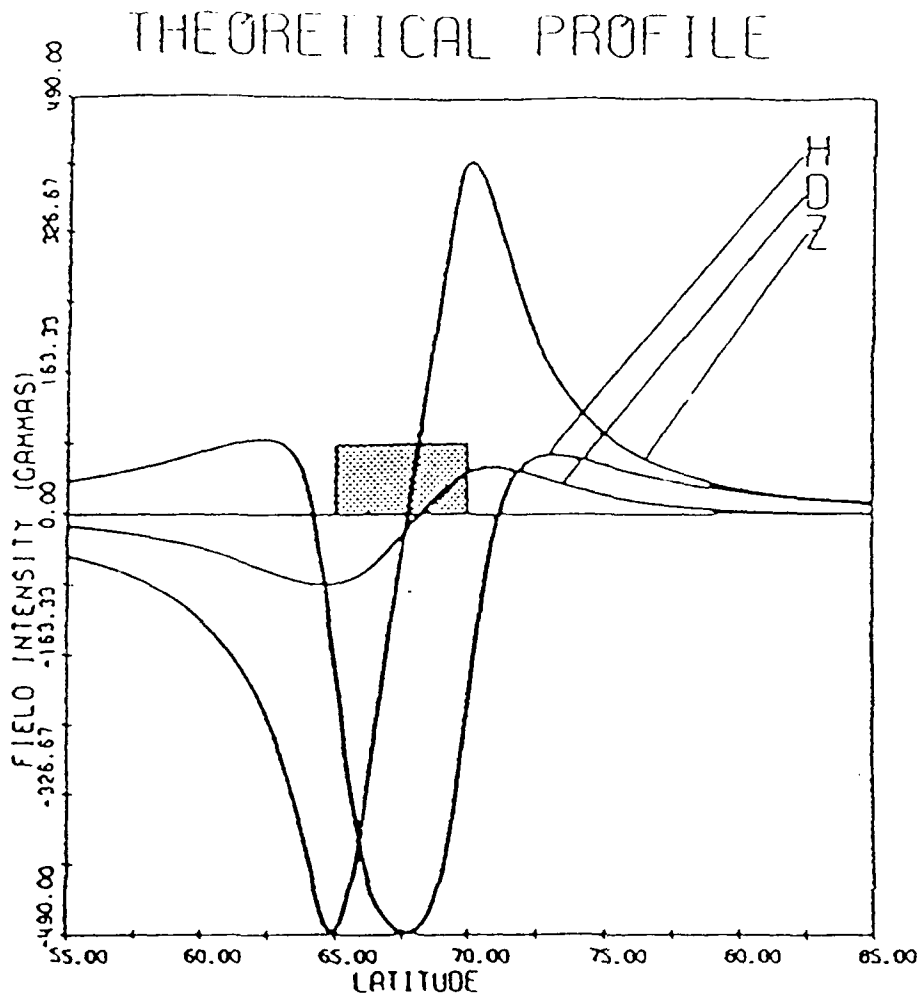


Figure 6 Model Magnetometer Profiles Due to a Horizontal Current Source

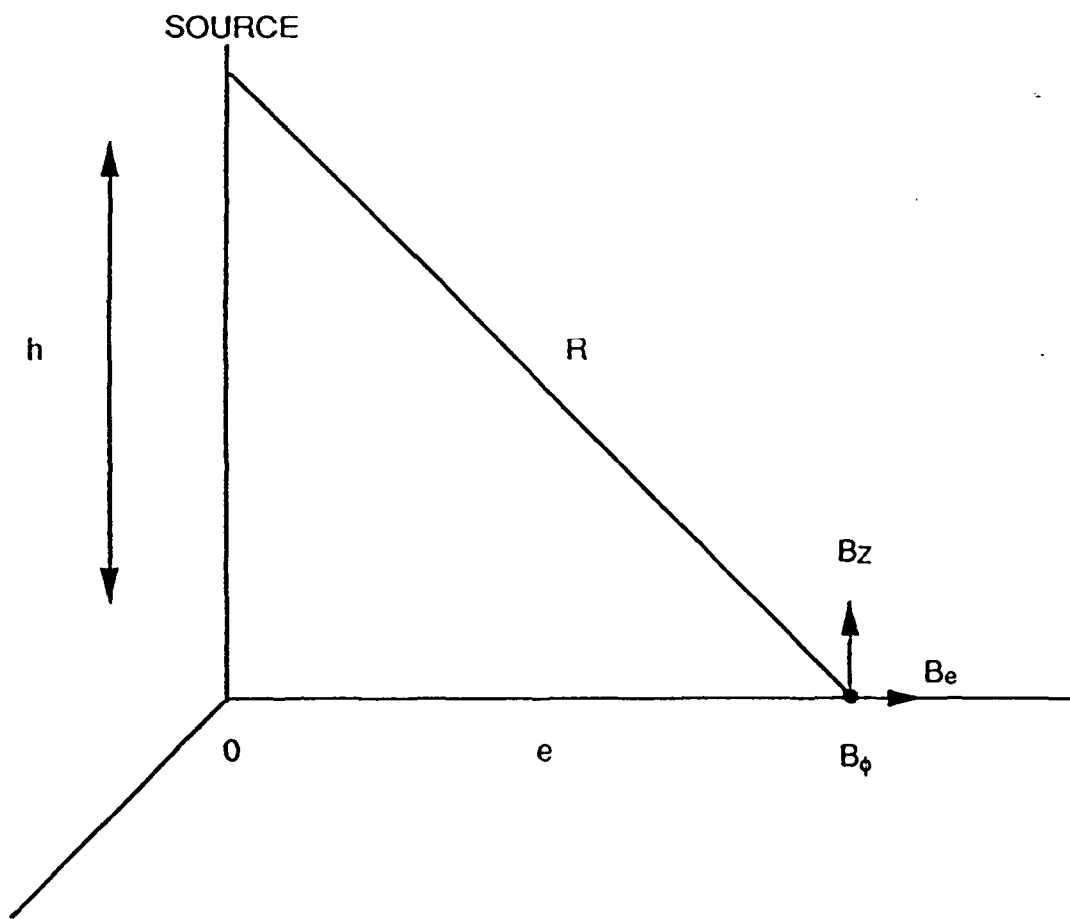


Figure 7 Coordinate System and Notation

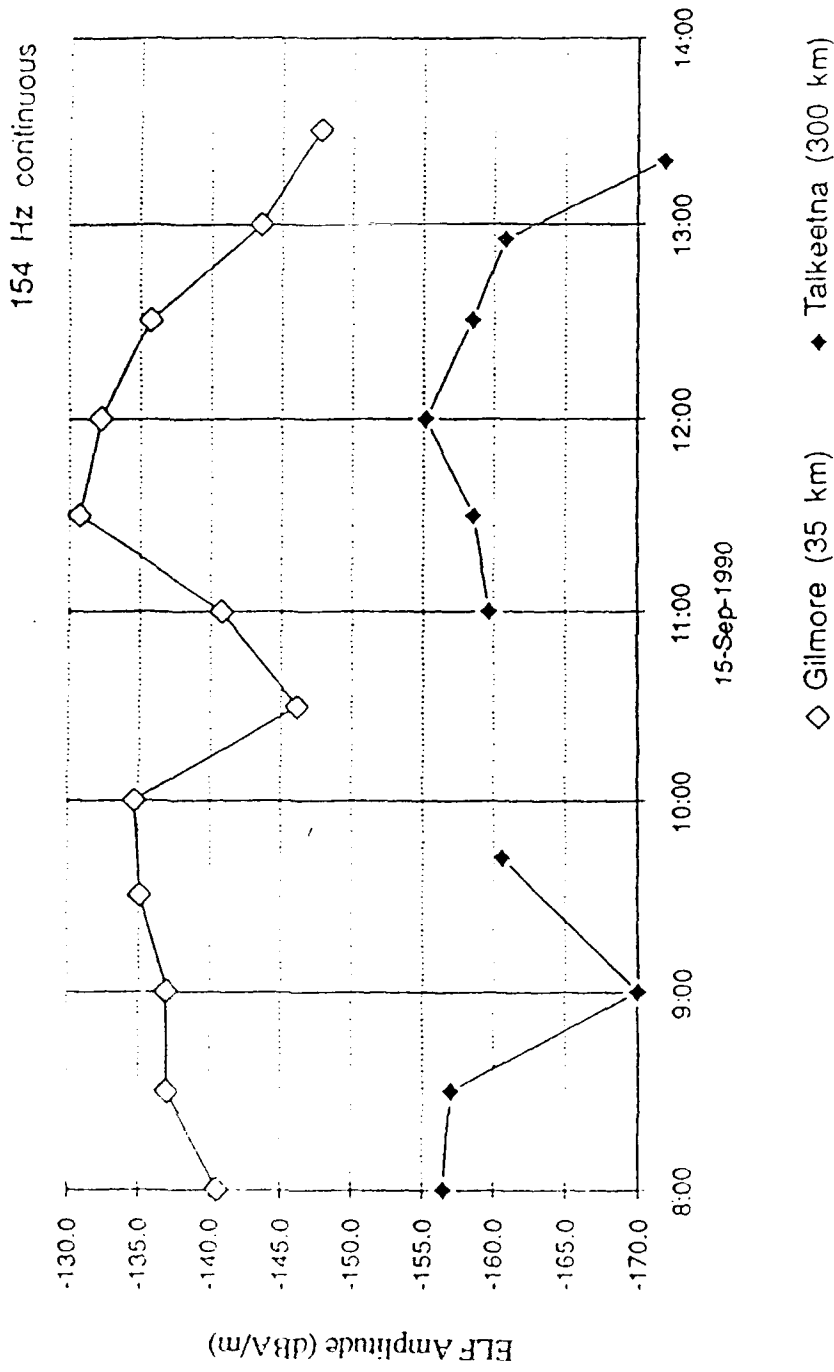


Figure 8 (a) Comparison of ELF Amplitudes Received in Talkeetna and the NOAA Site During the September 1990 Campaign

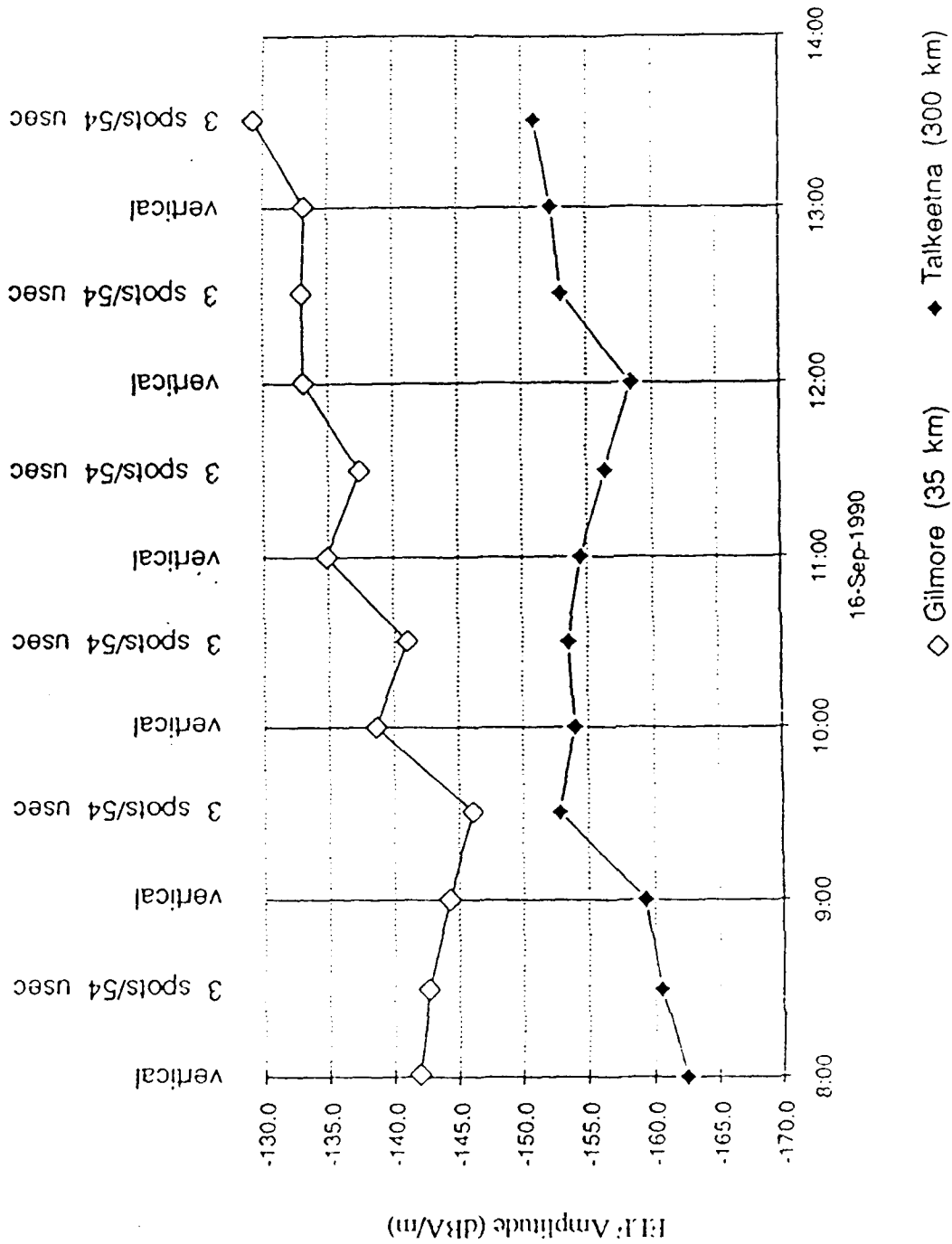


Figure 8 (b)

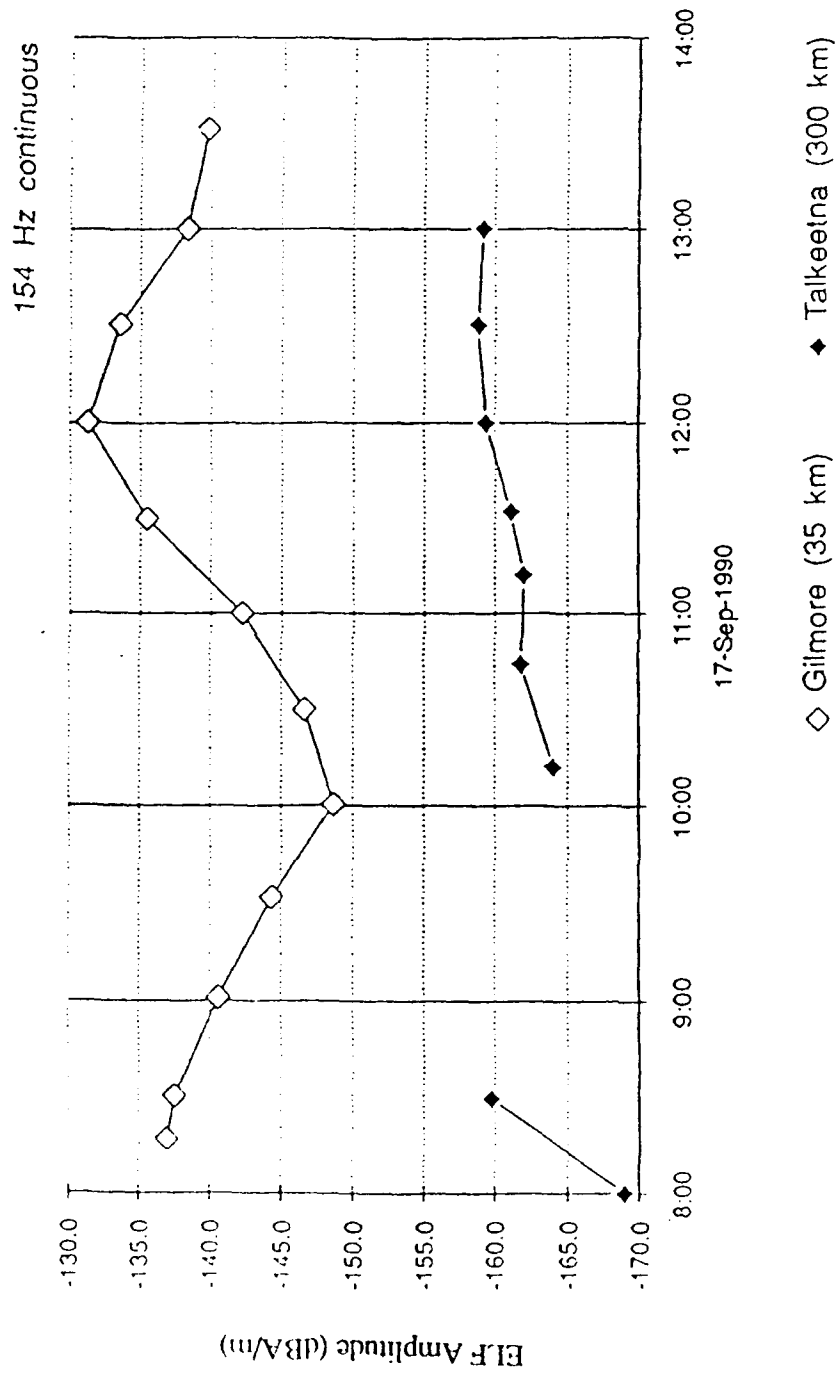
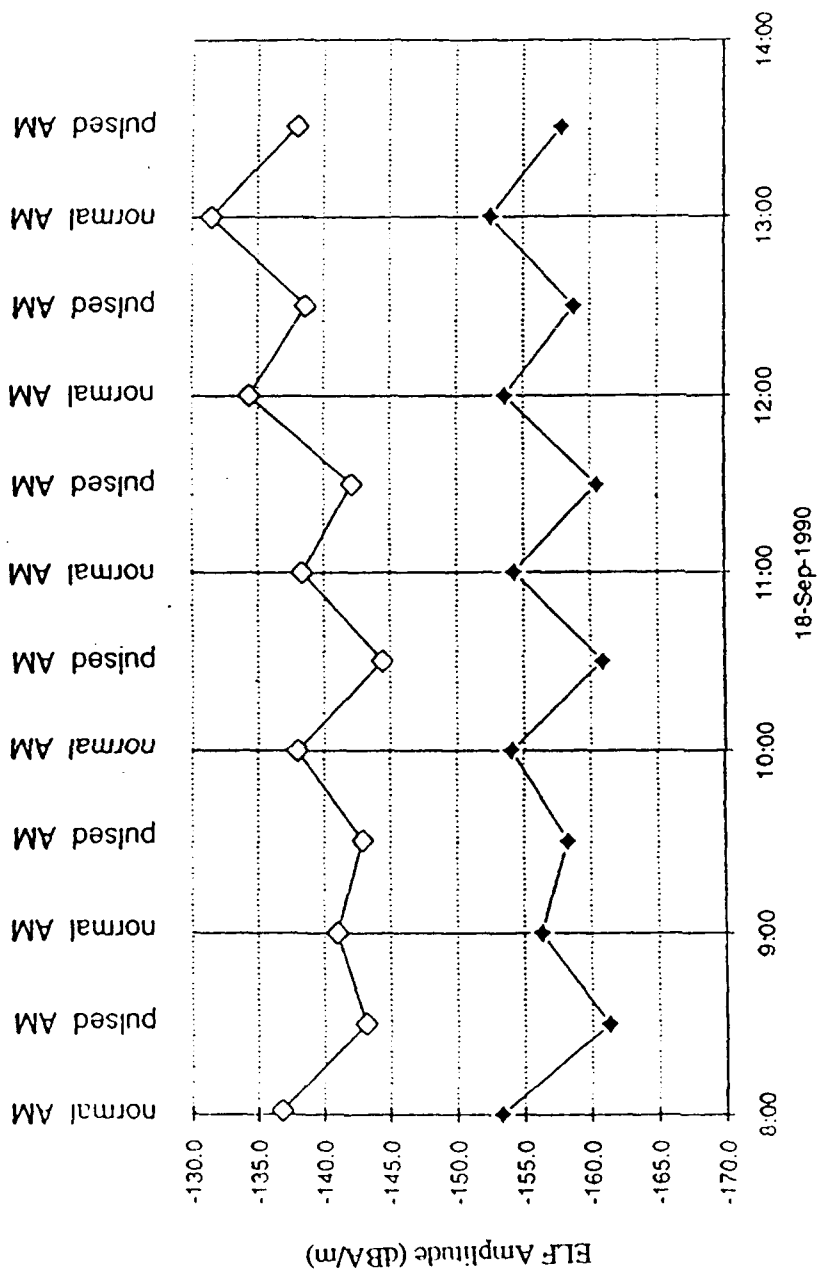


Figure 8 (c)



3.2 msec

normal AM

pulsed AM

54 usec on/108 usec off

Figure 8 (d)

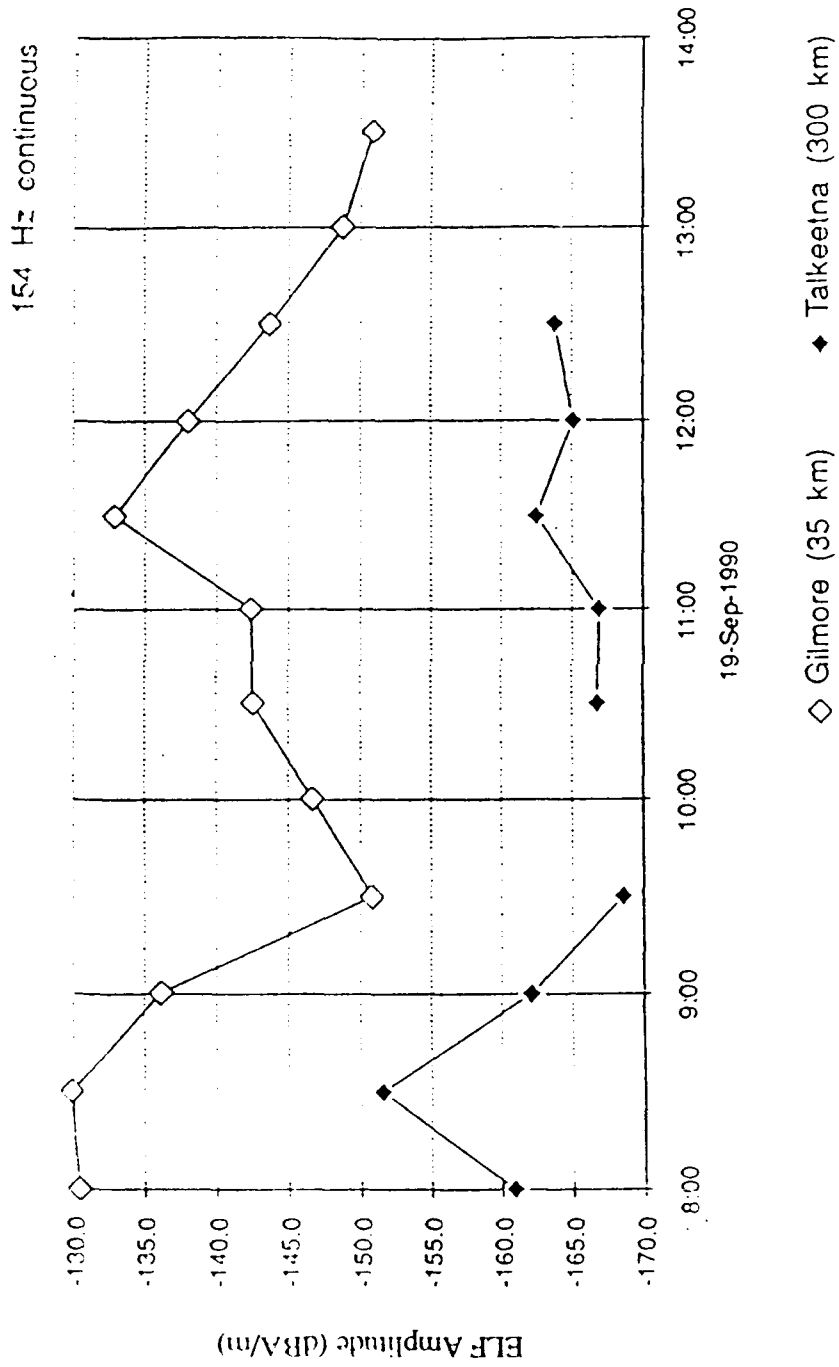


Figure 8 (e)

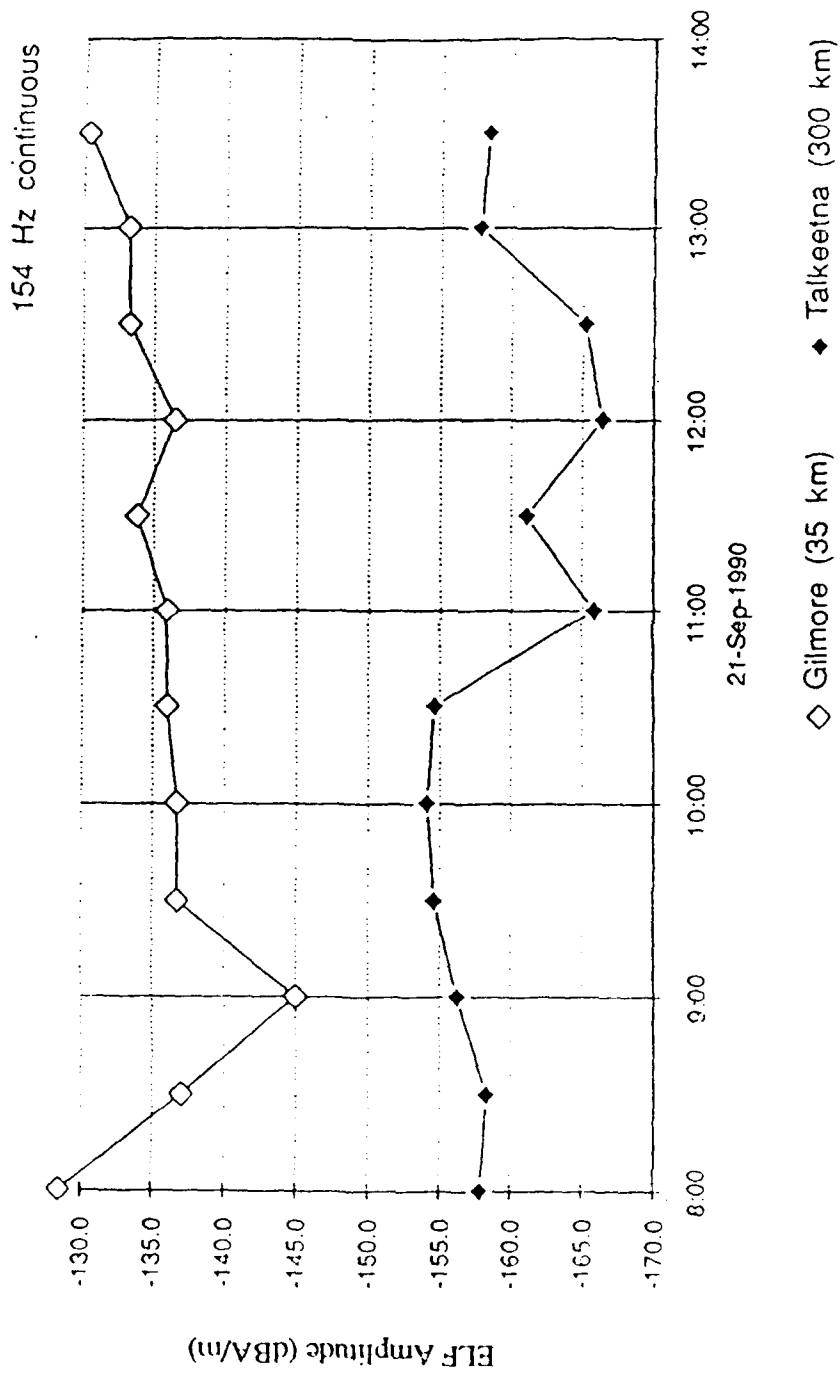


Figure 8 (f)

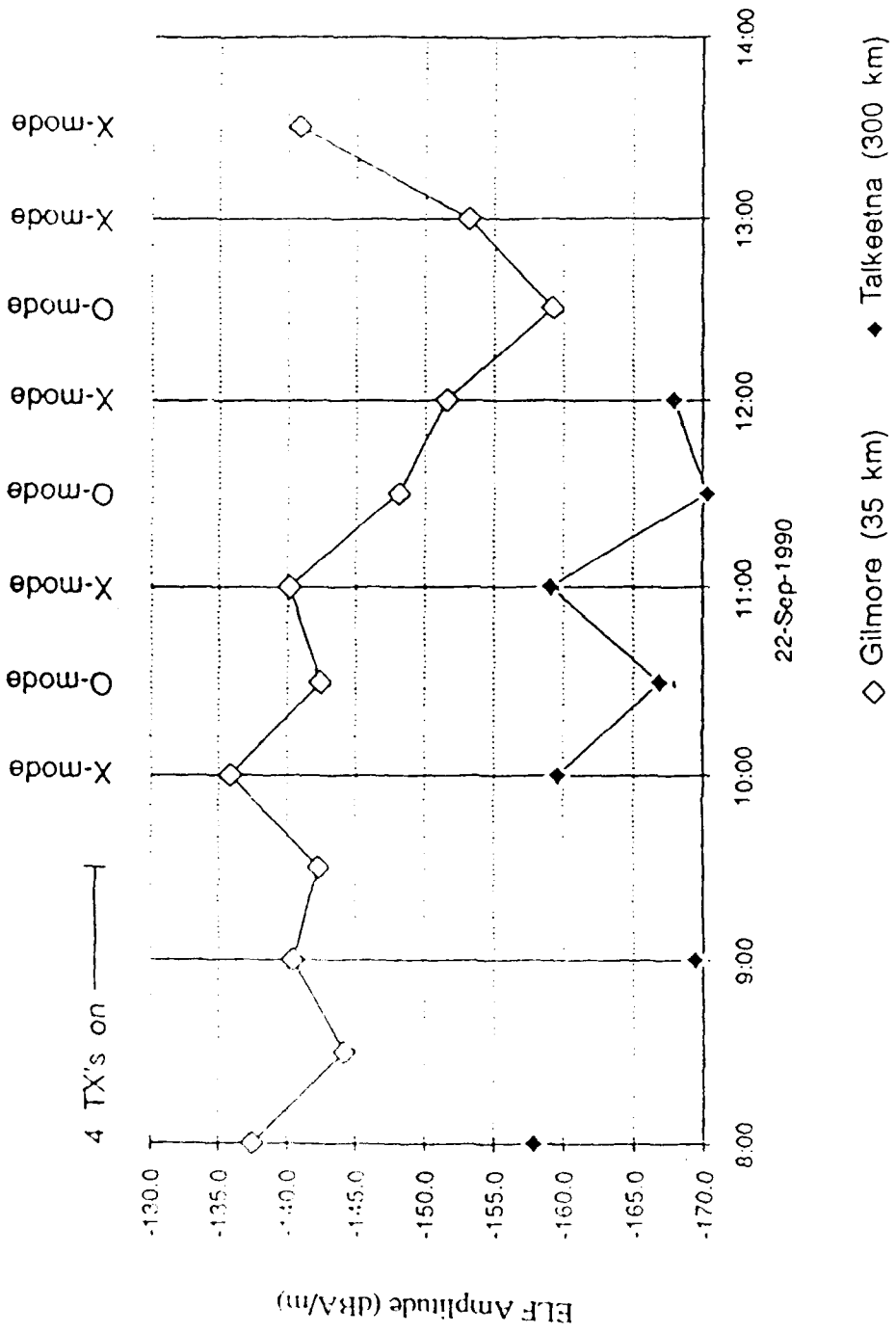


Figure 8 (g)

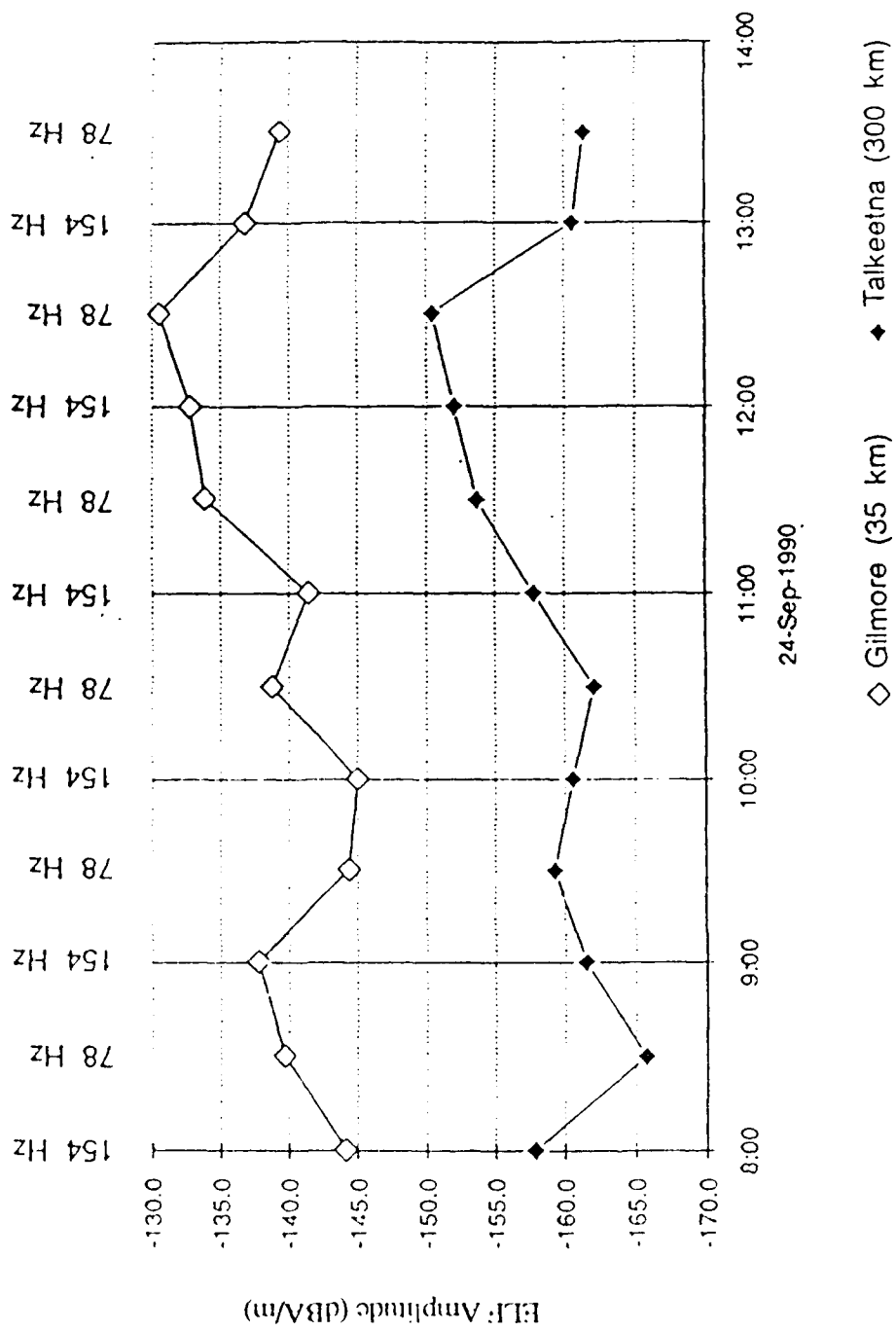


Figure 8 (h)

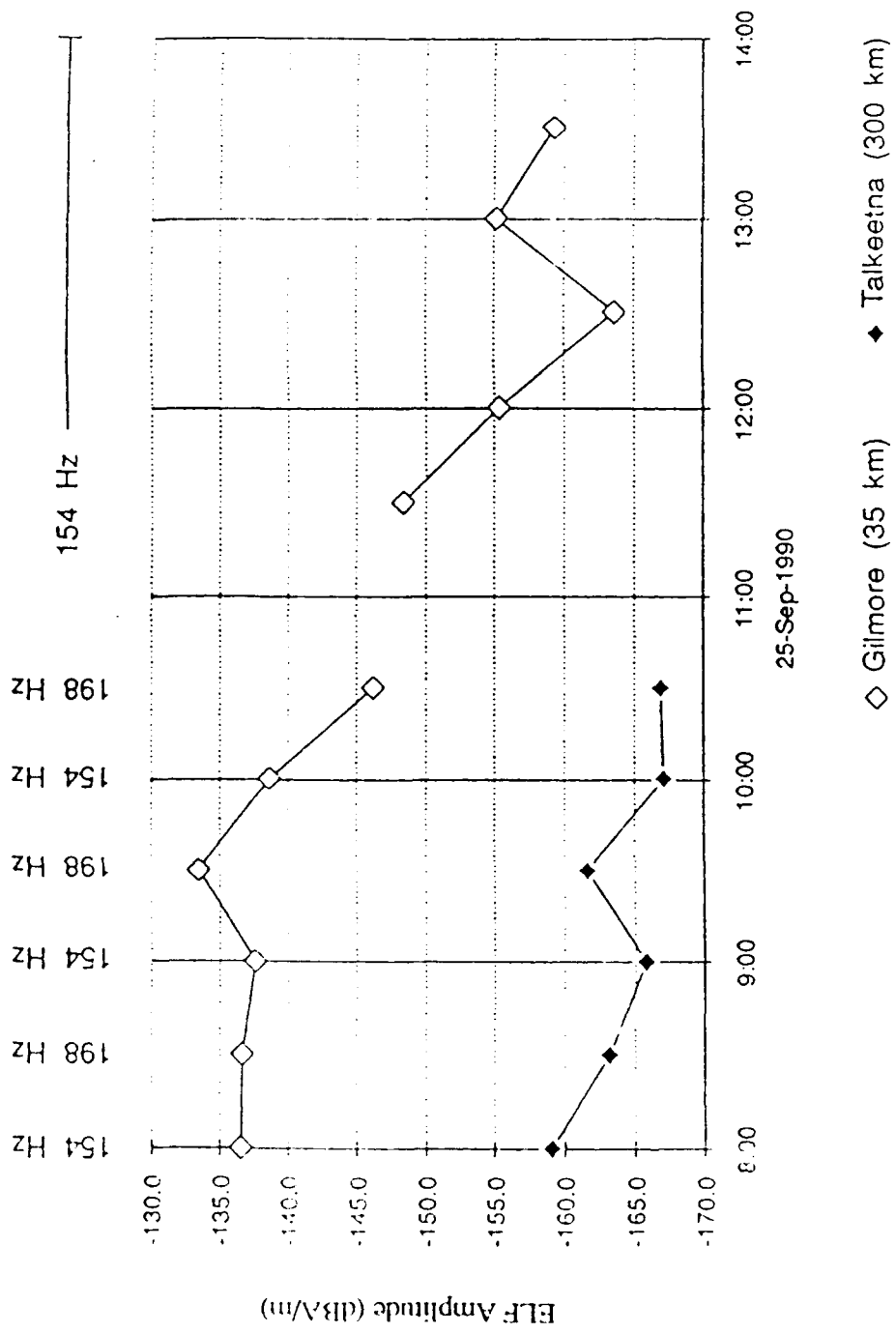


Figure 8 (i)

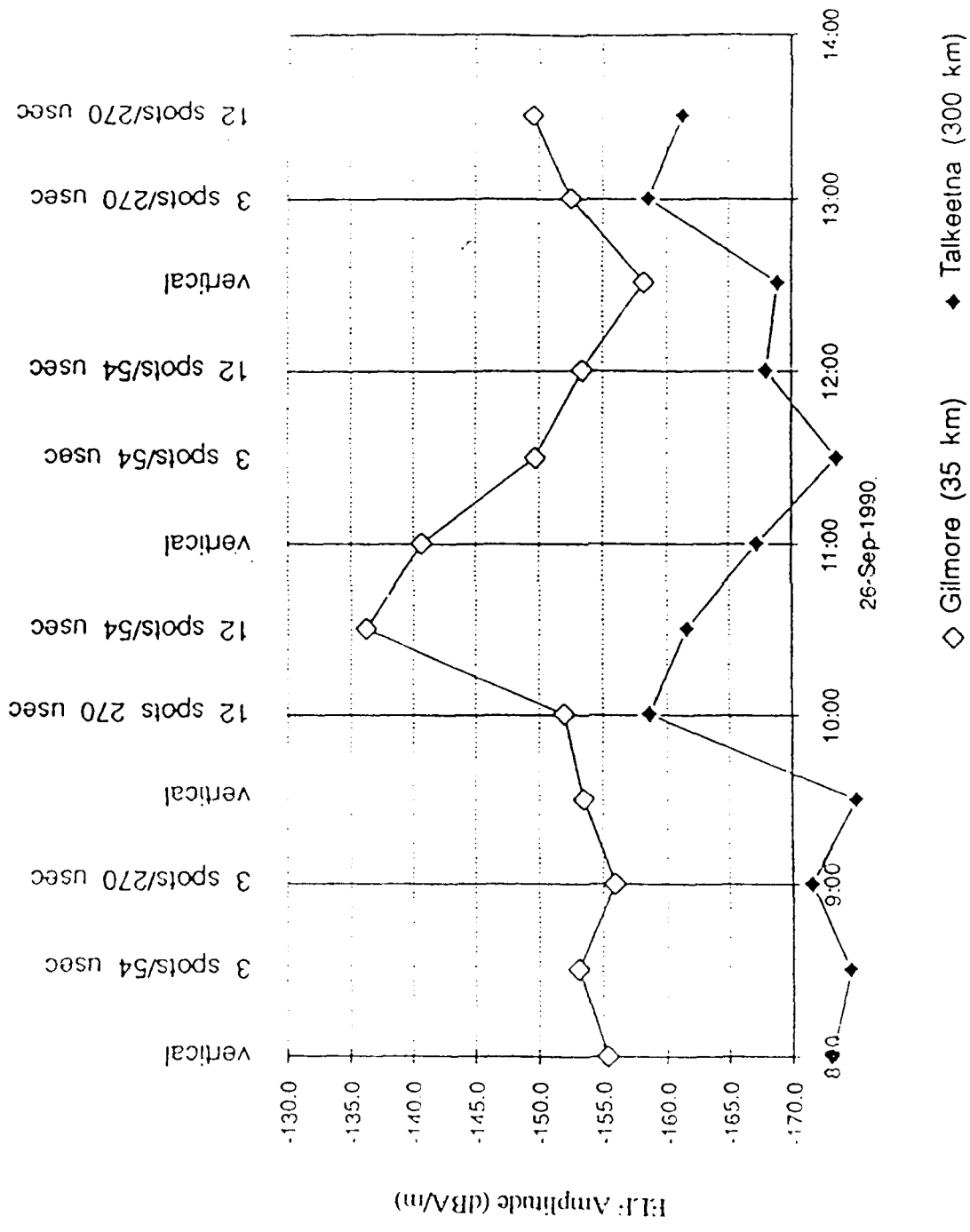


Figure 8 (j)

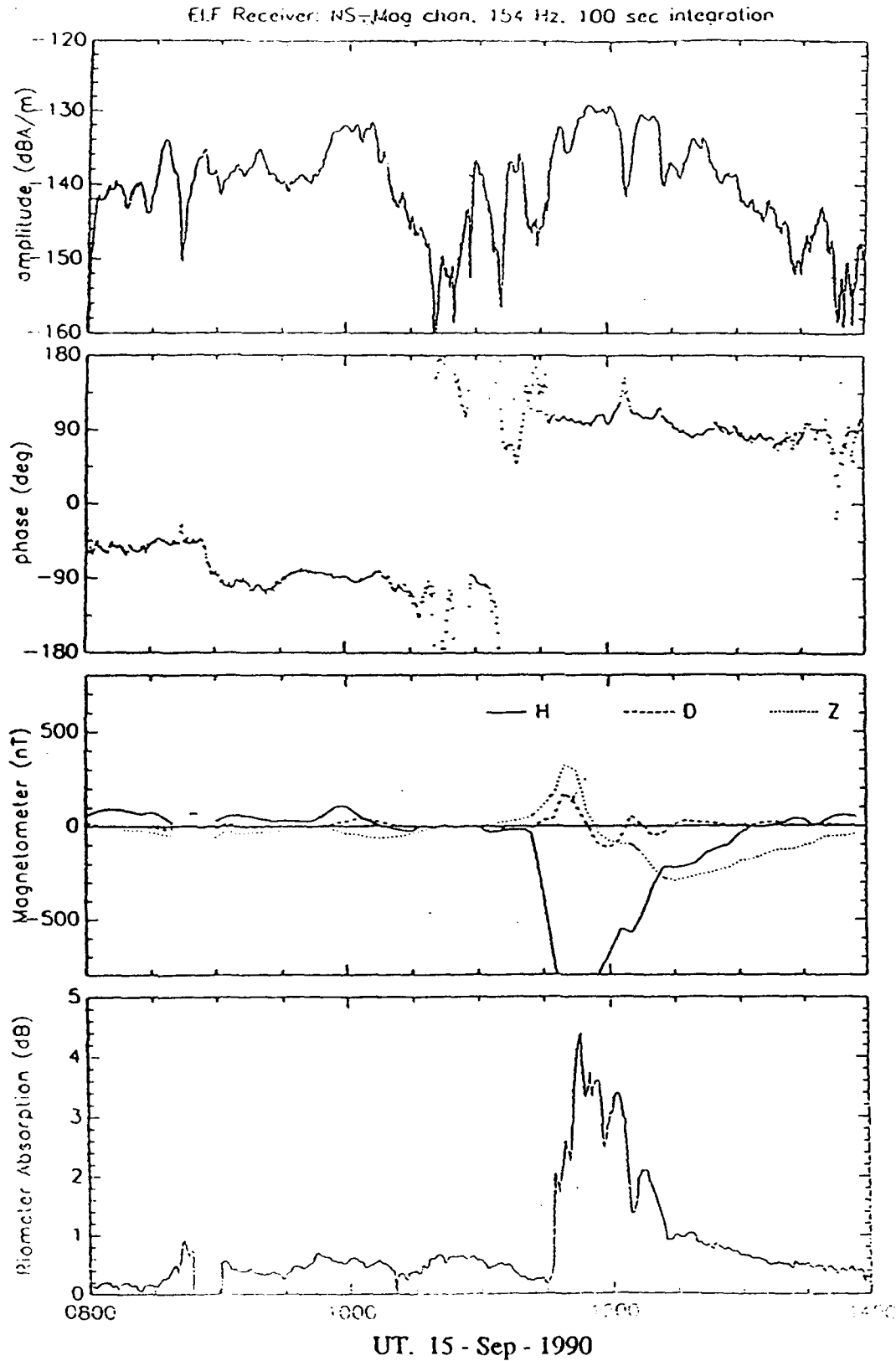
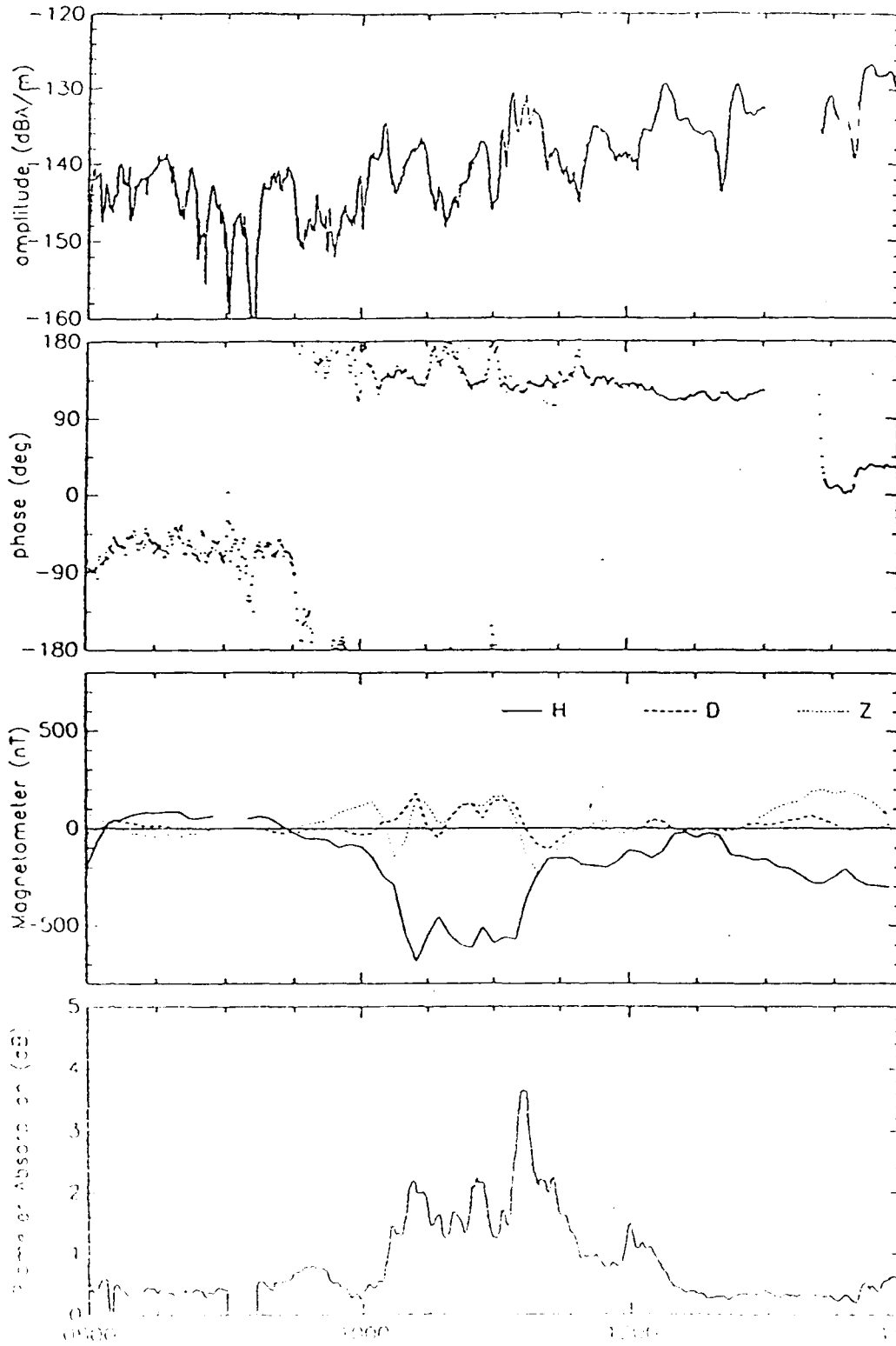


Figure 9 (a) Complete Set of NOAA Data Along with Magnetometer and Riometer Data from the College Station for the September 1991 Campaign

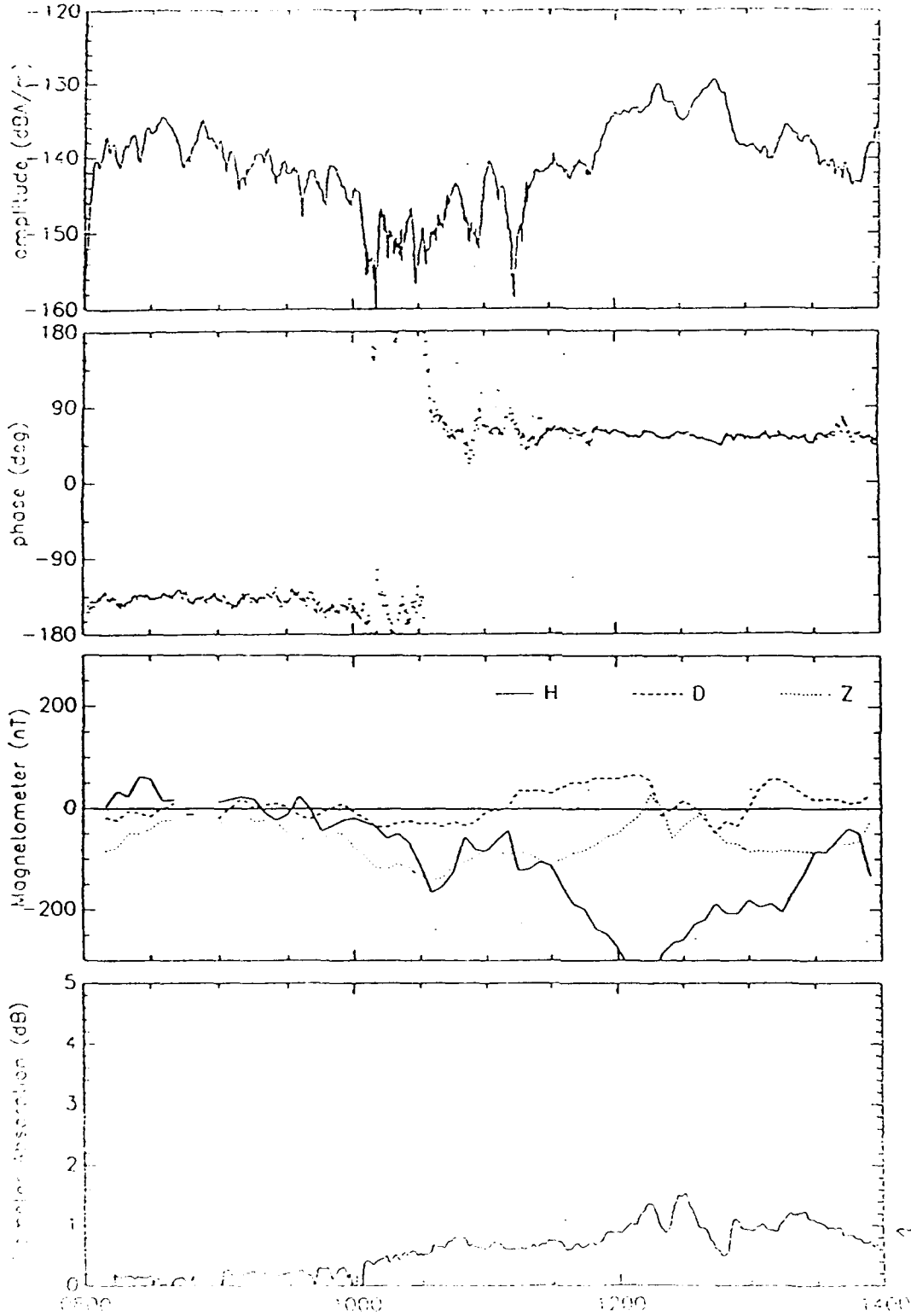
ELF Receiver: NS-Mag chan. 154 Hz, 100 sec integration



UT. 16 - Sep - 1990

Figure 9 (b)

III Receiver NS-Mag chan, 154 Hz, 100 sec integration



UT. 17 - Sep - 1990

Figure 9 (c)

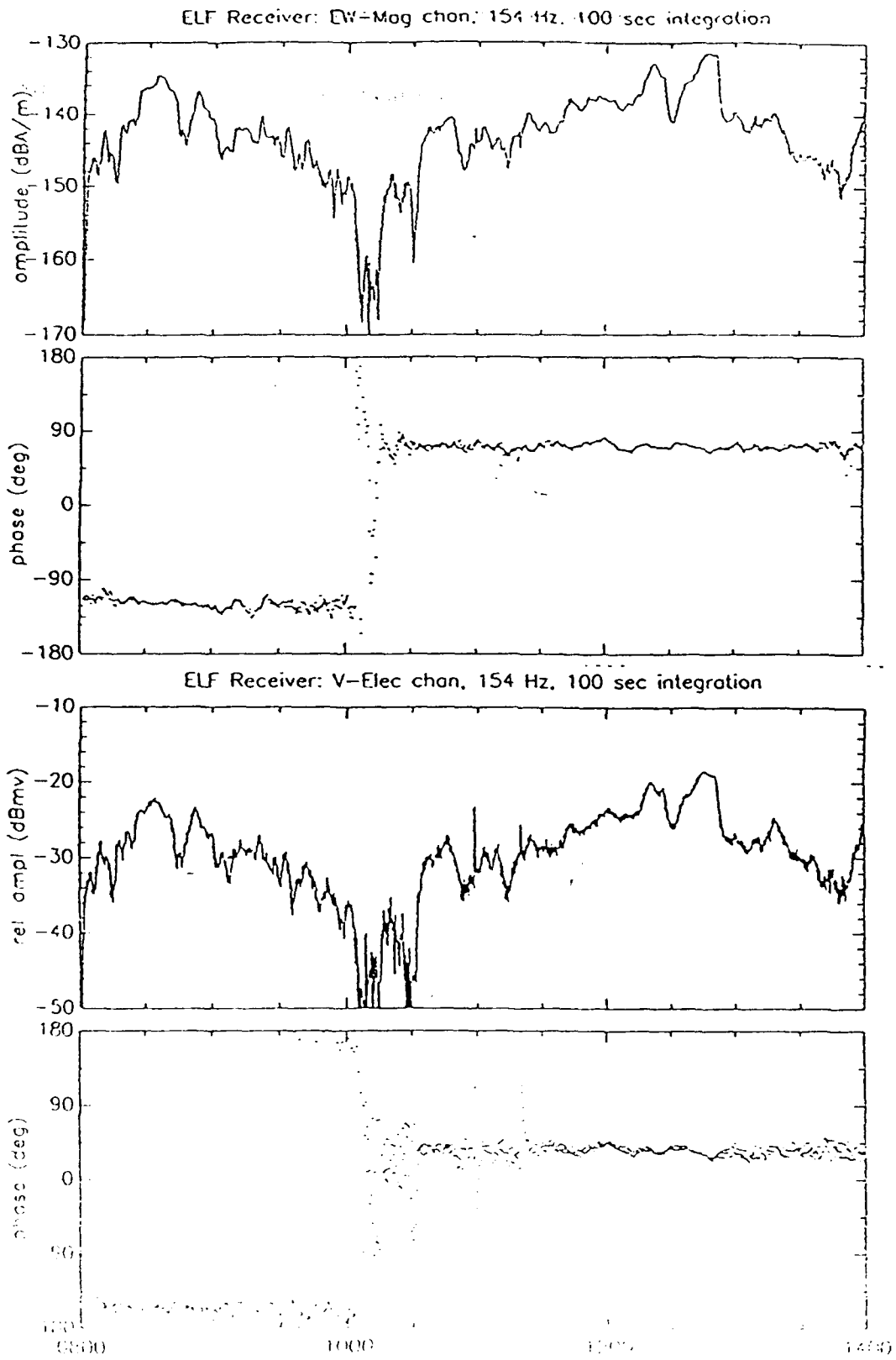
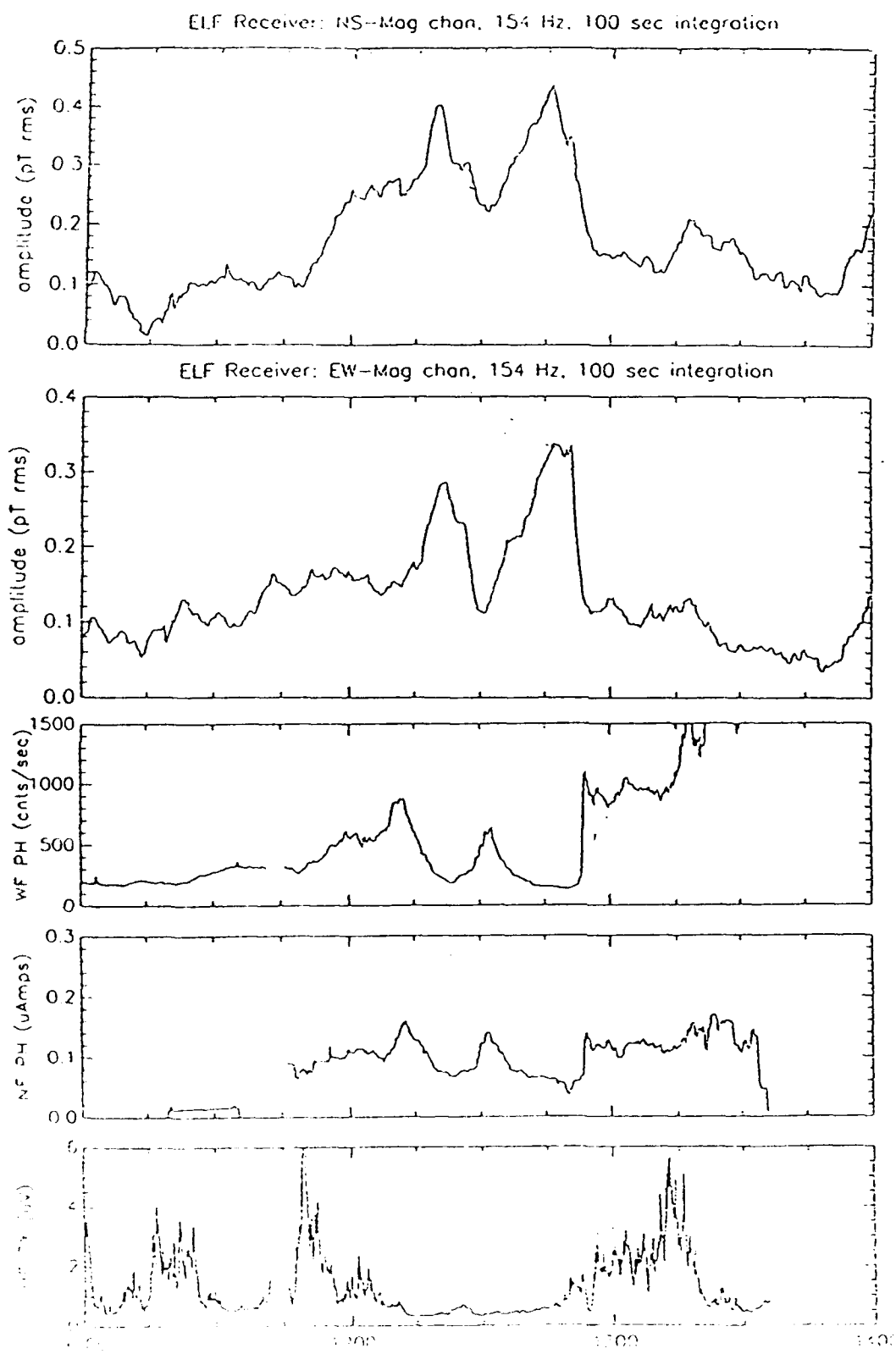


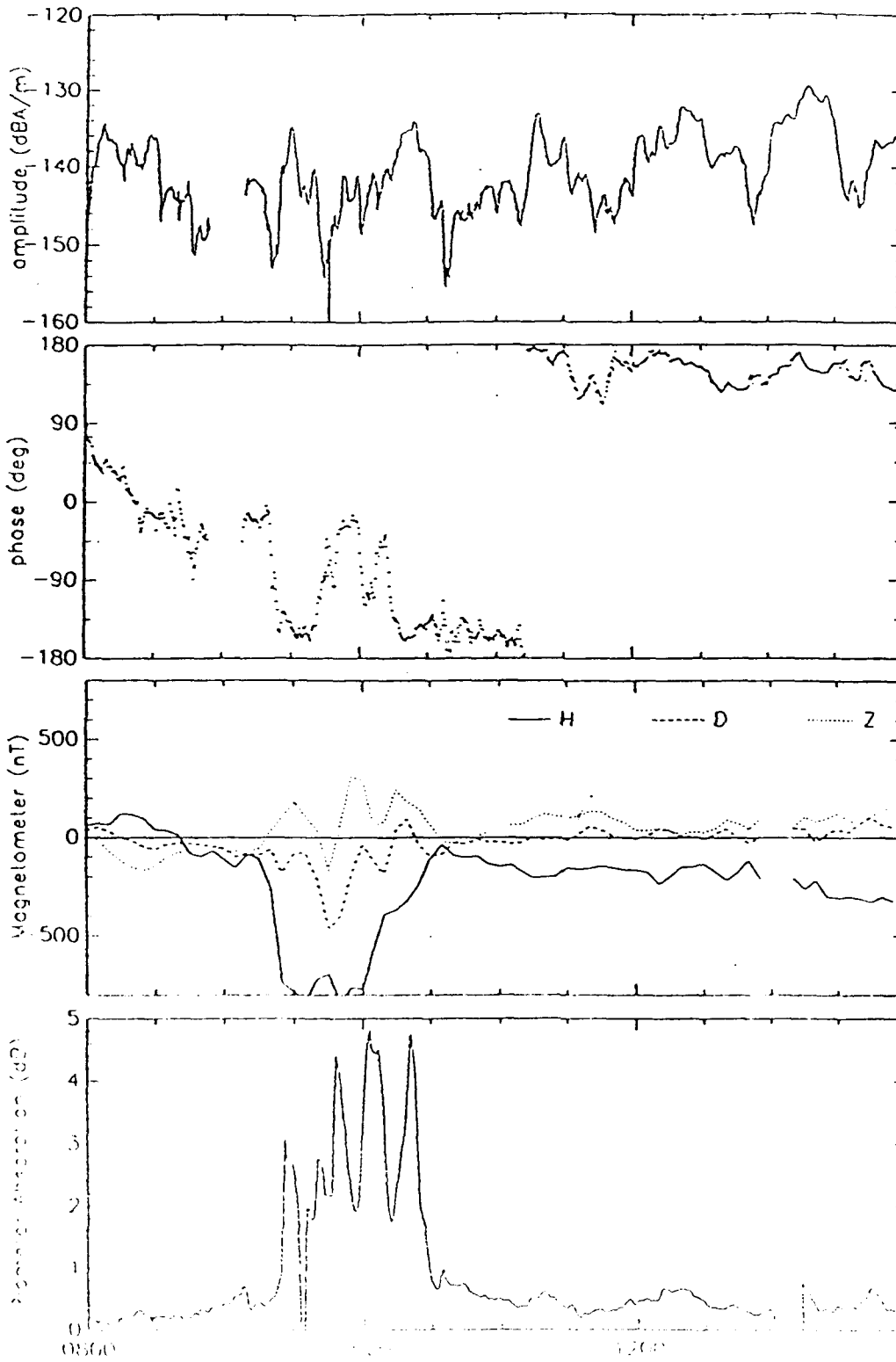
Figure 9 (d)



UT. 17 - Sep - 1990

Figure 9 (e)

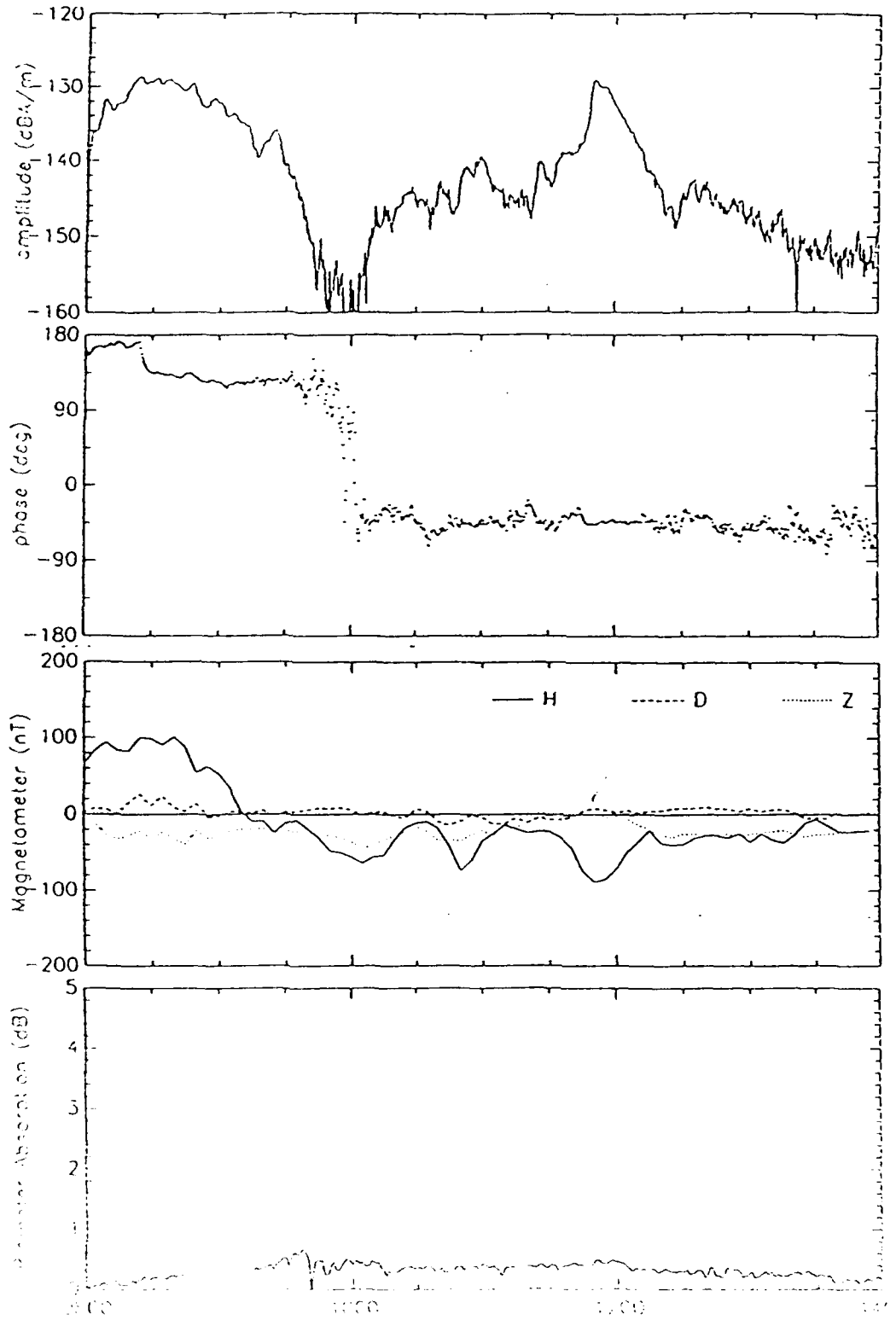
ELF Receiver: NS-Mag chan. 154 Hz. 100 sec integration



UT. 18 - Sep - 1990

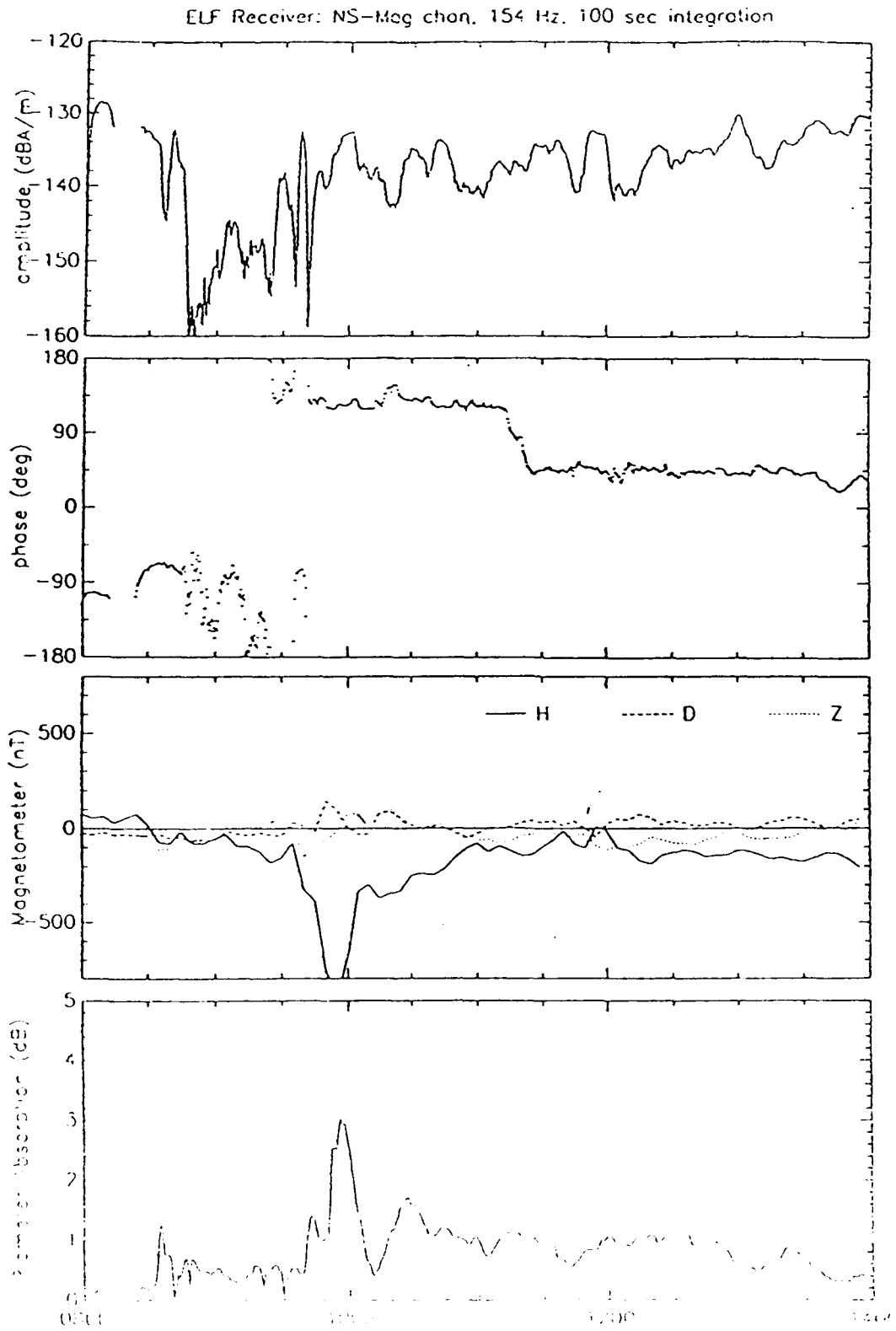
Figure 9 (f)

ELF Receiver: NS-Mog chan, 154 Hz, 100 sec integration



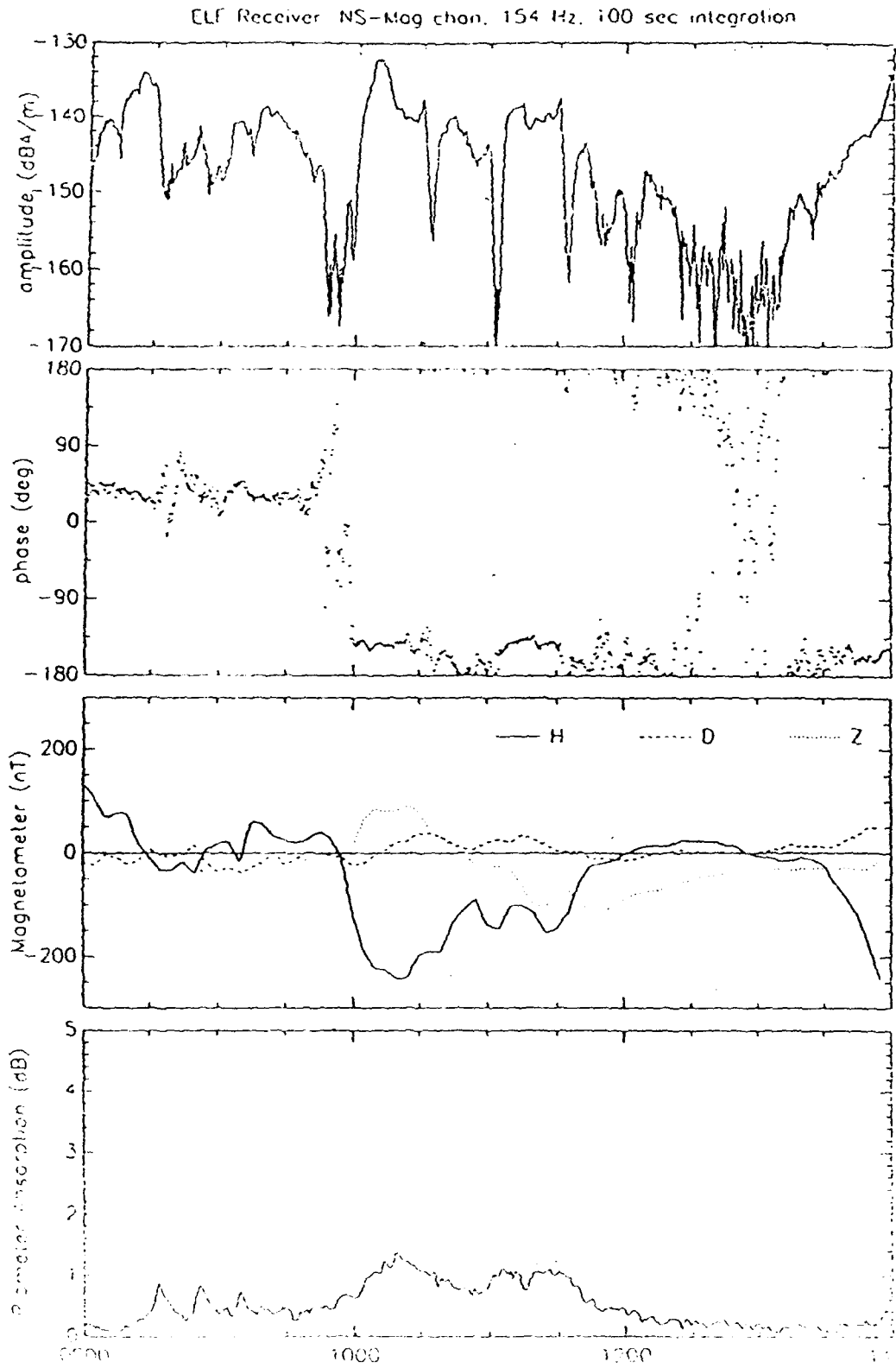
UT. 19 - Sep - 1990

Figure 9 (g)



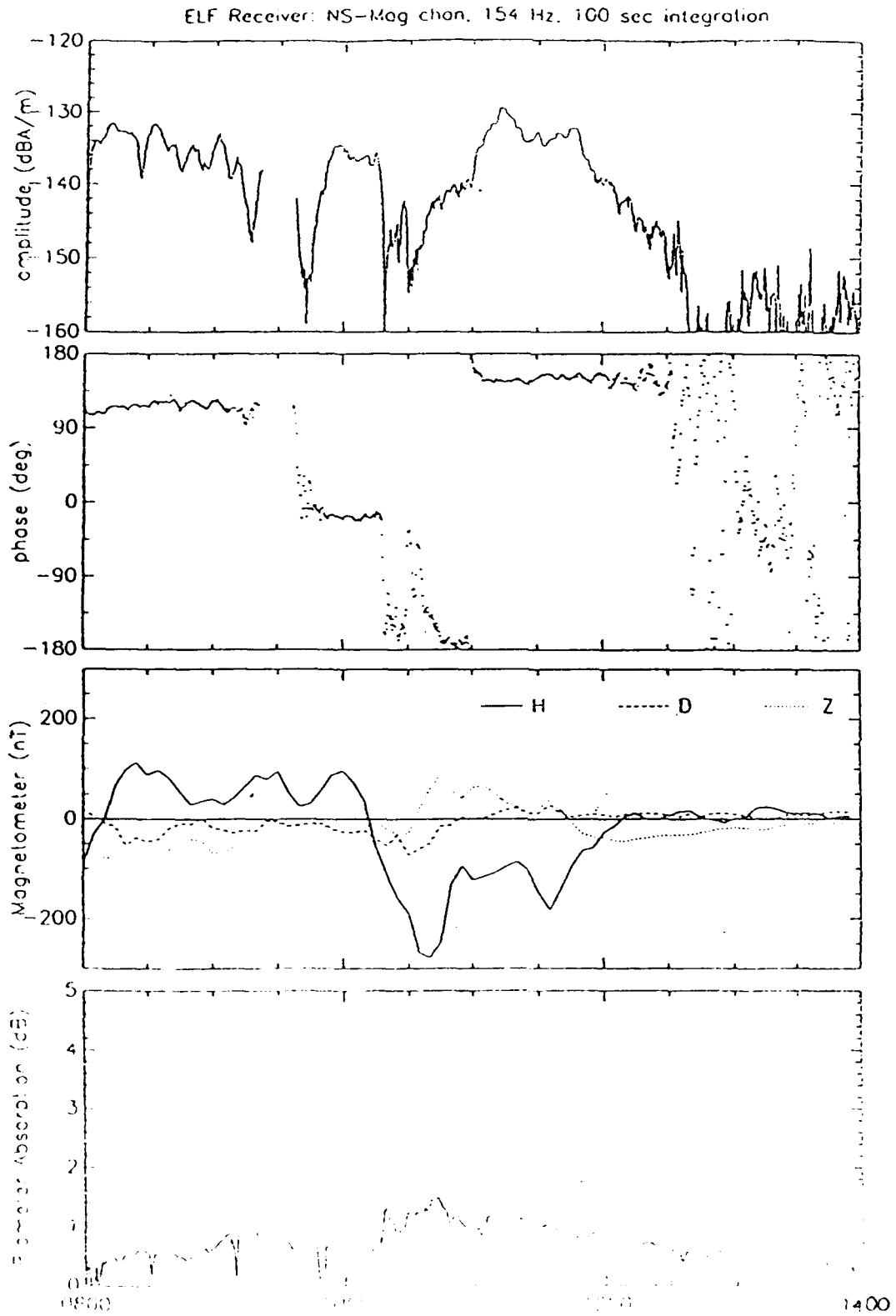
UT. 21 - Sep - 1990

Figure 9 (h)



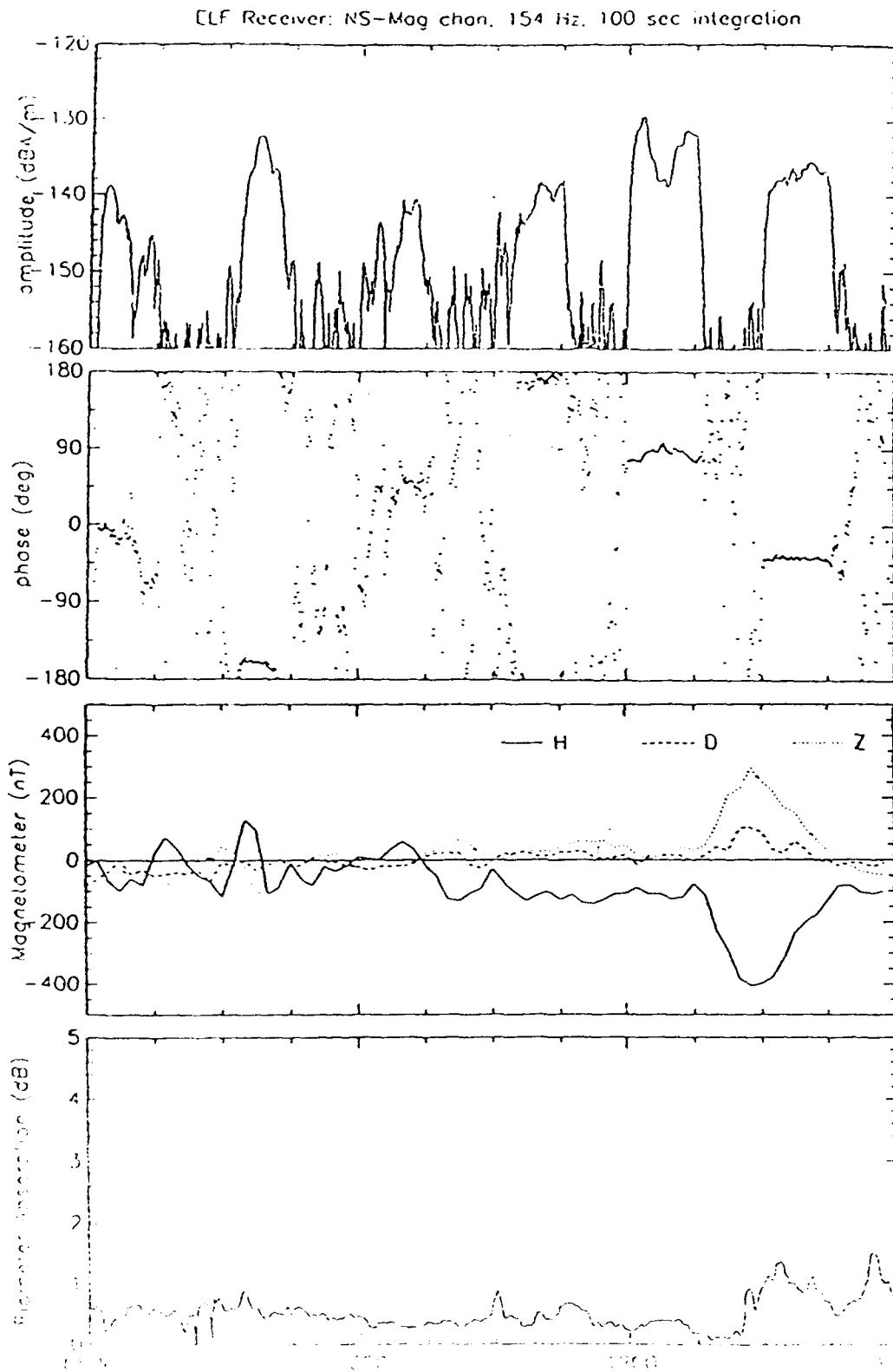
UT. 22 - Sep - 1990

Figure 9 (i)



UT. 23 - Sep - 1990

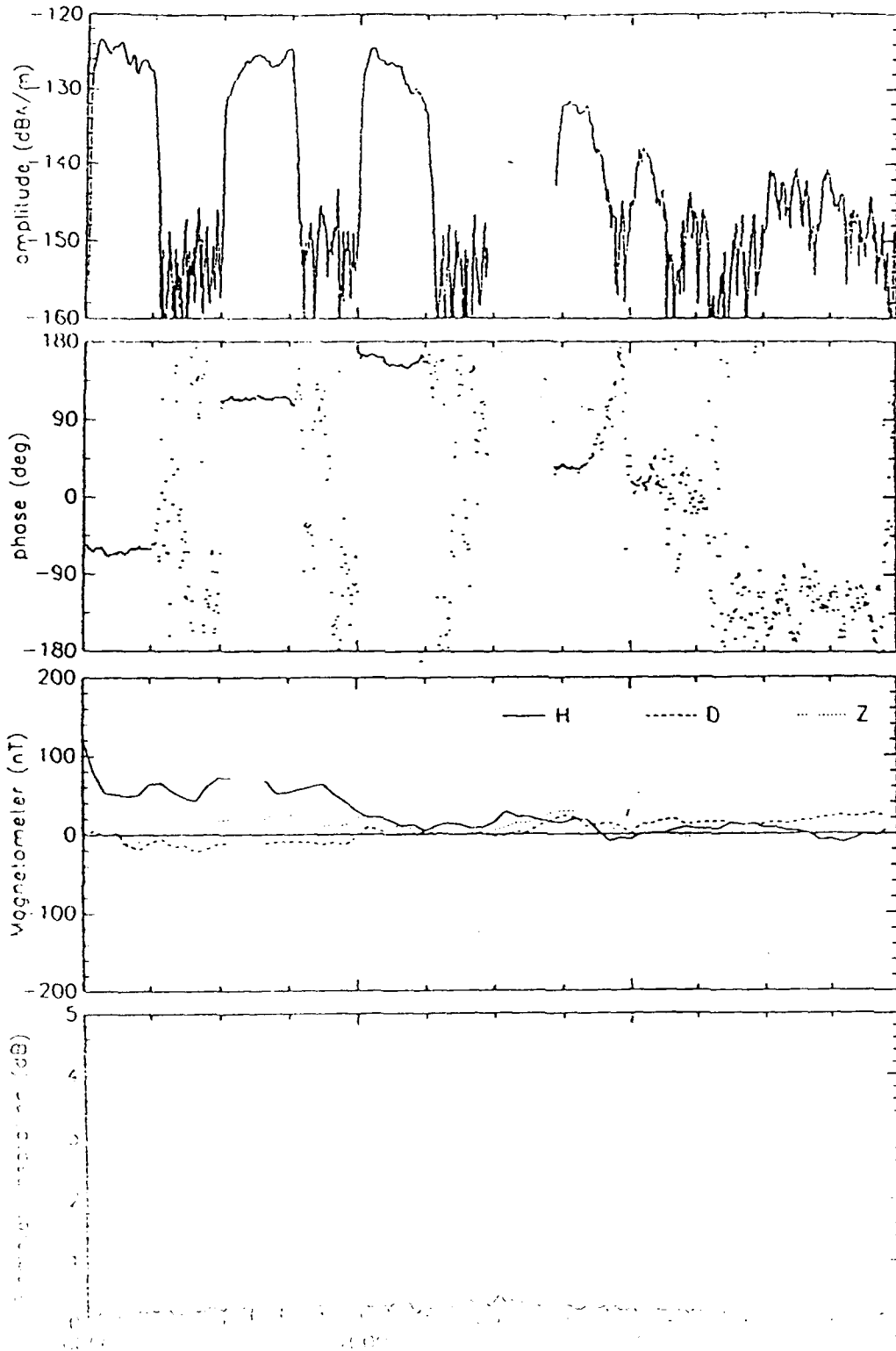
Figure 9 (j)



UT. 24 - Sep - 1990

Figure 9 (k)

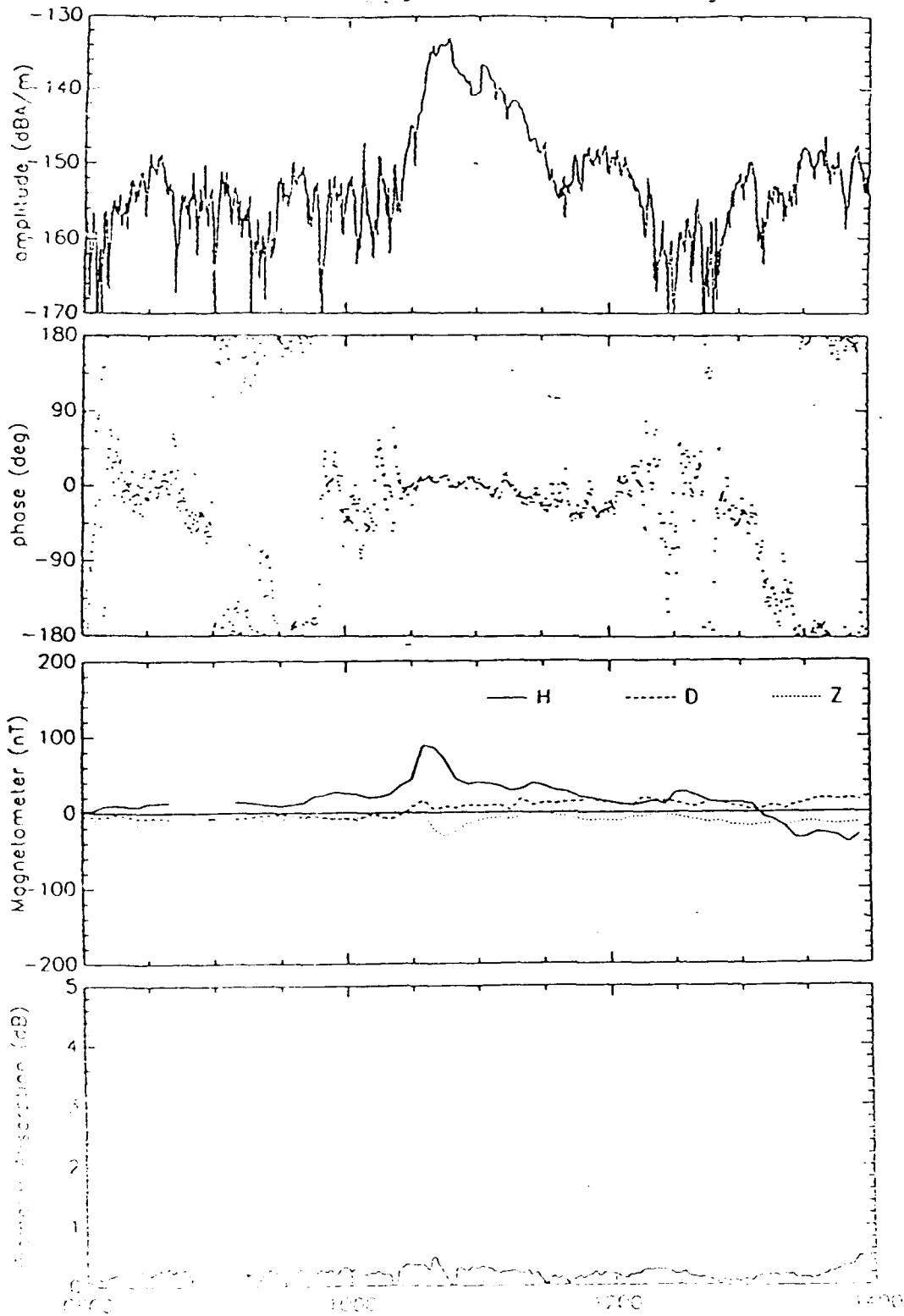
ELF Receiver: NS-Mag chan. 154 Hz. 100 sec integration



UT. 25 - Sep - 1990

Figure 9 (I)

ELF Receiver: NS-140g chon. 154 Hz. 100 sec integration



UT. 26 - Sep - 1990

Figure 9 (m)

SEPTEMBER 1990 CAMPAIGN
0000-0600 ADST NIGHTLY AVERAGES

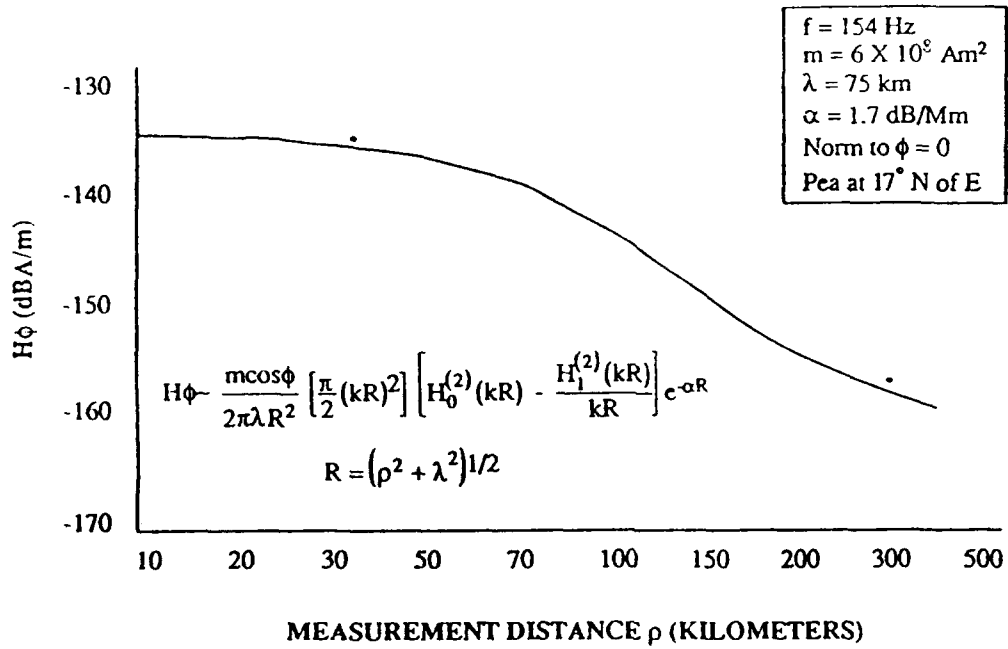


Figure 10 (a) Nightly Average Signal Received in Talkeetna During the September Campaign (Bannister 1990)

SEPTEMBER 1990 CAMPAIGN
HIGH VALUE AVERAGES
(VALUES > NIGHTLY AVGS)

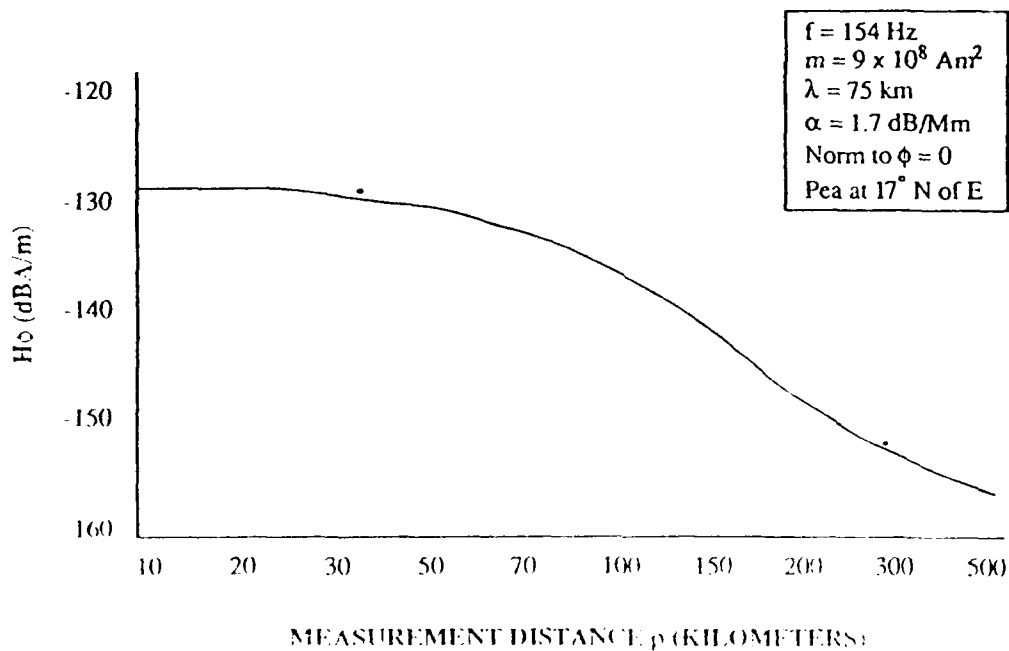
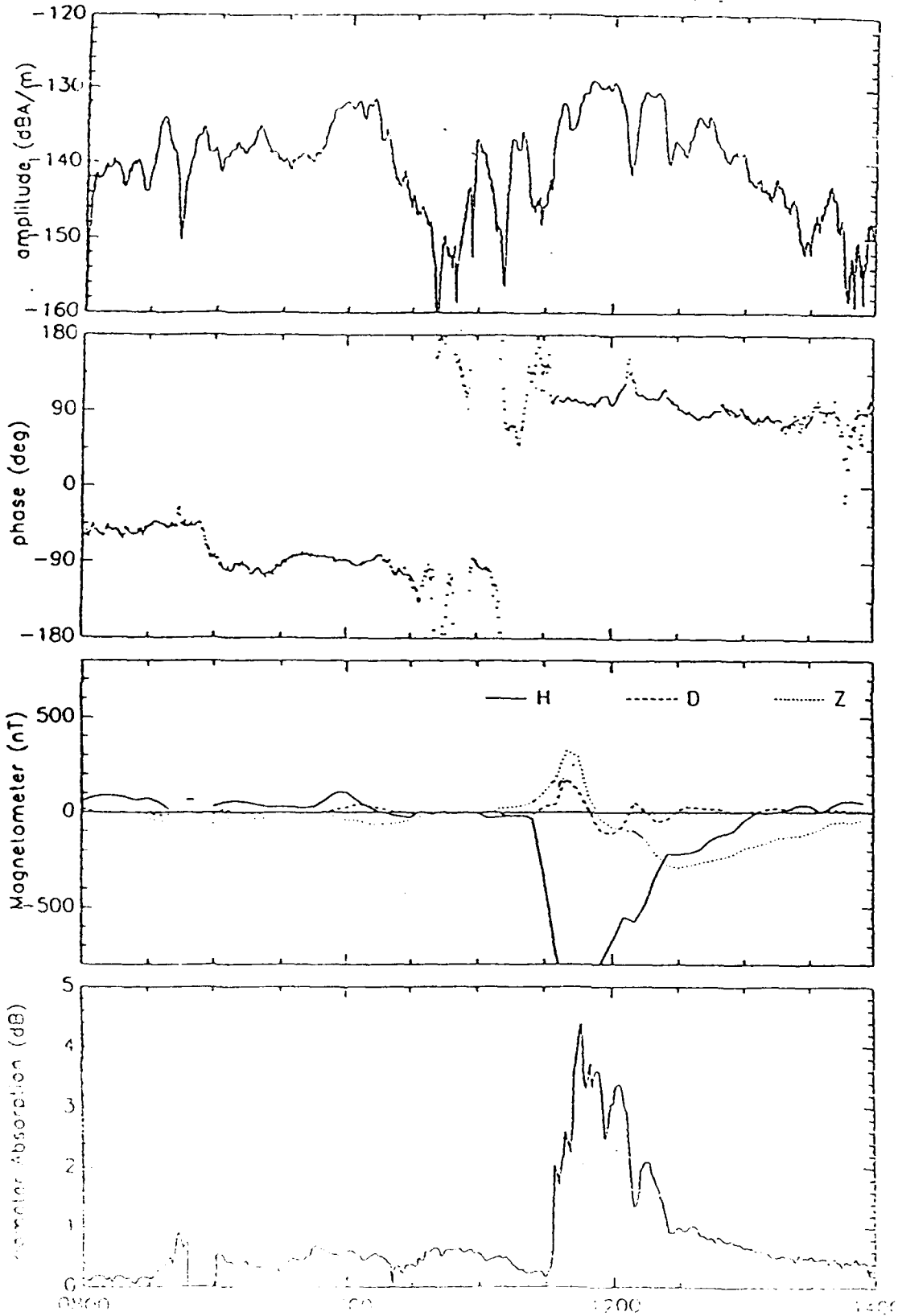


Figure 10 (b)

ELF Receiver: NS-Mag chan, 154 Hz, 100 sec integration



UT 15 - Sep - 1990

Figure 11 ELF Data in Conjunction with Magnetometer Data Indicating Clearly the Ionospheric Origin of the ELF Source

hipas.out

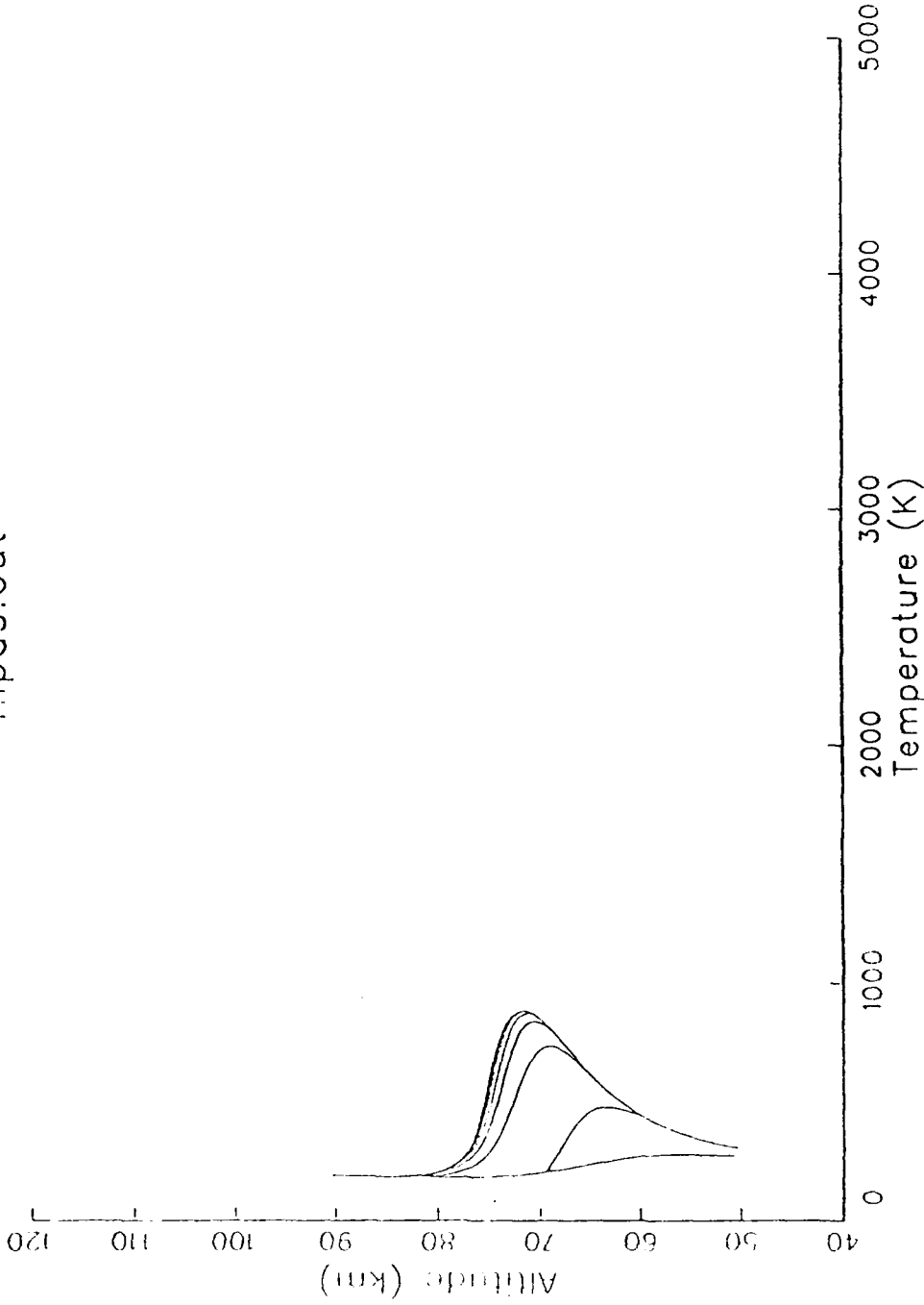


Figure 12 (a) Theoretical Prediction of Expected Temperature and Conductivity Modifications for Average Ionospheric Density Profile

hipas.out

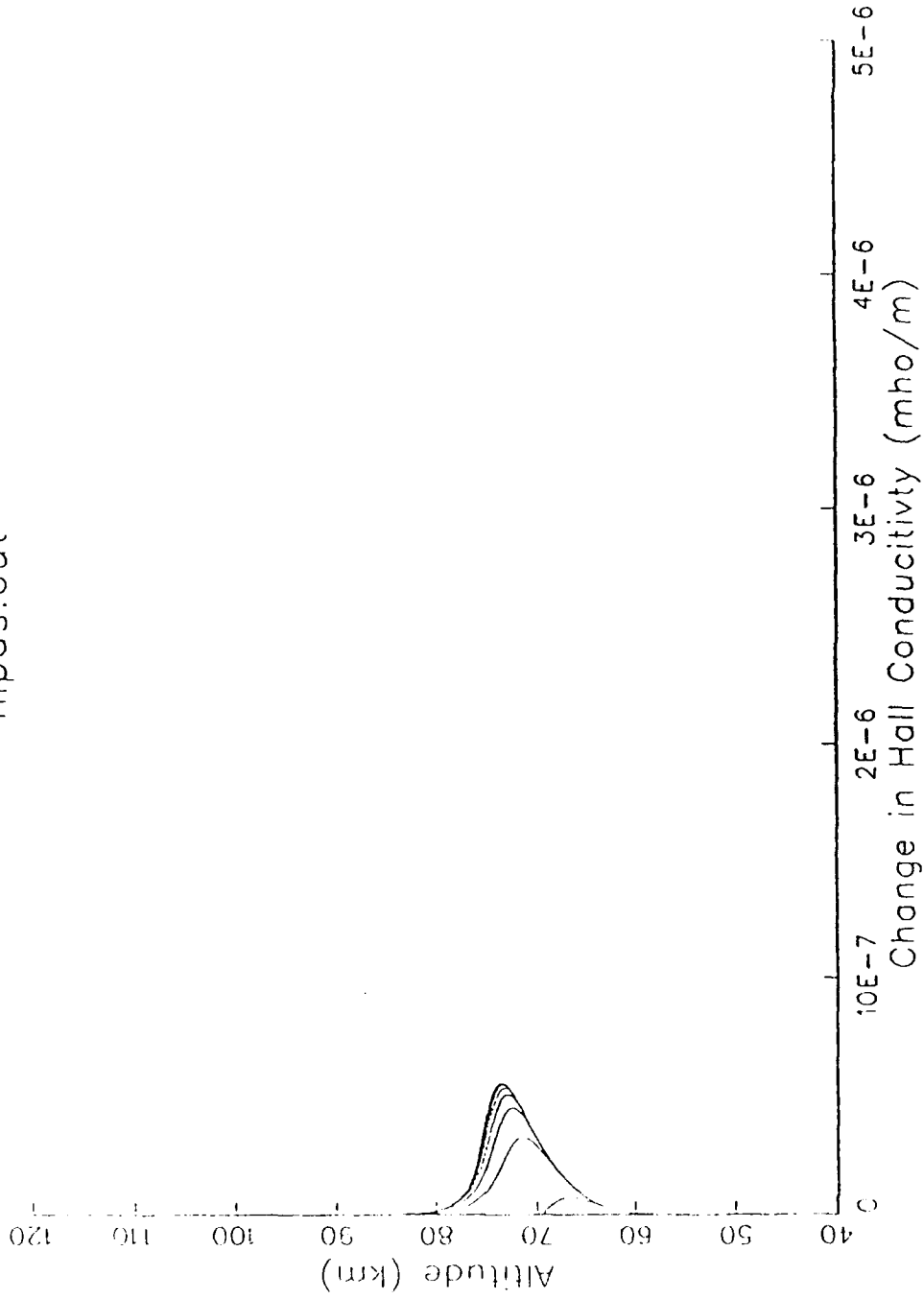


Figure 12 (b)

hipas.out

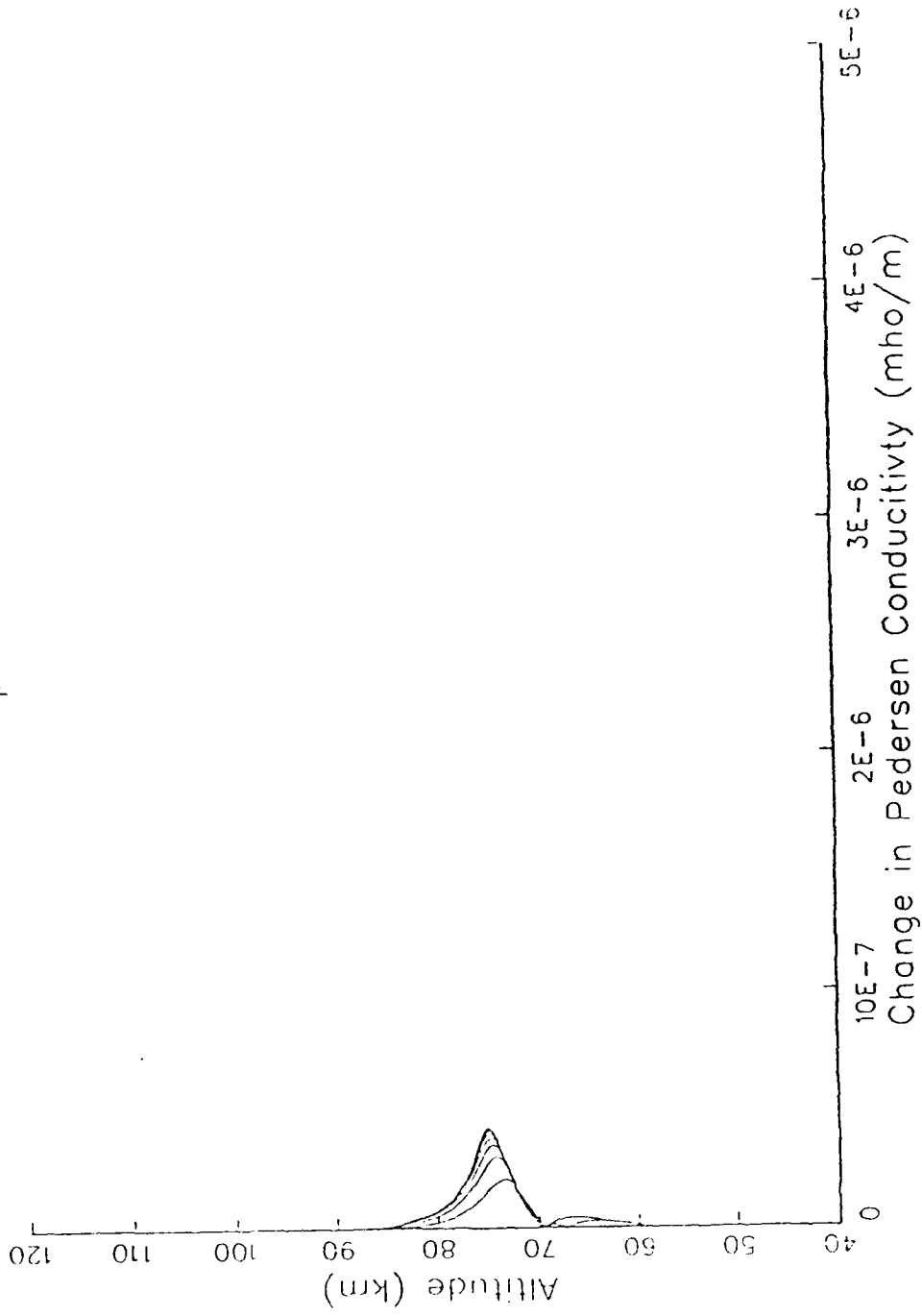


Figure 12 (c)

hipas2.out

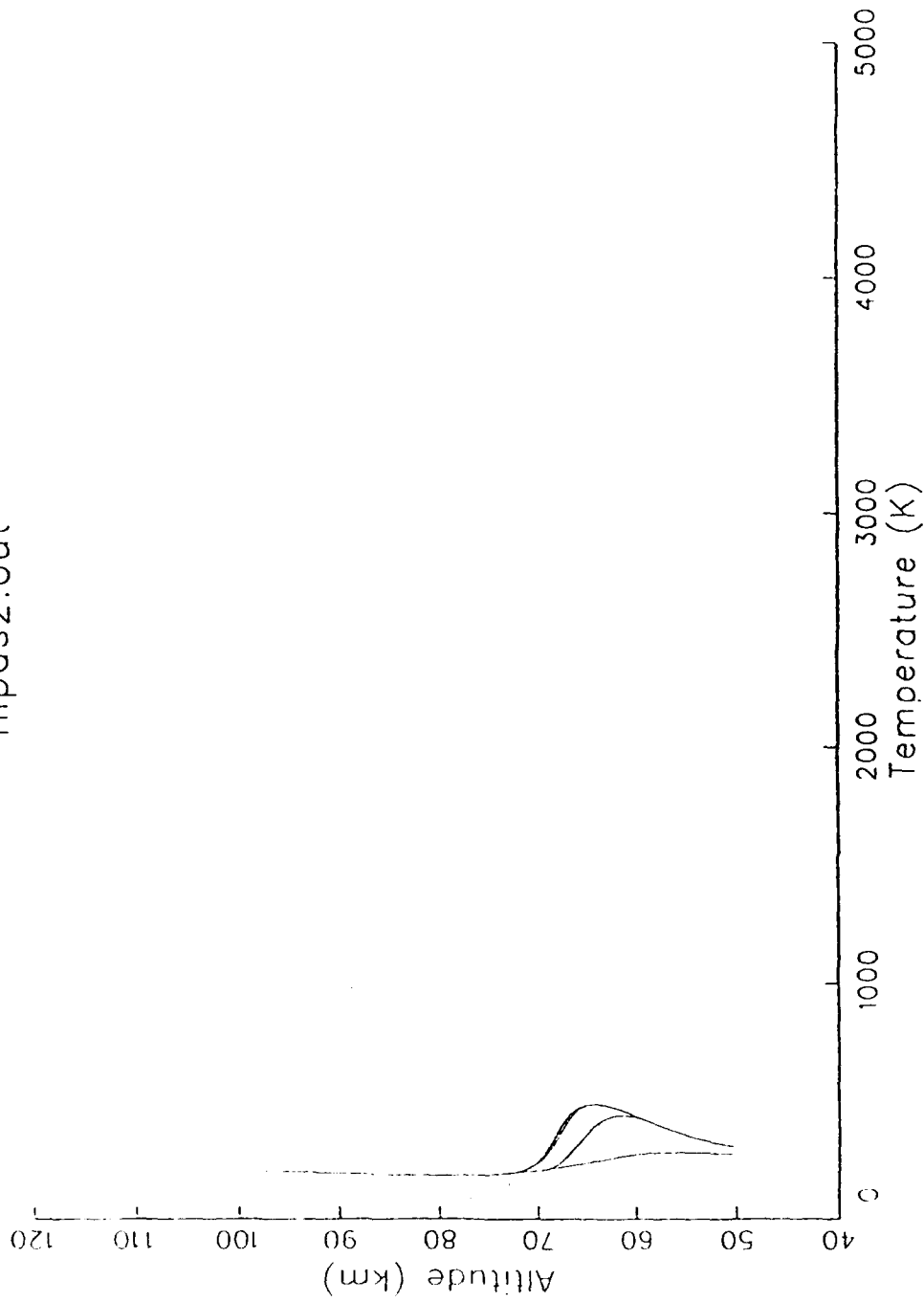


Figure 13 (a) Theoretical Prediction of Expected Temperature and Conductivity Modifications for a High Density Profile

hipas2.out

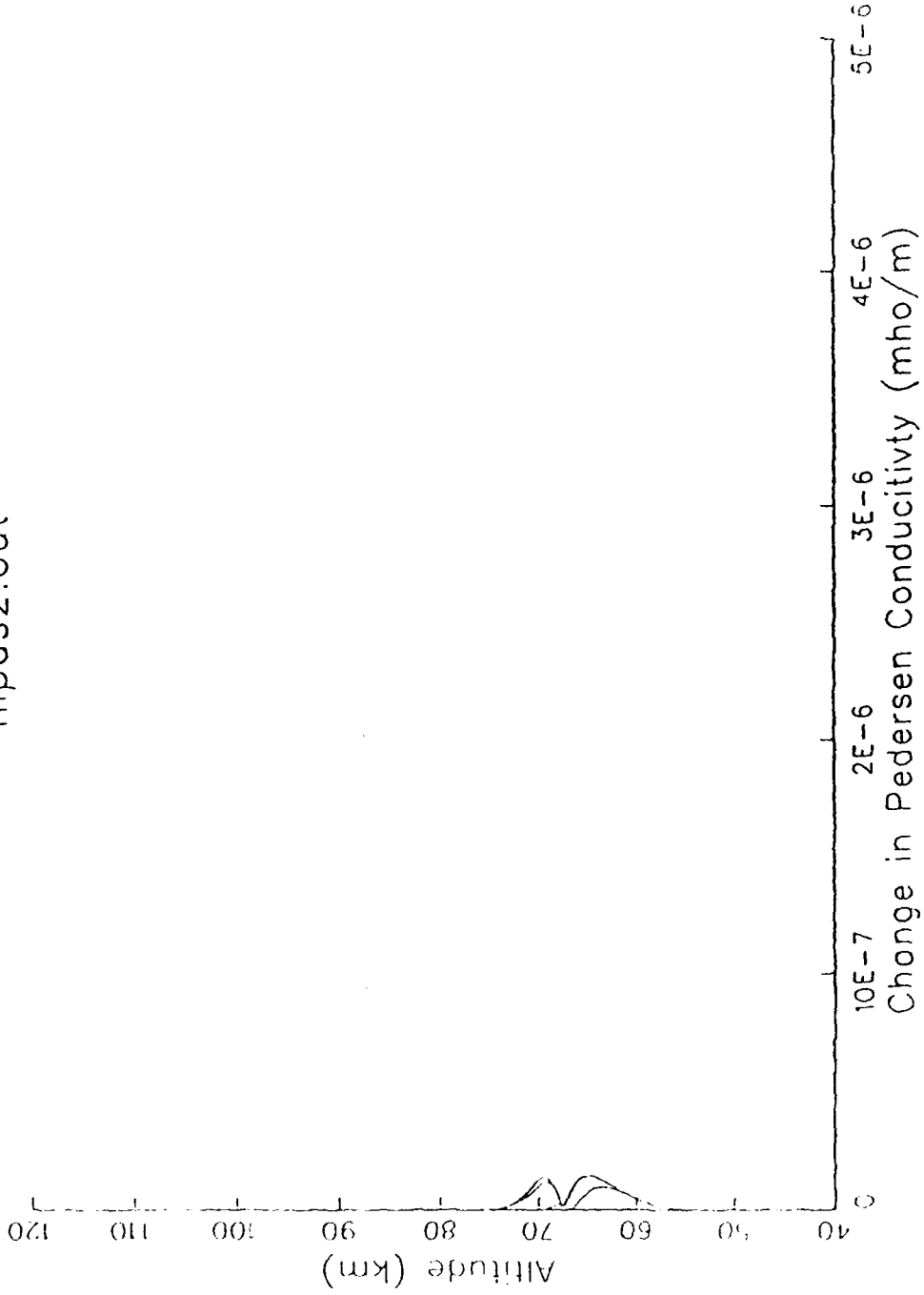


Figure 13 (b)

hipas2.out

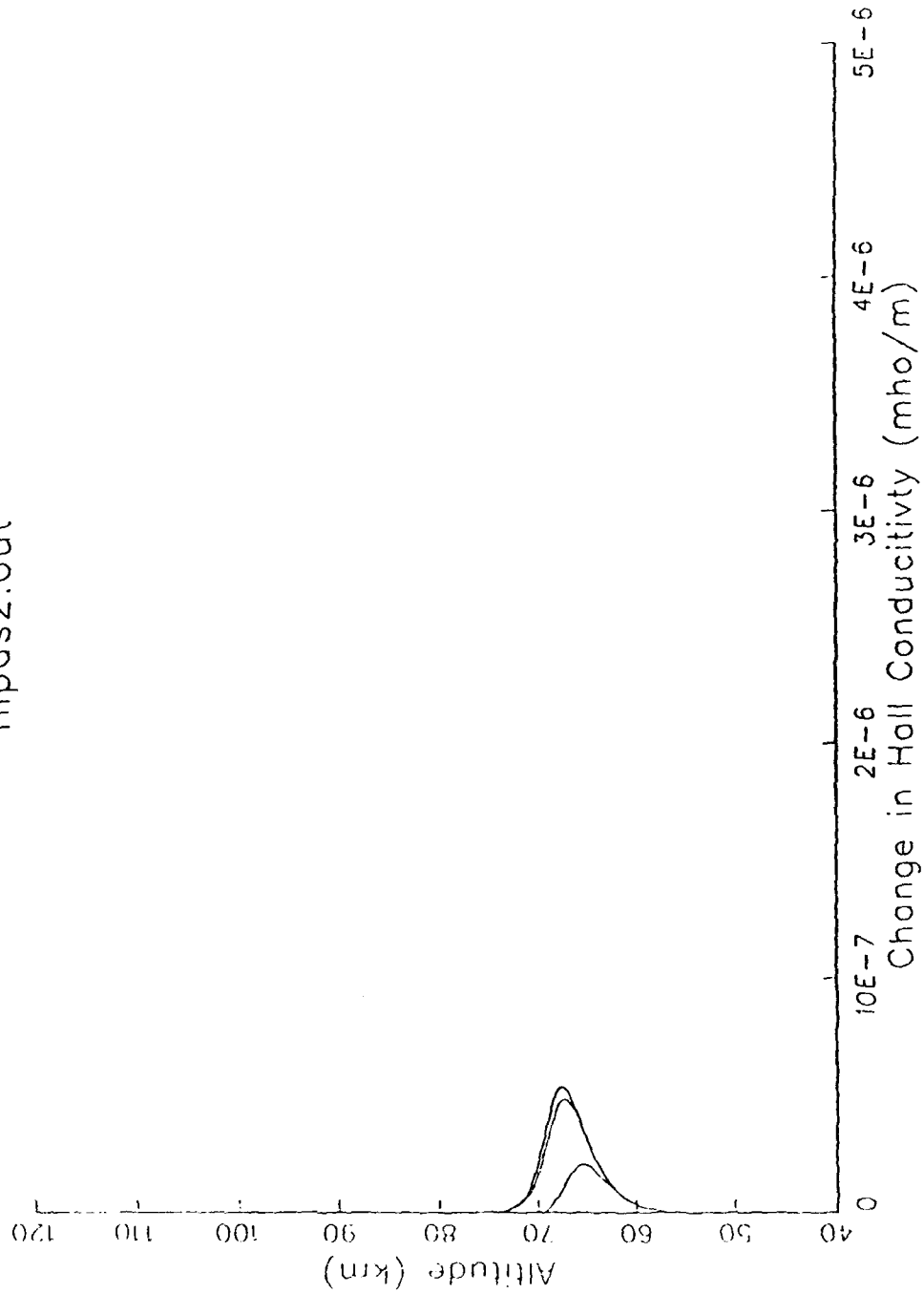


Figure 13 (c)

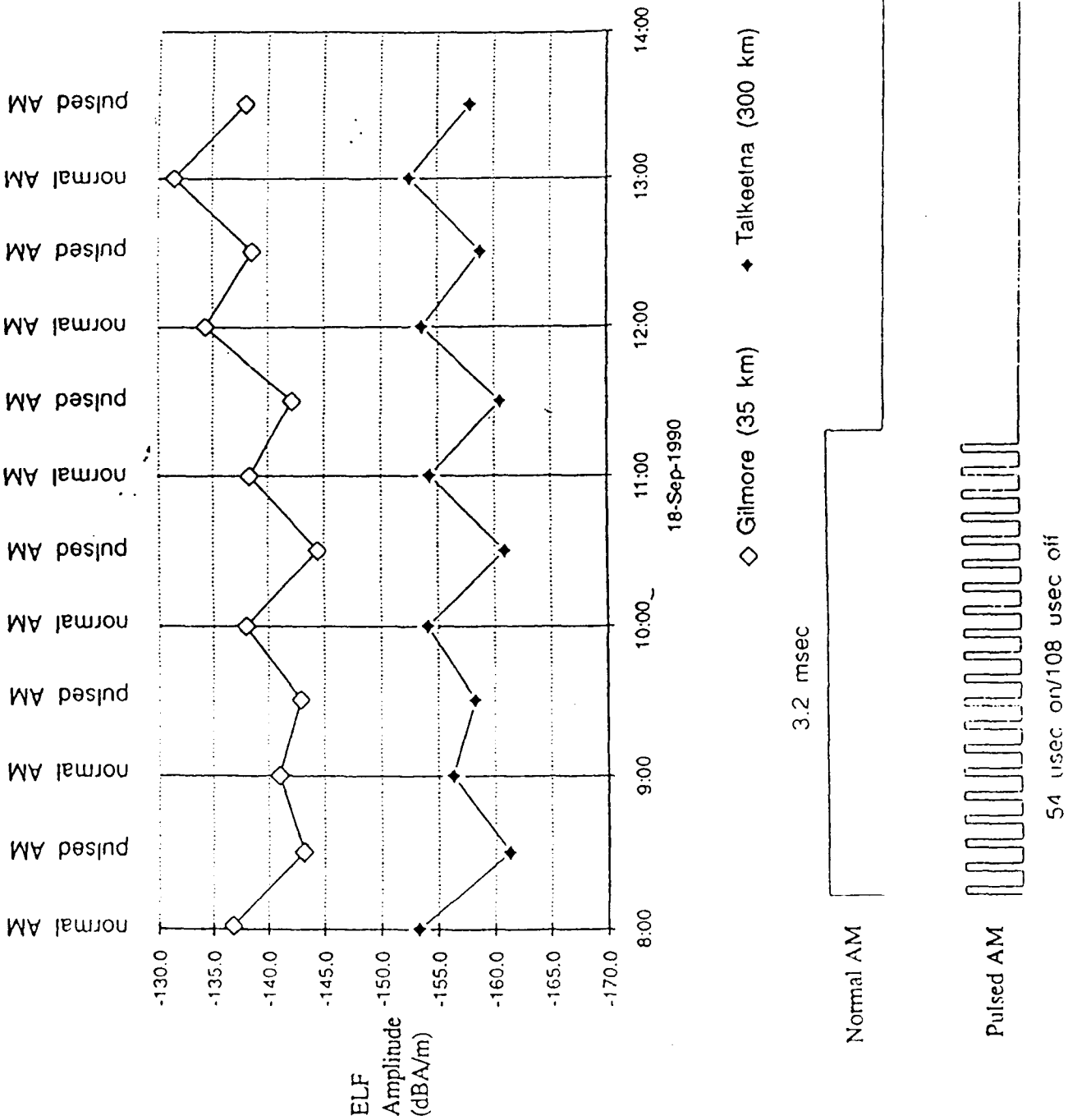


Figure 14 (a) Comparison of NOAA vs Talkeetna Signals for Selected Operating Periods

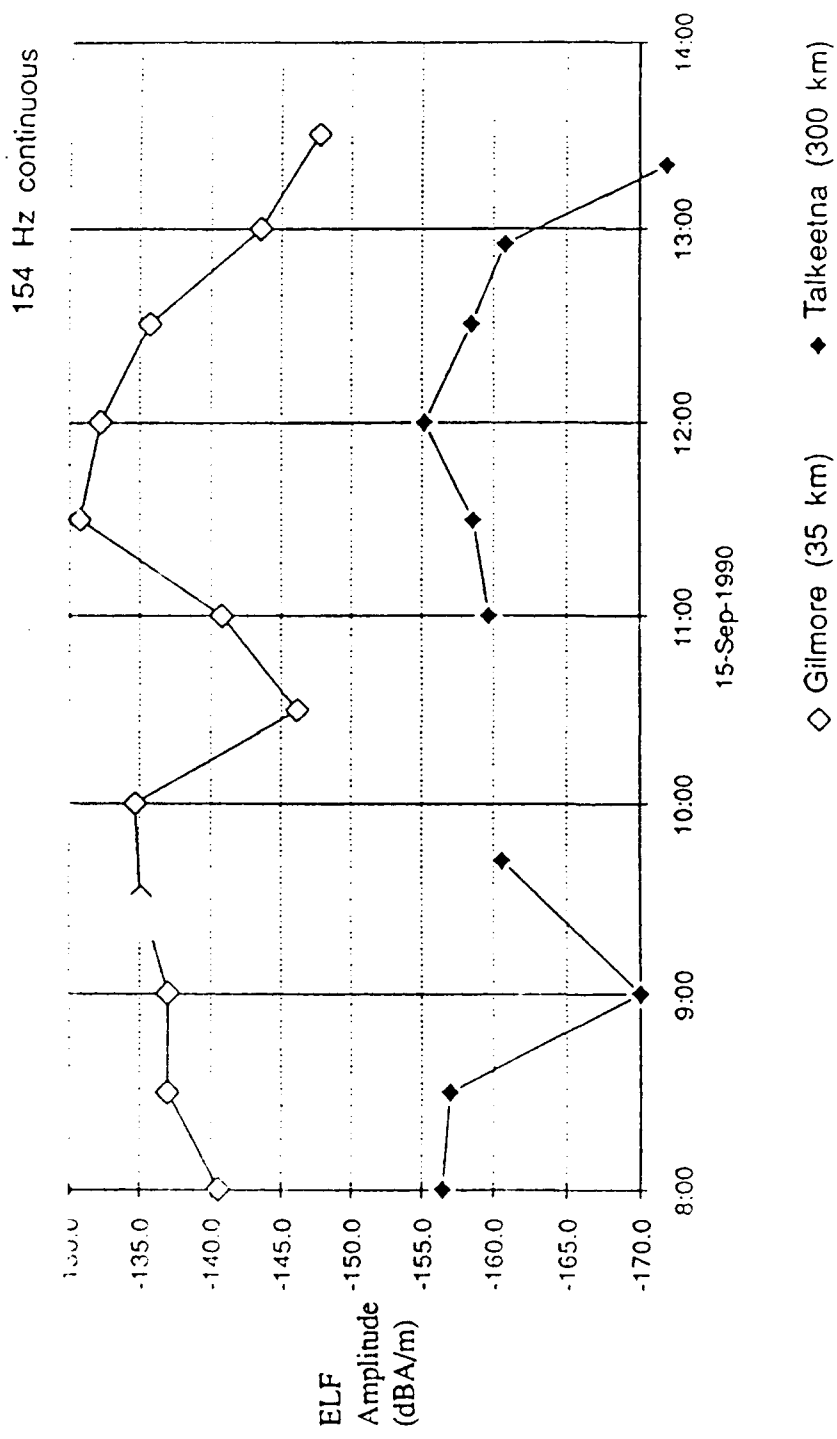


Figure 14 (b)

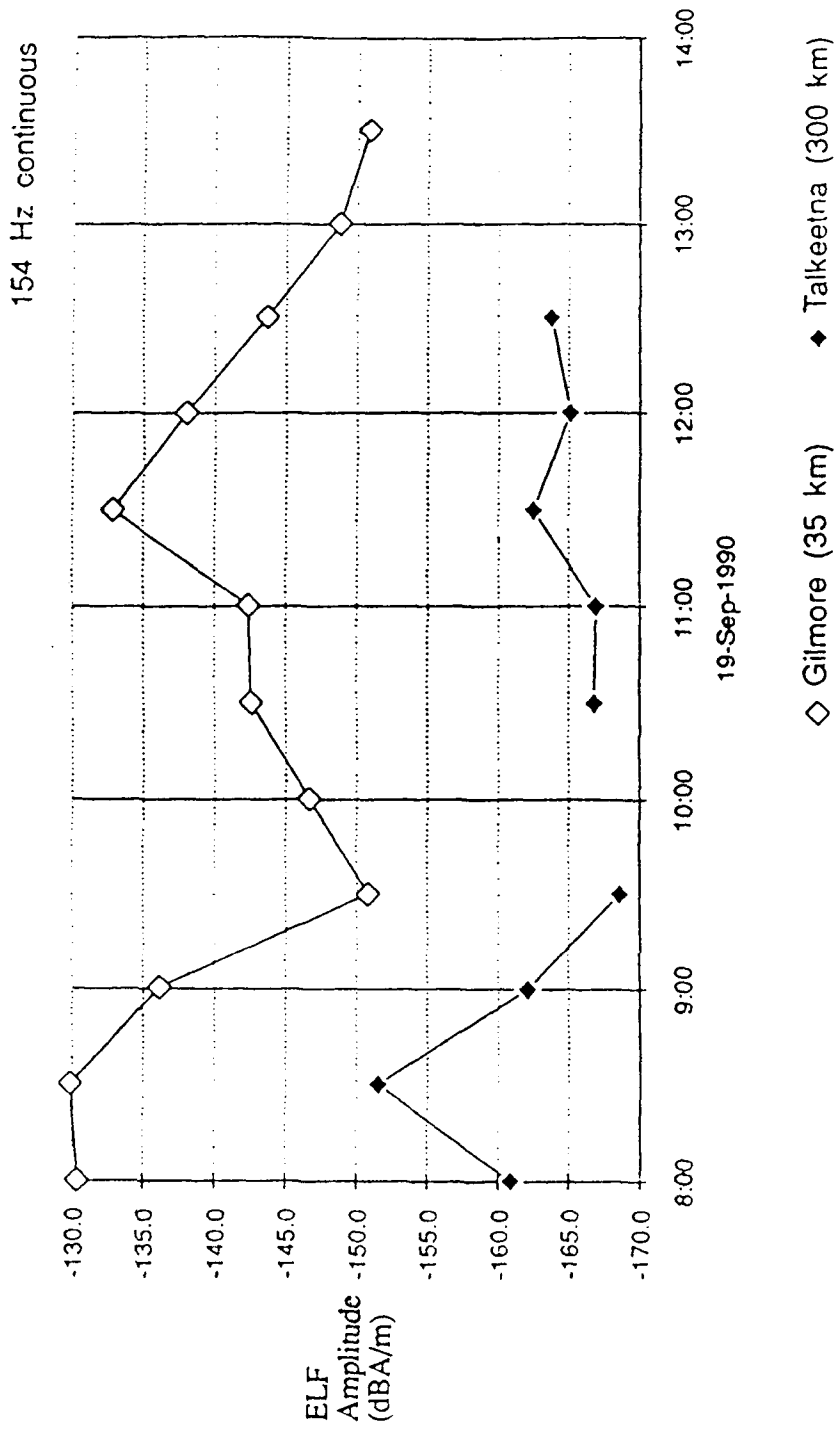


Figure 14 (c)

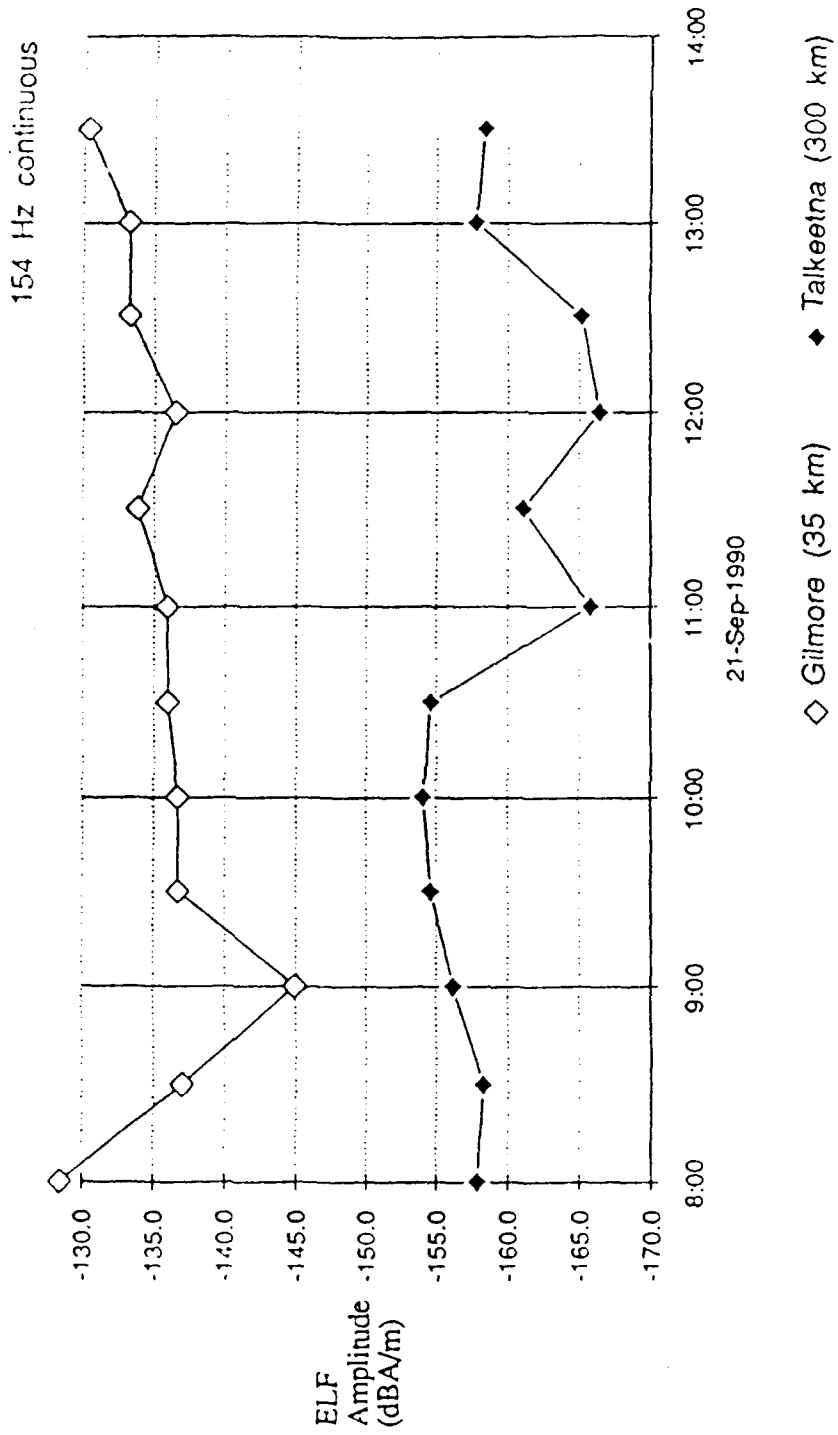


Figure 14 (d)

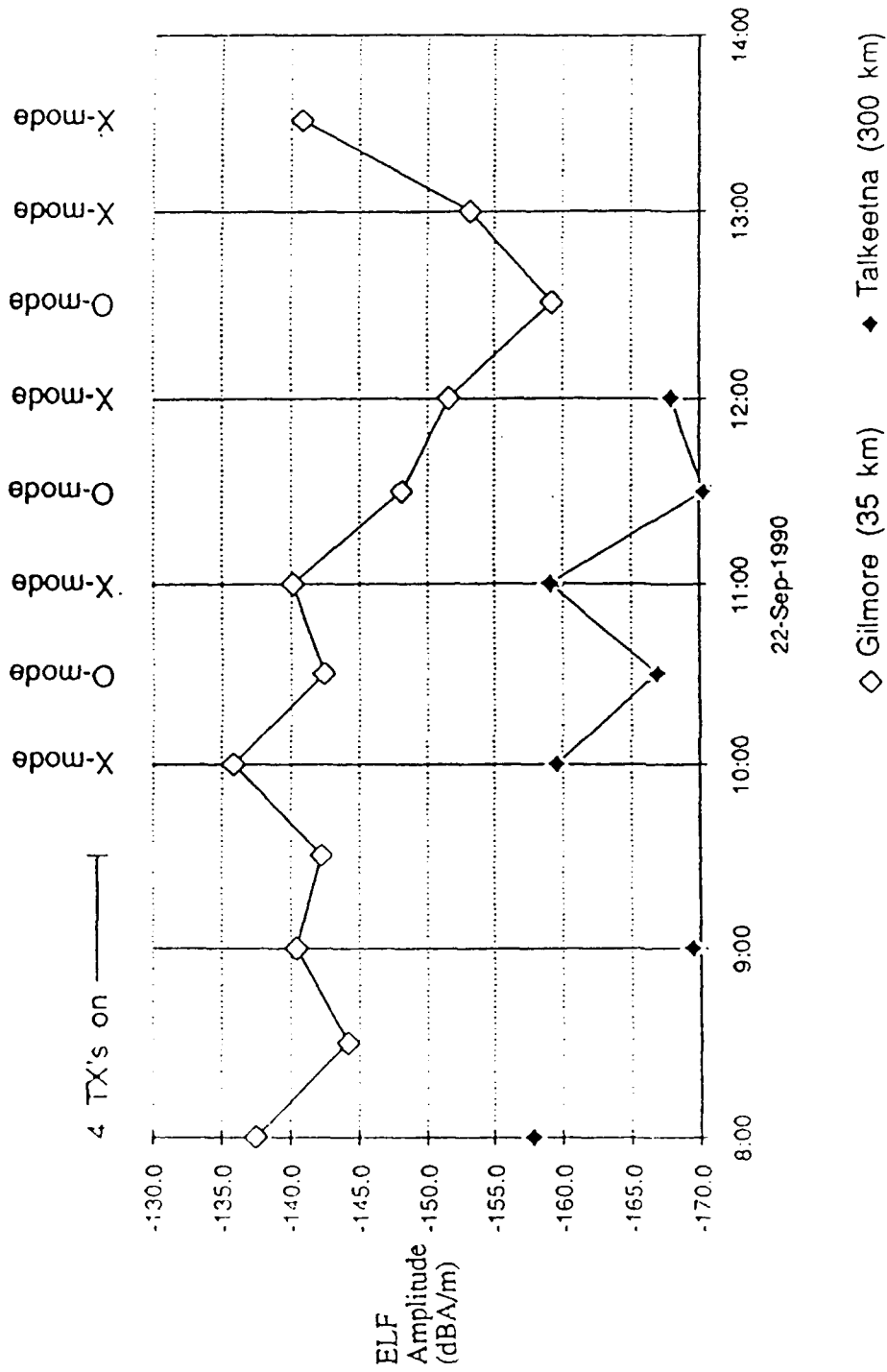


Figure 15 Comparison of O vs X Mode Operation

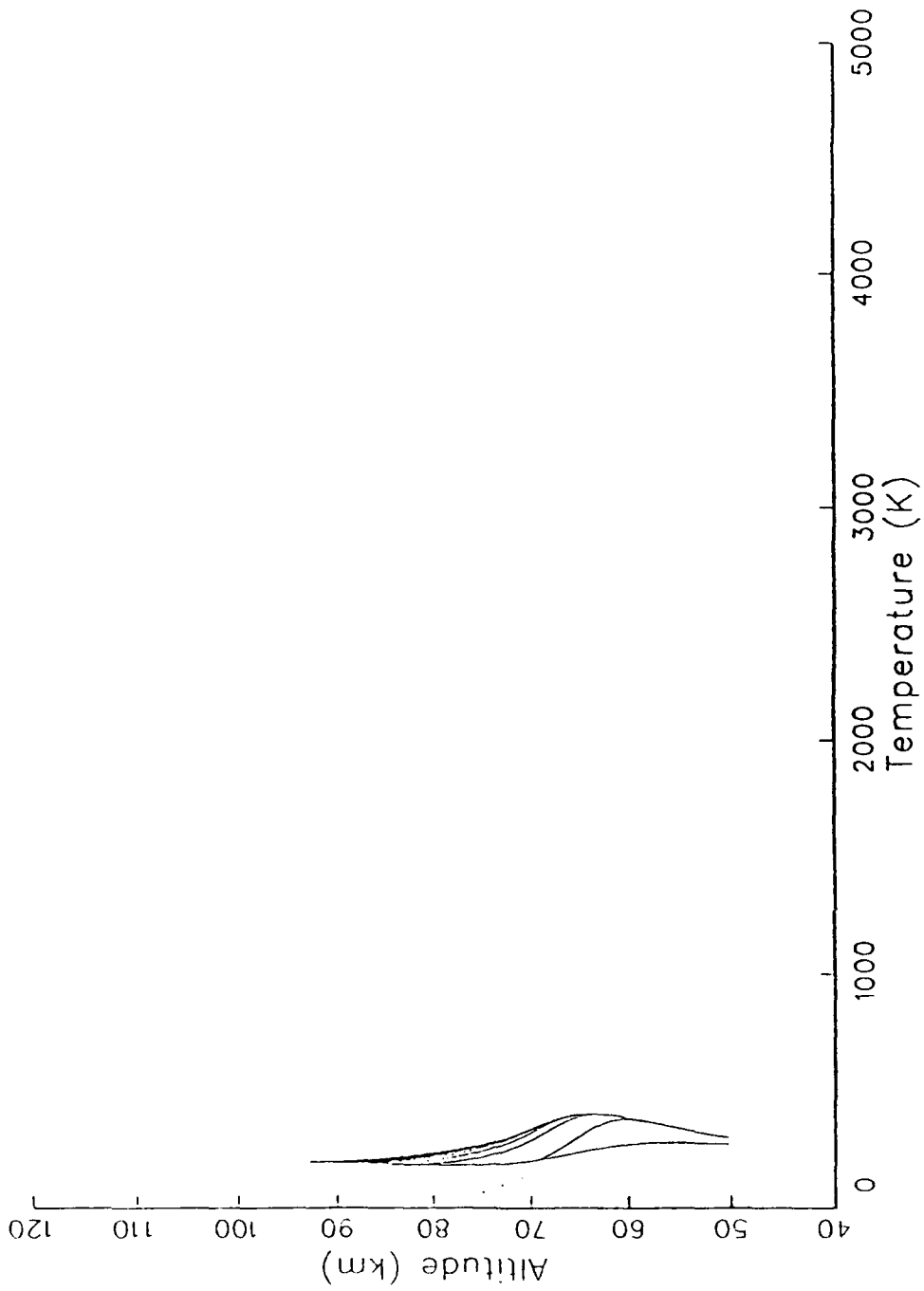


Figure 16 (a) Numerical Profiles for O-Mode Operation

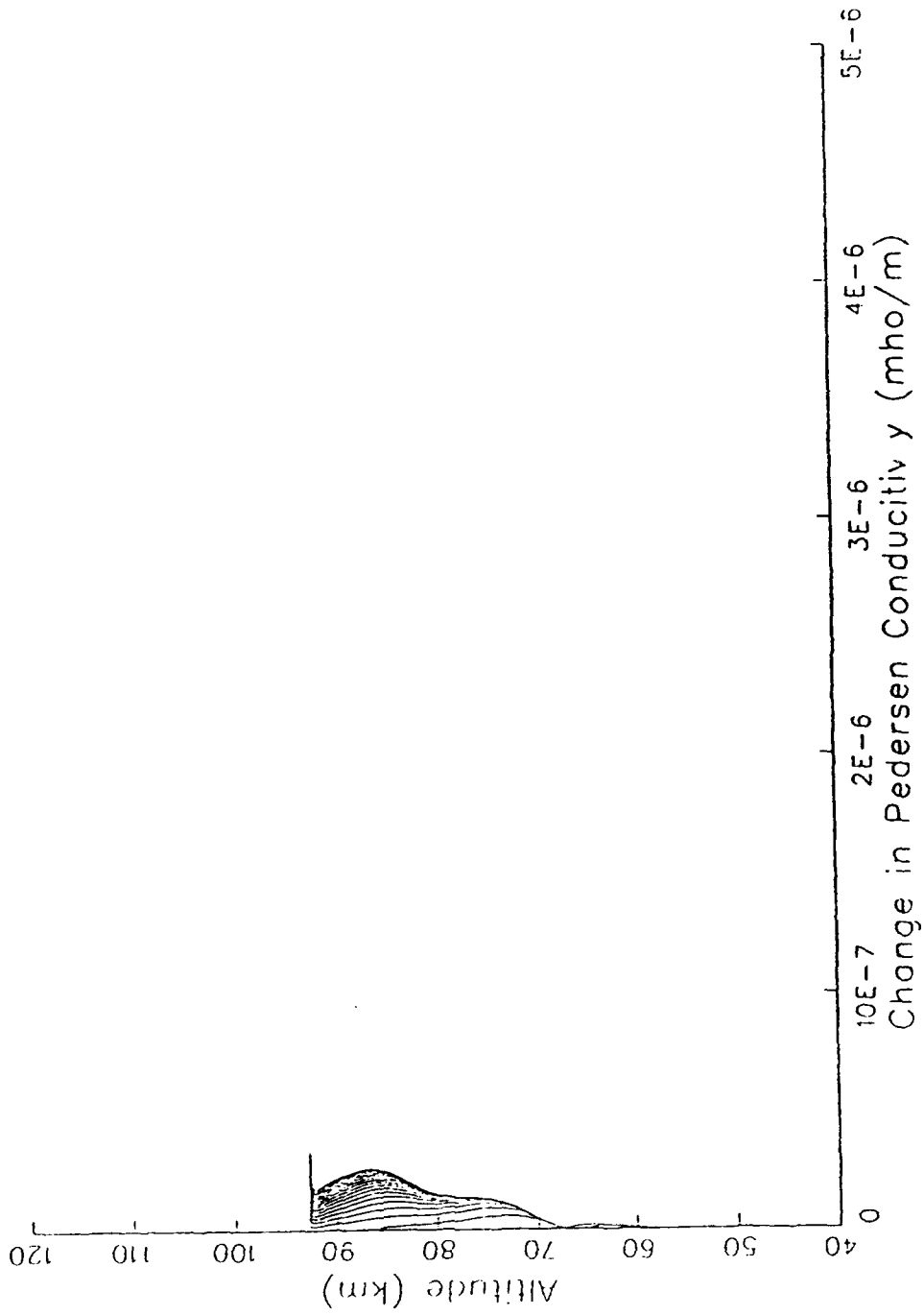


Figure 16 (b)

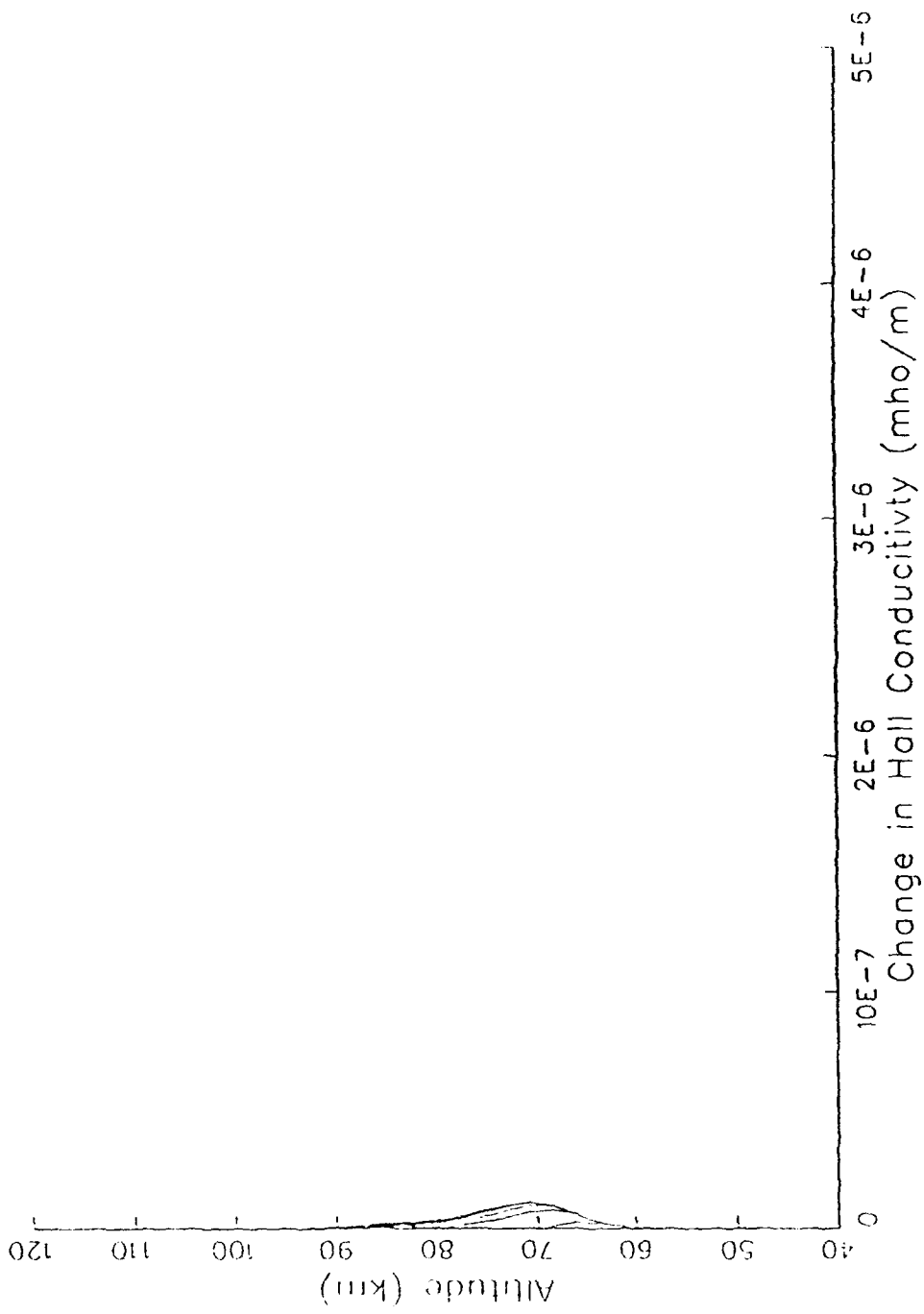


Figure 16 (c)

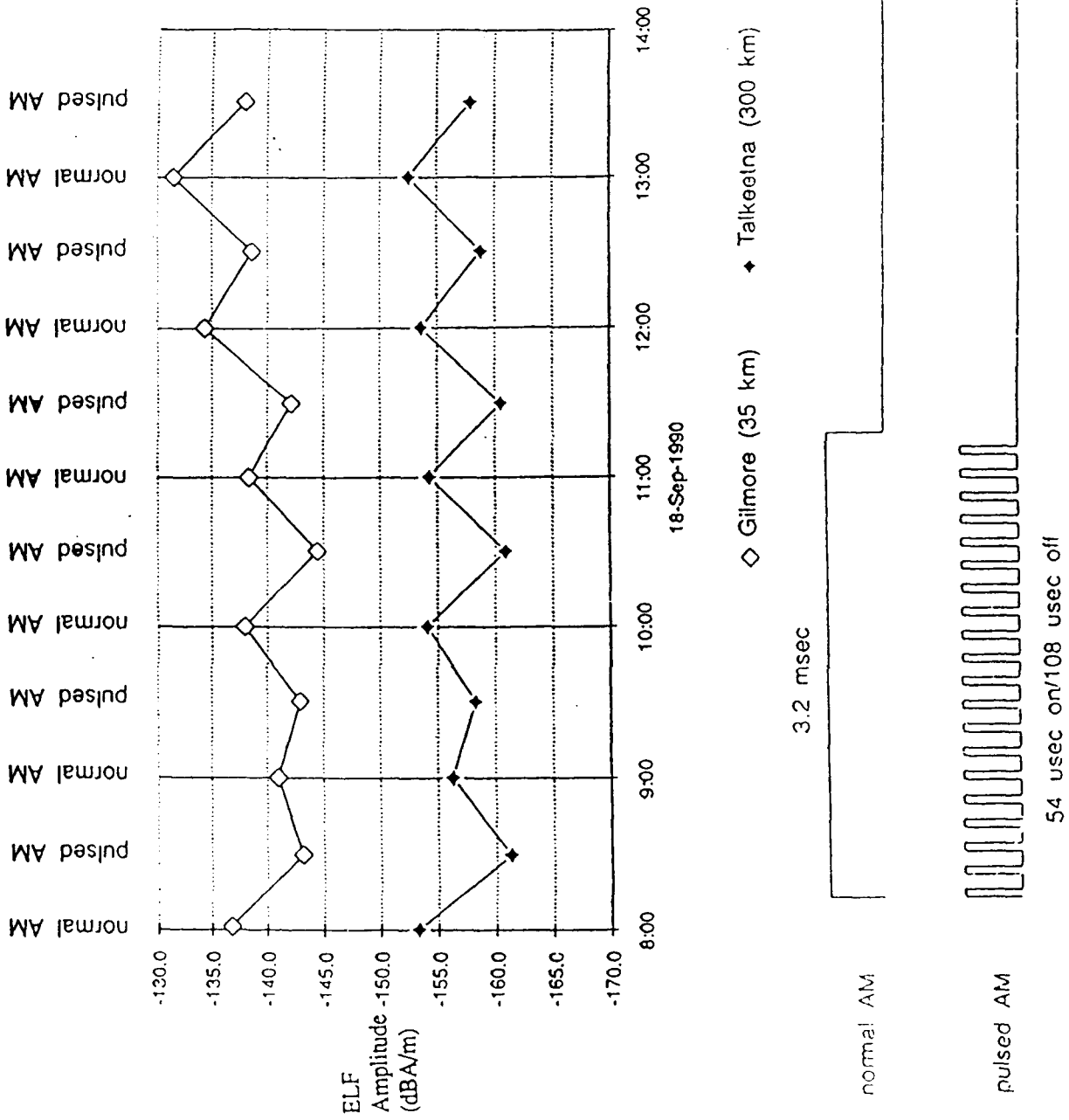


Figure 17 Experimental; Results for Low Duty Heater Operation

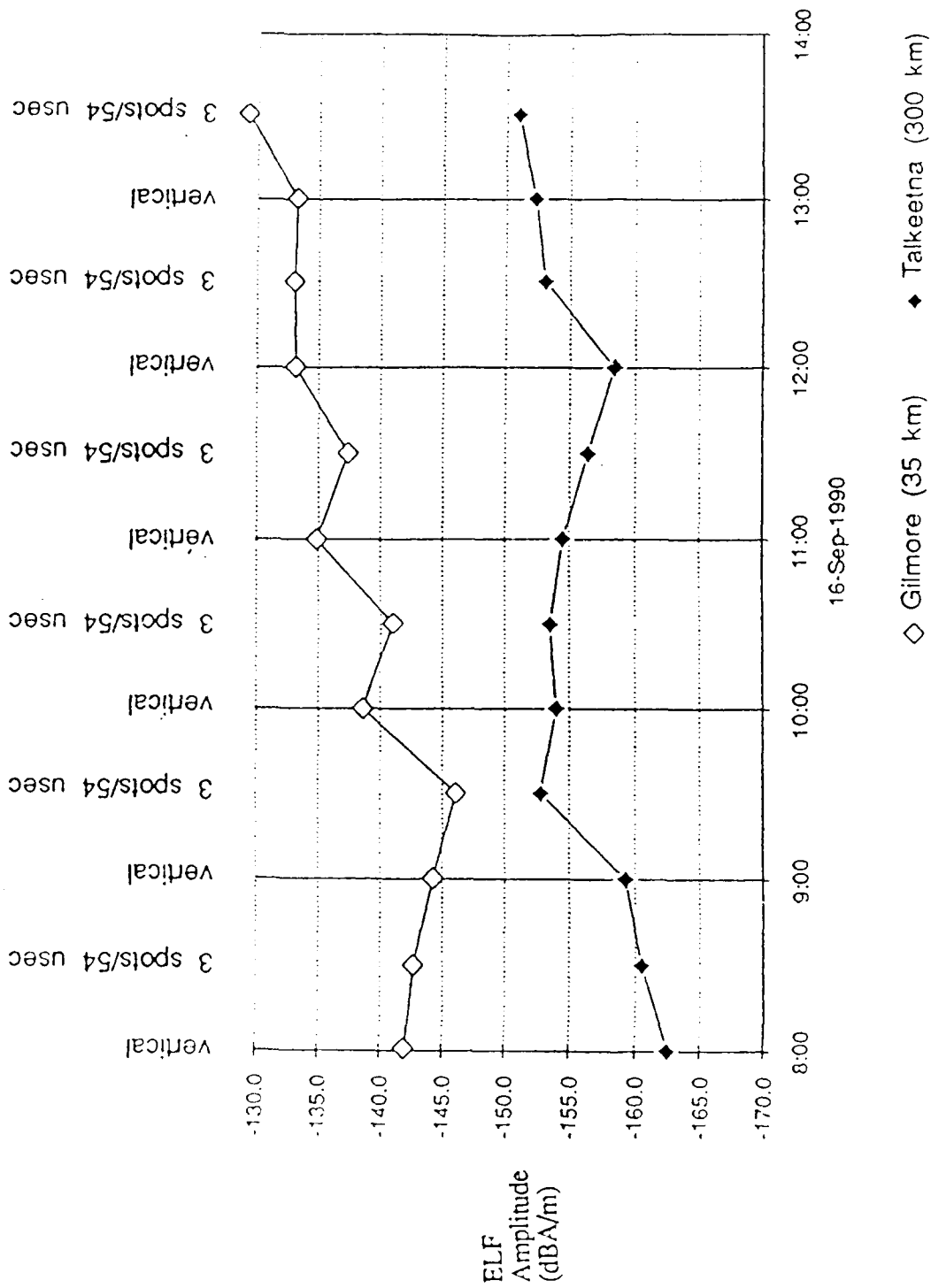


Figure 18 Painting Experiments with 3 Spots

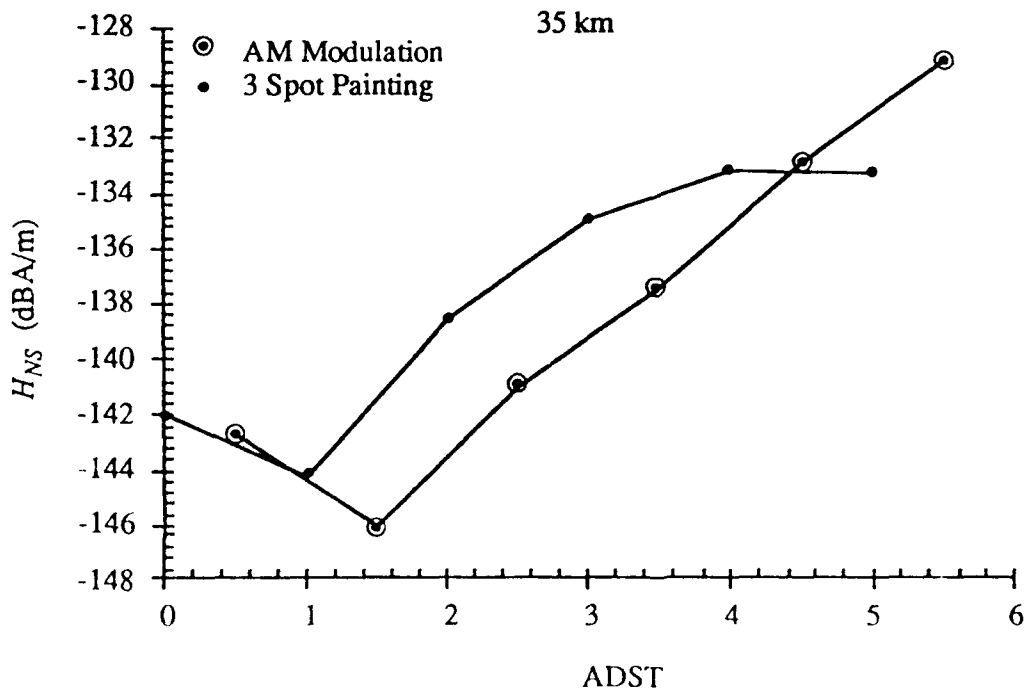
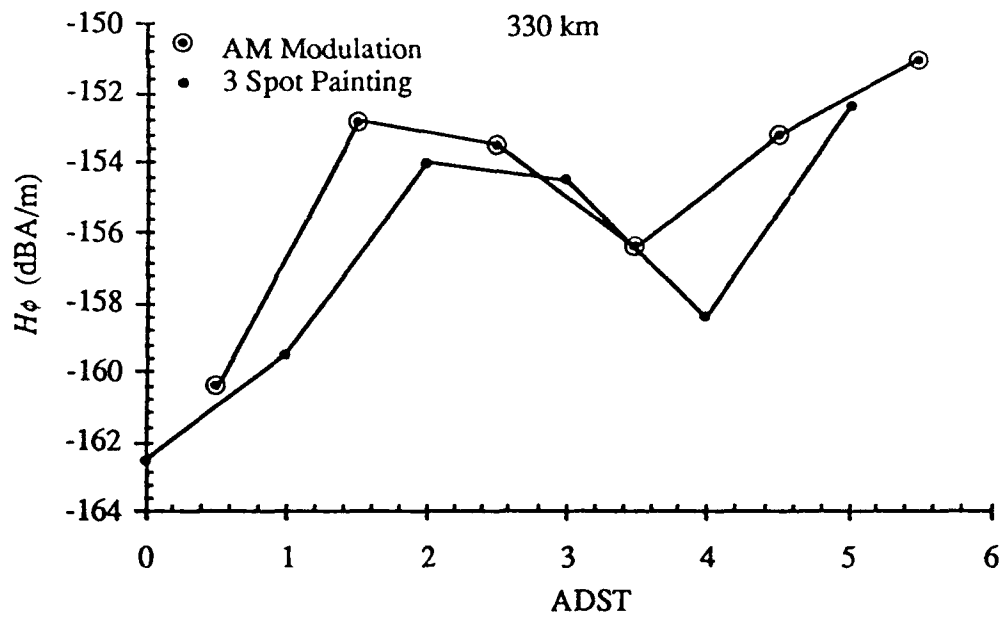


Figure 18 (b)

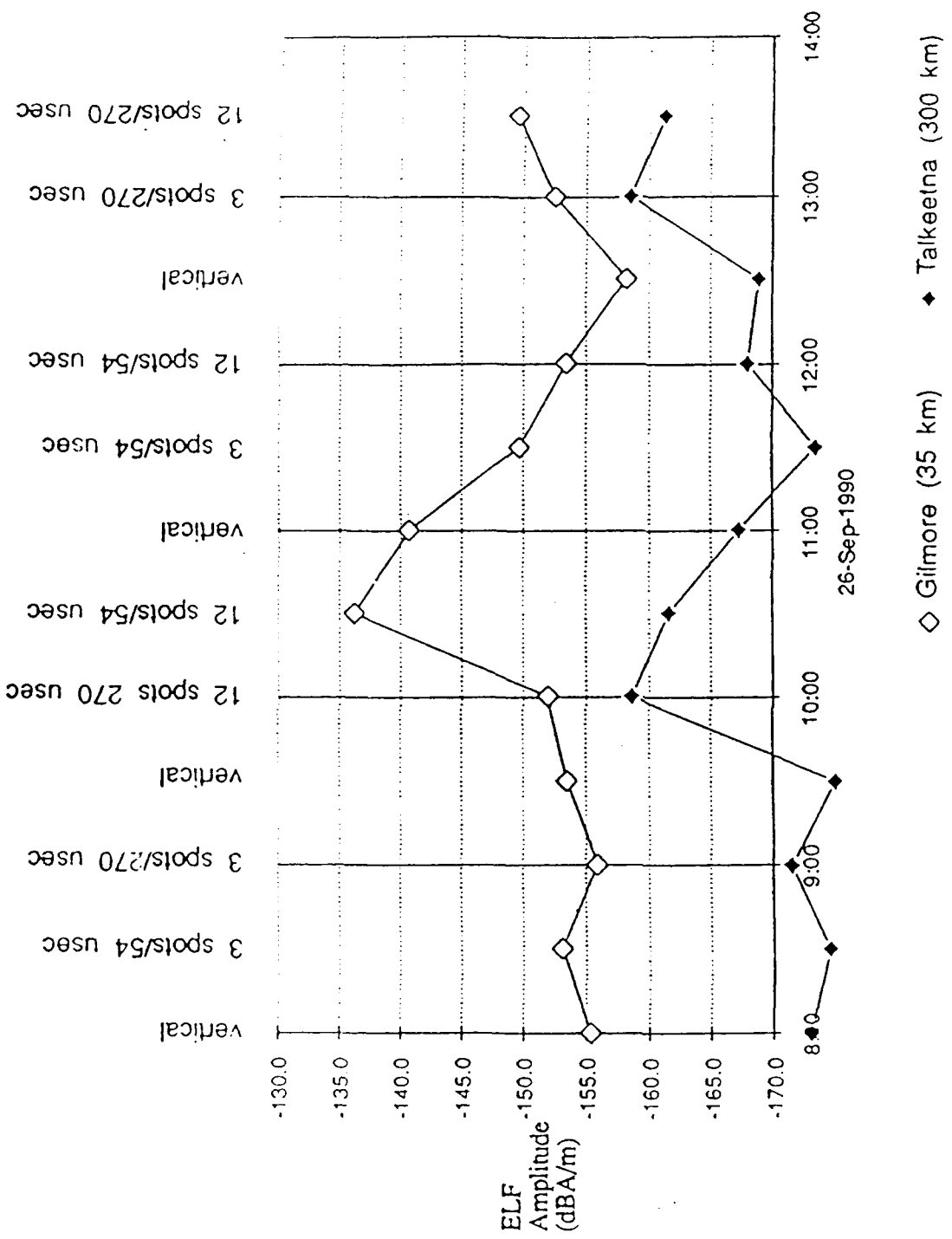


Figure 19(a) Painting Experiments with 3 and 12 Spots Alternating

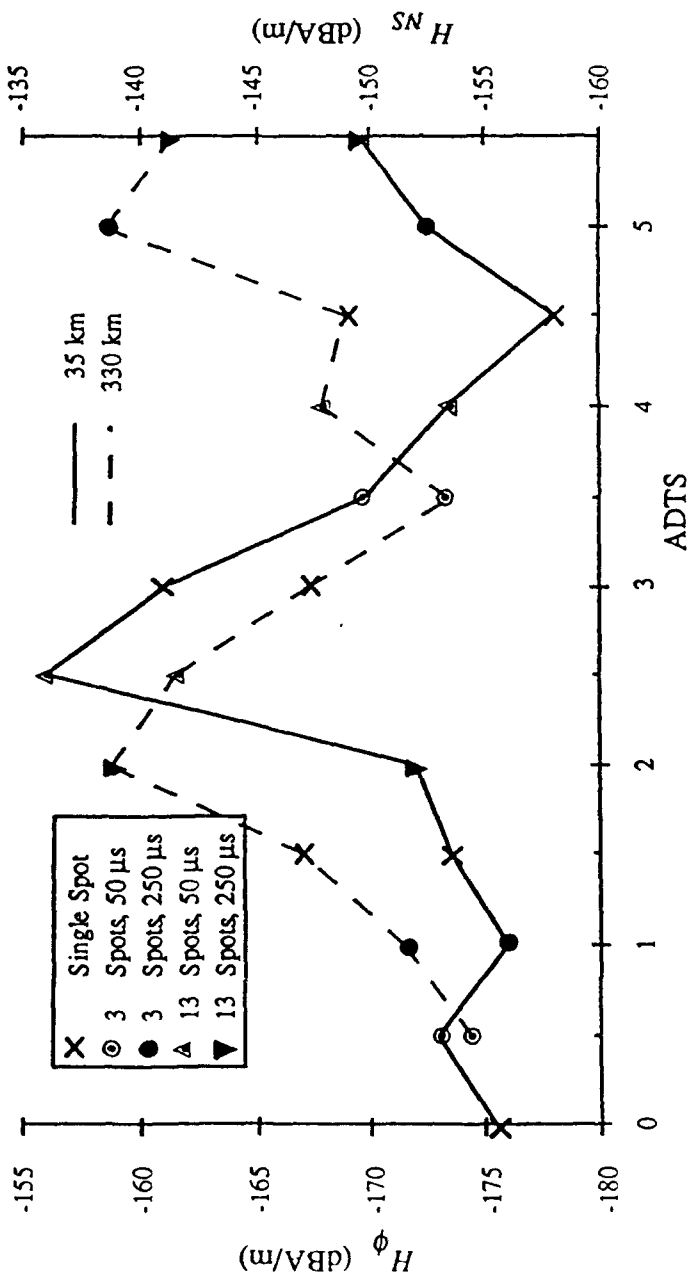


Figure 19 (b)

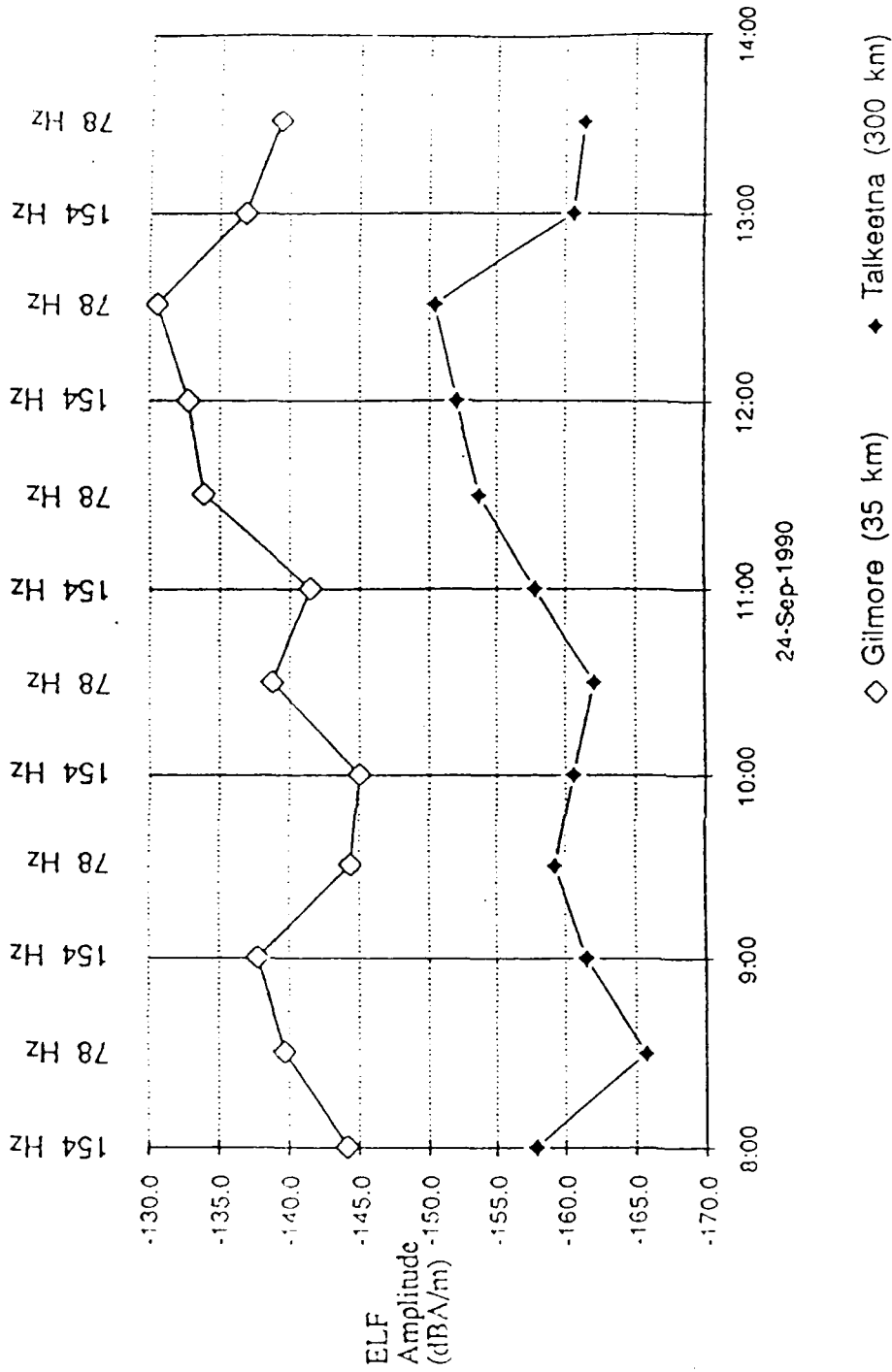


Figure 20 (a) Comparison of Signals at 78 Hz and 154 Hz

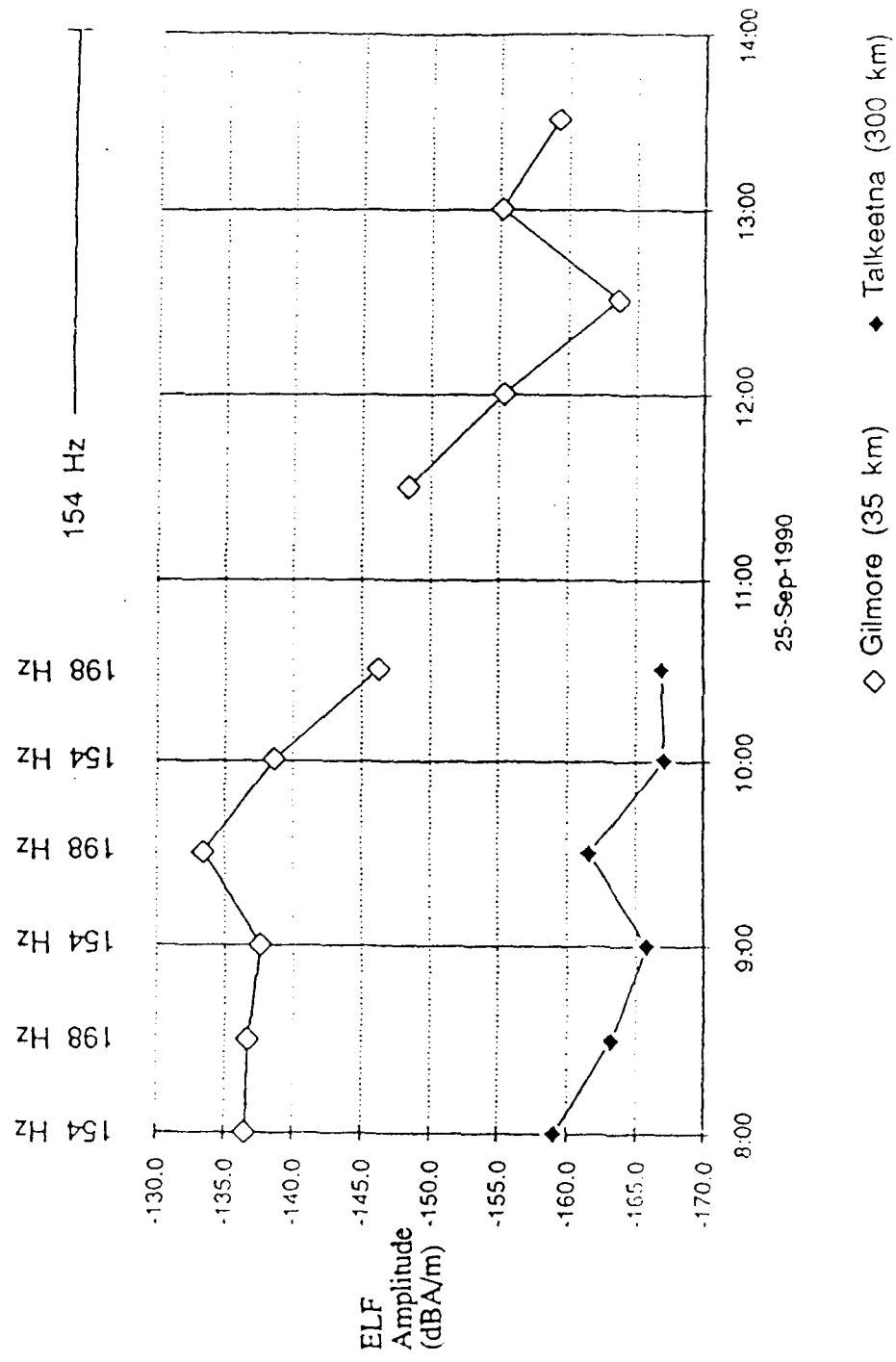


Figure 20 (b)

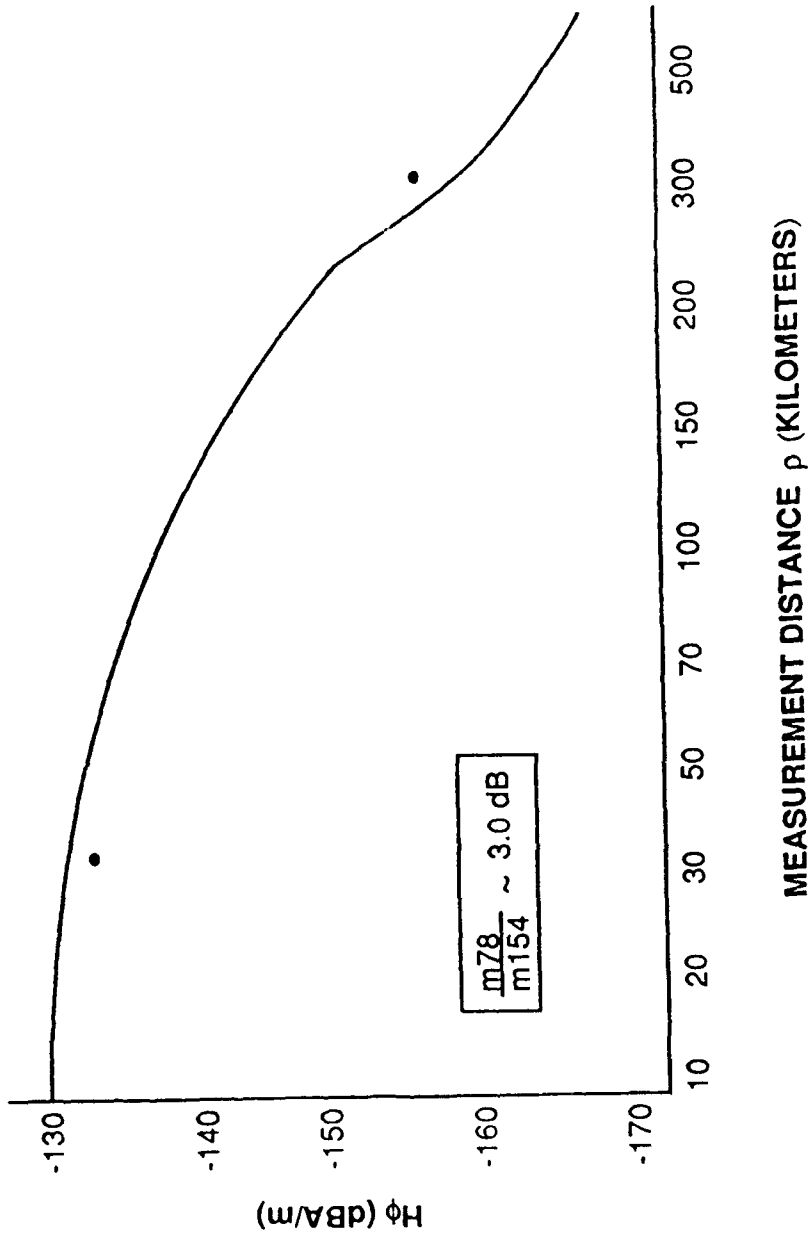


Figure 21 Propagation Model Fitting 78 H7
Data to HMD at 75km